Title
Measurement and Control of Particulate Matter Emissions from Mobile Sources

Author
Quiros, David Christopher

Publication Date
2014

Peer reviewed|Thesis/dissertation

UNIVERSITY OF CALIFORNIA

Los Angeles

Measurement and Control of Particulate Matter Emissions from Mobile Sources

A dissertation submitted in partial satisfaction of the

requirements for the degree

Doctor of Environmental Science and Engineering

by

David Christopher Quiros

2014

ABSTRACT OF THE DISSERTATION

Measurement and Control of Particulate Matter Emissions from Mobile Sources

by

David Christopher Quiros

Doctor of Environmental Science and Engineering

University of California, Los Angeles, 2014

Professor Yifang Zhu, Chair

Controlling mobile source emissions is a key strategy for reducing ambient particulate matter (PM) emissions and to comply with the National Ambient Air Quality Standards (NAAQS). The California Air Resources Board (ARB) has adopted new regulations, strengthened existing regulations, and implemented control programs for reducing emissions of PM from light-duty vehicles (LDV) and heavy-duty diesel trucks (HDDT). Since model year (MY) 2007, all HDDTs are certified to a stringent PM emissions standard of 0.01 g PM per brake-horsepower-hour using diesel particulate filter (DPF) aftertreatment. Recently, ARB adopted the Low Emission Vehicle (LEV) III regulations, which will reduce the PM emissions for LDVs over the Federal Test Procedure (FTP) to 3 mg/mi beginning with MY 2017, and to 1 mg/mi beginning with MY 2025. This dissertation discusses and investigates some of the key issues for reducing PM emissions from both HDDTs and LDVs. It is subdivided into the

following five chapters: an introduction (Chapter 1), three chapters of original research (Chapters 2-4), and a discussion of the implications and conclusions of the work (Chapter 5).

Chapter 2 evaluates PM emissions during a process called diesel particulate filter (DPF) regeneration, which is the periodic oxidization of accumulated soot into mostly carbon dioxide. The PM emissions released during this process are noteworthy and need to be controlled. However, the total PM emissions, following equal treatments of loading, decreased by over an order of magnitude between the MY 2007 and 2010 HDDT.

Chapters 3 and 4 evaluate particle size distribution, effective density, and an alternative method called Integrated Particle Size Distribution (IPSD) to further support measurement of PM from vehicles emitting below 1 mg/mi. The evaluation of the IPSD method provided a better understanding of the variability of PM emissions of vehicles meeting the LEV III standards. The implementation of the 1 mg/mi standard is currently scheduled to begin with MY 2025 vehicles, and serves to prevent emissions backsliding associated with the introduction of newer and more fuel-efficient engine designs that could result in excess PM emissions.

At the time of filing, Chapter 2 has been published in the Journal of Aerosol Science (JAS), Chapter 3 has been submitted to JAS, and Chapter 4 is in preparation for submission to Environmental Science & Technology.

The dissertation of David Christopher Quiros is approved.

Ann Carlson

Harry Dwyer

Tao Huai

Suzanne Paulson

Yifang Zhu, Committee Chair

University of California, Los Angeles

2014

TABLE OF CONTENTS

LIST OF ABBREVIATIONS

ACC	Advanced Clean Cars
APM	Aerosol Particle Mass analyzer
APS	Aerodynamic Particle Sizer
ARB	Air Resources Board
ATD	Arizona Test Dust (ISO-12103-1 A1)
bhp-hr	brake-horsepower-hr
CA	California
CAA	Clean Air Act
CFM	Cubic Feet per Minute
CFR	Code of Federal Regulations
CMD	Count Median Diameter
CPC	Condensation Particle Counter
CPMA	Centrifugal Particle Mass Analyzer
CVS	Constant Volume Sampler
D_{50}	Diameter corresponding to 50% detection efficiency
DISI	Direct Injection Spark Ignition
DMA	Differential Mobility Analyzer
DMM	Dekati Mass Monitor
DOC	Diesel Oxidation Catalyst
DOS	Dioctyl Sebacate
DPF	Diesel Particulate Filter

DPM	Diesel Particulate Matter
DTT	Dithiothreitol
EAD	Electrical Aerosol Detector
EC	Electrostatic Classifier
EEPS	Engine Exhaust Particle Sizer
EGR	Exhaust Gas Recirculation
ELPI	Electrical Low Pressure Impactor
EMFAC	on-road EMissions FACtor model (ARB)
EU	European Union
FMPS	Fast Mobility Particle Sizer
FTP	Federal Test Procedure
GDI	Gasoline Direct Injection
GPF	Gasoline Particulate Filter
GSD	Geometric Standard Deviation
GVWR	Gross Vehicle Weight Rating
HDDT	Heavy Duty Diesel Truck (GVWR > 33,000 lbs)
HDV	Heavy-Duty Vehicle
HDVIP	Heavy Duty Vehicle Inspection Program
HEPA	High Efficiency Particulate Arrestor
HSL	Haagen-Smit Laboratory (ARB)
IPSD	Integrated Particle Size Distribution
LDD	Light-Duty Diesel Vehicle equipped with a Diesel Particulate Filter
LDV	Light-Duty Vehicle

LEV	Low Emission Vehicle
M_{GRAV}	PM Mass Measured using Gravimetric Method (40 CFR 1065)
M_{IPSD}	PM Mass Measured using IPSD Method
MMD	Mass Median Diameter
MSS	Micro Soot Sensor
MY	Model Year
NAAQS	National Ambient Air Quality Standards
N_{IPSD}	Total PM Number Measured using IPSD Method
NIST	National Institute of Standards and Technology
NOx	Nitrogen Oxides, NO + NO_2
NTDE	New Technology Diesel Exhaust
OBD	On-Board Diagnostics
PEMS	Portable Emissions Measurement Systems
PFI	Port Fuel Injection
PM	Particulate Matter
$PM_{1.0}$	PM mass (submicron) with aerodynamic diameter < 1 µm
$PM_{2.5}$	PM mass (fine) with aerodynamic diameter < 2.5 µm
PM_4	PM mass with aerodynamic diameter < 4 µm
PM_{10}	PM mass (coarse) with aerodynamic diameter < 10 µm
PM_{Total}	See TSP
PMP	Particle Measurement Programme
PNC	Particle Number Concentration
PSD	Particle Size Distribution

PSIP	Periodic Smoke Inspection Program
PSL	Polystyrene Latex
RH	Relative Humidity
RMS	Root Mean Square
ROS	Reactive Oxygen Species
SAE	SAE International
SA_{IPSD}	Surface area measured by IPSD method ($d^{1.4}$)
SCAB	South Coast Air Basin
SCFM	Standard Cubic Feet per Minute
SCR	Selective Catalytic Reduction
SFTP	Supplemental FTP (same as US06)
SJVAB	San Joaquin Valley Air Basin
SMPS	Scanning Mobility Particle Sizer
SOP	Standard Operation Procedure
SPLAT	Single Particle Laser Ablation Time-of-Flight Mass Spectrometer
SPN	Solid Particle Number
SS	Steady State
ST	Simulated Transient
SwRI	Southwest Research Institute
TAC	Toxic Air Contaminant
TC	Turbocharger
TDE	Traditional Diesel Exhaust
TDI	Turbo Direct Injection

THC	Total Hydrocarbon
TSP	Total Suspended Particulate (no upper size cutoff)
TWC	Three Way Catalyst
U.S. EPA	United States Environmental Protection Agency
UFP	Ultrafine Particle
US06	Supplemental FTP Cycle
WHO	World Health Organization

LIST OF TABLES

LIST OF FIGURES

COPYRIGHT

DISCLAIMER

Whereas this dissertation was written in conjunction with my employment with ARB, the findings and conclusions do not represent the official position of ARB. The mention of trade names, products, and organizations does not constitute endorsement or recommendation for use. ARB is a department of the California Environmental Protection Agency. ARB's mission is to promote and protect public health, welfare, and ecological resources through effective reduction of air pollutants while recognizing and considering effects on the economy. ARB oversees all air pollution control efforts in California to attain and maintain health-based air quality standards.

ACKNOWLEDGEMENTS

This dissertation was made possible by means of skills developed over the past twenty-two years of education, and the support of many individuals that need to be acknowledged. First, I acknowledge my advisor Dr. Yifang Zhu of the School of Public Health at UCLA, whose modern scientific training and optimism enabled me to begin developing into a scholar and critical thinker.

I express additional gratitude to the other members of my doctoral committee, Prof. Ann Carlson, Dr. Harry Dwyer, Dr. Tao Huai, and Dr. Suzanne Paulson, as well as other faculty of the Environmental Science and Engineering Program, Dr. Irwin "Mel" Suffet and Dr. Arthur Winer. I also need to acknowledge several other important individuals.

Dr. Shaohua Hu and Dr. Tao Huai for providing me the daily guidance, training, and critique that have helped me develop into a professional scientist and policymaker.

Dr. Alberto Ayala, Dr. Michael Benjamin, and Dr. Todd Sax, whose mentorship in air quality science and policy have enabled me to jumpstart my career within the ARB.

Mark Burnitzki, Don Chernich, Bruce Frodin, Dr. Satya Sardar, and others at ARB whose generous and kind laboratory support, practical knowledge, and lunchtime barbeques have made emissions testing possible.

Dr. Alex Revchuk, a dear friend and teammate, whose scientific prowess and mentorship were highly influential in my pursuit of a doctoral education.

Dr. Nina Brandt, for all of your kind and loving support.

My parents, Pamela and Victor Quiros, whose support and patience from day one made all of the above a reality, for which I am forever grateful.

VITA

2005	Diploma Mater Dei High School Santa Ana, CA
2007 – 2009	Undergraduate Research Assistant University of California, Los Angeles
2009	B.S., Environmental Science Institute of the Environment University of California, Los Angeles
2010	Legislative Intern Climate Action Reserve Los Angeles, CA
2009 – 2012	Graduate Student Researcher Department of Environmental Health Sciences School of Public Health University of California, Los Angeles
2010	M.S., Civil & Environmental Engineering Henry Samueli School of Engineering and Applied Science University of California, Los Angeles
2012 –	Air Resources Engineer Monitoring & Laboratory Division California Air Resources Board Sacramento, CA

PUBLICATIONS

1. **Quiros, D.C.**, Zhang, Q., Choi, W., He, M., Paulson, S.E., Winer, A.M., Wang, R., Zhu, Y. "Air Quality Impacts of a scheduled 36-h closure of a major highway". Atmospheric Environment 67: 404-414, 2013.

2. **Quiros, D.C.**, Lee, E.S., Wang, R., Zhu, Y. "Ultrafine particle exposures while walking, cycling, and driving along an urban residential roadway". Atmospheric Environment 73: 185-193, 2013.

3. Hu, S., Zhang, S., Sardar, S., Chen, S., Dzhema, I., Huang, S-M., **Quiros, D.C.**, Sun, H., Laroo, C., Sanches, L.J., Watson, J., Chang, O.M-C., Huai, T., Ayala, A., "Evaluation of Gravimetric Method to Measure Light-Duty Vehicle Particulate Matter Emissions at Levels below One Milligram per Mile (1 mg/mile)." SAE 2014-01-1571.

4. Li, Y., Xue, J., Johnson, K., Durbin, T., Villela, M., Pham, L., Hosseini, S., Zheng, Z., Short, D., Karavalais, G., Asa-Awuku, A., Jung, H., Wang, X., **Quiros, D.C.**, Hu, S., Huai, T., Ayala, A. "Determination of Suspended Exhaust PM Mass for Light-Duty Vehicles". SAE 2014-01-1594.

5. **Quiros, D.C.**, Yoon, S., Dwyer, H.A., Collins, J.F., Zhu, Y., Huai, T. "Measuring particulate matter emissions during parked active diesel particulate filter regeneration of heavy-duty diesel trucks". Journal of Aerosol Science 73: 48-62, 2014.

6. Dwyer, H.A., Yoon, S., **Quiros, D.C.**, Burnitzki, M., Riemersma, R., Chernich, D., Collins, J.F., Herner, J. "Ambient Emission Measurements from Parked Regenerations of 2007 and 2010 Diesel Particulate Filters". SAE 2014-01-2353.

7. Shu, S., **Quiros, D.C.**, Wang, R., Zhu, Y. "Changes of street use and on-road air quality before and after complete street retrofit: An exploratory case study in Santa Monica, California". Transportation Research Part D: Transport and the Environment 32: 387-396, 2014.

8. **Quiros, D.C.**, Hu, S., Hu, S. Lee, E.S., Sardar, S., Wang, X., Olfert, J.S., Jung, H.S., Zhu, Y., Huai, T. "Particle effective density and mass during steady-state operation of GDI, PFI, and diesel passenger cars." Submitted to Journal of Aerosol Science, August 2014.

9. Xue, J., Li, Y., Wang, X., Durbin, T.D., Johnson, K.C., Karavalakis, G., Awuku-Awa, A., Villela, M., **Quiros, D.C**., Hu, S., Huai, T., Ayala, A., Jung, H.S. "Comparison of vehicle exhaust particle size distributions measured by SMPS and EEPS during steady-state conditions." Submitted to Aerosol Science & Technology, September 2014.

10. **Quiros, D.C.**, Zhang, S., Sardar, S., Kamboures, M.A., Eiges, D., Zhang, M., Jung, H.S., Chang, O.M-C., Ayala, A., Zhu, Y., Huai, T., Hu, Shaohua. "Demonstration of particulate matter (PM) measurement below 1 mg/mi using Integrated Particle Size Distribution (IPSD)". In preparation for submission to Environmental Science & Technology.

11. Bahreini, R., Xue, J., Li, Y., Jonson, K.C., Durbin, T.D., **Quiros, D.C.**, Hu, S., Huai, T., Ayala, A., Jung, H. "Characterizing Particulate Matter Emissions from Light-duty Gasoline Vehicles" In preparation for submission to Environmental Science & Technology.

12. Yoon, S., **Quiros, D.C.**, Dwyer, H.A., Collins, J.F., Burnitski, M., Chernich, D., Herner, J.D. "Characteristics of Particle Number and Mass Emissions during Heavy-Duty Diesel Truck Parked Active DPF Regeneration in an Ambient Air Dilution Tunnel". Submitted to Environmental Science & Technology.

PRESENTATIONS

1. *Integrated Particle Size Distribution (IPSD) for Particulate Matter (PM) Measurement.* **David Quiros**. Staff presentation to the Manufacturers of Emissions Controls Association (MECA) on November 19, 2014. Sacramento, CA (2014).

2. *Determination of Suspended Exhaust PM Mass for Light Duty Vehicles Using IPSD.* Heejung S. Jung, Yang Li, Jian Xue, Kent Johnson, Thomas D. Durbin, Mark Villela, Liem Pham, Seyedehsan Hosseini, Zhongqing Zheng, Daniel Short, Georgios Karavalakis, Akua Asa-Awuku, Xiaoliang Wang, **David Quiros**, Shaohua Hu, Tao Huai, Alberto Ayala. 33rd Annual Conference of the American Association for Aerosol Research. October 20 to 24, 2014, Orlando, FL.

3. *The Air Resources Board's Mobile Source Measurement Capabilities*. **David Quiros**, Tao Huai, Michael Benjamin. Staff presentation to the California Air Resources Board. Board Item 14-5-2. Sacramento, CA (2014).

4. *Determination of Suspended PM Mass for Light Duty Vehicles Using IPSD*. Yang Li, Jian Xue, Kent Johnson, Thomas Durbin, Mark Villela, Liem Pham, Seyedehsan Hosseini, Zhongqing Zheng, Daniel Short, George Karavalakis, Akua Asa-Awuku, and Heejung Jung, **David Quiros,** Shaohua Hu, Tao Huai, Alberto Ayala. Air & Waste Management Association Annual Conference. Long Beach, CA (2014).

5. *High-speed Portable FTIR Measurements of Ammonia and Nitrous Oxides From Heavy Duty CNG Transit Buses.* Xu Wang, Saroj Pradhan, Arvind Thiruvengadam, Marc Besch, **David Quiros**, Tao Huai. Portable Emissions Measurement System (PEMS) International Conference & Workshop, University of California, Riverside (2014).

6. *Evaluation of the Gravimetric Method to Measure Light-Duty Vehicle Particulate Matter Emissions at Levels Below One mg/mile*. Suiyun Zhang, M.C. Oliver Change, Tao Huai, Michael Kamboures, Shaohua Hu, Satya Sardar, Shiyan Chen, Inna Dzhema, Shiou-Mei Huang, **David Quiros**, Huawei Sun, Jim Watson, Alberto Ayala. 24th Coordinating Research Council (CRC) Real World Emissions Workshop. San Diego, CA (2014).

7. *Determination of Suspended Exhaust PM Mass for Light Duty Vehicles.*Yang Li, Jian Xue, Kent Johnson, Thomas Durbin, Mark Villela, Liem Pham, Seyedehsan Hosseini, Zhongqing Zheng, Daniel Short, George Karavalakis, Akua Asa-Awuku, Xiaoliang Wang, **David Quiros**, Shaohua Hu, Tao Huai, Alberto Ayala, Heejung Jung. Poster presentation at the 24th Coordinating Research Council (CRC) Real World Emissions Workshop, San Diego, CA (2014).

8. *Determination of Suspended Exhaust PM Mass for Light Duty Vehicles*. Yang Li, Jian Xue, Kent Johnson, Thomas Durbin, Mark Villela, Liem Pham, Seyedehsan Hosseini, Zhongqing Zheng, Daniel Short, George Karavalakis, Akua Asa-Awuku, Xiaoliang Wang, **David Quiros**, Shaohua Hu, Tao Huai, Alberto Ayala, Heejung Jung. Poster presentation at the

Portable Emissions Measurement System (PEMS) International Conference & Workshop. College of Engineering, University of California, Riverside (2014).

9. *Measuring Particulate Matter Emissions During Parked Active Diesel Particulate Filter Regeneration of Heavy-Duty Trucks.* **David Quiros**, Seungju Yoon, Mark Burnitzki, Harry Dwyer. Air Quality Measurement, Methods and Technology. Air & Waste Management Association, Sacramento, CA (2013).

10. *Air Quality Impacts of a Scheduled 36-hour Closure of a Major Highway.* **David Quiros**, Qunfang Zhang, Suzanne Paulson, Rui Wang, Wonsik Choi, Arthur Winer, Yifang Zhu 31st Annual Conference of the American Association for Aerosol Research, Minneapolis, MN (2012).

11. *Ultrafine Particle Exposure of Street Users Walking, Cycling, and Driving Along an Urban Residential Roadway*. **David Quiros**, Eon Lee, Yifang Zhu, Rui Wang. 31st Annual Conference of the American Association for Aerosol Research. Minneapolis, MN (2012).

12. *Evaluating Which TOC Size Fractions Produce the Most THMFP from Different Drinking Water Resources*. **David Quiros**, Judy Billica, Irwin (Mel) Suffet. 82nd Annual Conference of the California Water Environment Association. Sacramento, CA (2010).

1 BACKGROUND AND MOTIVATION

1.1 Motivation For Regulating Mobile Sources

The Clean Air Act of 1970 (CAA) established the National Ambient Air Quality Standards (NAAQS), which set health-based air quality standards to protect public health and welfare. The NAAQS regulate six pollutants, including particulate matter (PM). The first PM standard was 75 $\mu g/m^3$ for total suspended particulate (TSP), averaged annually. The first standard for size-classified PM was established in 1987 for coarse particles (PM_{10}) at 50 $\mu g/m^3$ averaged annually, along with more lenient standards for shorter 24-hr periods. The first standard for fine particles ($PM_{2.5}$) was established in 1997, which limited annual average ambient concentrations to 15 $\mu g/m^3$, and recently an even more stringent standard limiting ambient concentrations to 12 $\mu g/m^3$ was promulgated in 2012. The successive reductions in the ambient fine particle standard have resulted from the growing body of evidence indicating that the concentration-response function is linear, and that additional public health benefits can be expected to be associated with additional reductions to ambient fine particle concentrations (Pope and Dockery 2006). This key review article also discusses the relative effects on morbidity and mortality associated with fine particle pollution. Based on extended reanalysis of two major cohort studies (the Harvard Six Cities and American Cancer Society studies), a 10-$\mu g/m^3$ increase in $PM_{2.5}$ is correlated with daily relative risk increases 6-16% for all-cause mortality, 9-28% for cardiopulmonary mortality, and 13-27% for developing lung cancer. Although epidemiological data suggest the only safe standard would be zero, the process for policymakers needs to ensure the defined standard is realistic and achievable. The United States Environmental Protection Agency (U.S. EPA) has been challenged repeatedly by interest groups for failing to set sufficiently stringent standards, which most recently is still more lenient than the World Health Organization (WHO) guidelines

of 10 $\mu g/m^3$ (WHO 2005). Nevertheless, the legal obligation to attain federal NAAQS has been the predominant driver and legal basis for the California Air Resources Board (ARB) adopting regulations to control emissions from mobile and stationary sources.

Within California, the South Coast Air Basin (SCAB), and San Joaquin Valley Air Basin (SJVAB) are the two regions that repeatedly fail to attain the national standards. The designation values for these two basins in 2012 still exceeded the NAAQS; the regions are non-attainment areas for two pollutants, ozone (O_3) and $PM_{2.5}$. The ARB emissions inventory calculations for criteria pollutants in calendar year 2012 indicated that mobile sources contributed 20% of statewide $PM_{2.5}$, which was slightly lower (17%) for the SJVAB and slightly greater (24%) for the SCAB. Prior to the implementation of numerous regulatory programs for mobile sources over the past decades, the contributions from these sectors were much larger. Nevertheless, mobile source emissions reduction programs continue to evolve, especially on-road mobile sources, which contributed an estimated 65 and 52% of total mobile source emissions in 2012 for the SCAB and SJVAB respectively (according to the ARB Emissions Factor (EMFAC) 2011 model).

Furthermore, significant health effects have been associated with exposure to PM from mobile sources. In 1998, California classified Diesel Particulate Matter (DPM) as a Toxic Air Contaminant (TAC) (CARB 1998). This designation has been a critical underpinning for multiple mobile source regulations over the past decade. Exposure to gasoline PM emissions has also been linked to adverse health outcomes by epidemiological studies (Laden et al. 2006; Beelen et al. 2007). One of the ongoing challenges for defining health outcomes is the evolution of chemical and physical properties of PM a result of new fuel regulations and engine technologies (Mulawa et al. 1997; Herner et al. 2009; Dallmann and Harley 2010; Herner et al.

2011). For example, the most recent standard for on-road heavy-duty engines (0.01 g PM/bhp-hr) resulted in the ubiquitous adoption of the Diesel Particulate Filter (DPF) to reduce the quantity of emissions. In addition to reducing emissions, the chemical composition of exhaust has changed drastically due to reductions in fuel sulfur content (U.S. EPA 2001; Ristovski et al. 2006) and catalytic treatment (Khalek 2005; Biswas et al. 2009; CRC 2009; CRC 2013). As described by a recent review article, "Traditional Diesel Exhaust," or TDE, was characterized by a high fraction of elemental carbon and a fractal-like particle morphology, whereas "New Technology Diesel Exhaust," or NTDE is dominated by organic carbon and sulfate fractions and particulates have more spherical morphology (Hesterberg et al. 2011). Accordingly, defining the health impacts associated with human exposure to mobile source PM emissions using incidental dose-response models is perhaps a fundamentally limited and flawed methodology. Instead, adopting a standardized series of toxicological assays (e.g. Kado et al. 2005), may provide more relevant information to assess the health benefits and impacts associated with a specific engine or control technology. Currently, strategies for reducing health effects associated with PM are purely quantitative. Regardless of chemical composition, total PM mass reductions are sought, which can be directed at reducing either primary PM emissions directly from the tailpipe of mobile sources, or at reducing the emission of precursor gases that can subsequently react to form PM in the atmosphere.

California is required under the CAA to submit periodic plans to demonstrate how air basins will attain or maintain the NAAQS, including the standards for PM. The State also has special authority under the CAA to regulate emissions from mobile sources, an authority that no other state possesses. For some classes of vehicles, ARB and U.S. EPA are aligned for their emissions standards, such as in the case of heavy-duty trucks. For light-duty vehicles (LDV), such as

passenger cars, the emissions standards are often similar, but differ based on the direction and regulatory needs of each jurisdiction. Although California has special authority to regulate emissions sources, ARB and U.S. EPA often work closely to develop harmonized standards to aid manufacturers certifying to both California and federal markets. Nevertheless, the most recent PM standards for LDVs, the Low Emission Vehicle (LEV) III and Tier 3 standards adopted by ARB and U.S. EPA respectively, have notable differences in the later stages of the implementation schedules.

1.2 Controlling Mobile Source PM Emissions

Regulation of mobile sources is one key strategy used by California and the United States to comply with provisions of the CAA. In the 1950s, Arie Haagen-Smit and other Southern California scientists determined that motor vehicles were one of the main sources of pollutants resulting in the photochemical smog and PM pollution blanketing the region. To address this problem, in 1959, the Legislature created the California Motor Vehicle Pollution Control Board, the predecessor to the ARB, and gave it the authority to test vehicle emissions and certify emission control devices. This was the beginning of ARB's mobile source emission measurement program which in its early years focused on controlling passenger car emissions on a car-by-car basis. California's ability to regulate mobile sources exists because the ARB already had established regulatory programs prior to the adoption of the CAA amendments in 1970. Since then, California has regulated its mobile sources to levels equal or more stringent than the federal government. In the 1990s, California shifted to regulate based on fleet averages, which allows some vehicles to have emissions greater than the standard, permitting that the sales-based fleet average remains below criteria pollutant standards.

1.2.1 Low Emission Vehicle (LEV) III Standards

In 1990, the low emission vehicle (LEV) program was created, which required compliance to more stringent emissions standards for vehicles beginning with MY 1994, allowed manufacturers to meet the standards based on fleet averages rather than for every individual vehicle produced by the manufacturer on a car-by-car basis. A decade later, a newly devised LEV II program was implemented beginning with MY 2004 vehicles. The success of the LEV programs were apparent, but the need for additional emissions control was identified, and in 2012, the ARB adopted the LEV III regulations as part of the Advanced Clean Cars (ACC) regulation, which will include the adoption of a PM emissions standard ten times more stringent than the LEV II standard. The existing 10 mg/mi standard will be lowered to 3 mg/mi beginning with MY 2017, and lowered again to 1 mg/mi beginning with MY 2025 over the Federal Test Procedure (FTP-75) (CARB 2011b). This is one distinct difference between U.S. EPA's Tier 3 program for LDVs, which does not currently have provisions to adopt any PM standard below 3 mg/mi over the FTP. The critical challenge for implementing the 1 mg/mi standard for the FTP in California is the emissions and measurement variability observed within the very low PM emissions rates. Although many conventional gasoline vehicles certified to the LEV II standards already meet the LEV III 1 mg/mi standard, the current regulatory measurement method has not been fully evaluated for its measurement capabilities at the very low PM emissions. That is, the ability of the existing measurement approach to differentiate between a compliant vehicle emitting less than 1 mg/mi and a non-compliant vehicle emitting slightly more than 1 mg/mi (e.g. 1.5 mg/mi) was unclear when the standards were adopted. The focus of my research for

LDVs is to better understand and quantify the emissions variability to implement the 1 mg/mi standard over the FTP.

Currently, emissions standards are expressed as a mass per distance measured over a predefined chassis dynamometer test schedule. PM is measured using a gravimetric filter-based method defined by the Code of Federal Regulations (CFR) Parts 1065 and 1066 (CFR 2011). PM is defined for the purpose of emissions measurement during dynamometer testing as the mass that collects onto a filter, under a defined set of dilution, temperature, and filter-face velocity conditions. Additional guidelines are provided for the design of the sampling system, the requirements for each stage of dilution, sampling pressure, and weigh-room conditions for analyzing filter media following a certification test.

Figure 1.1 shows the speed-time trace for the two certification cycles that are used during certification of LDVs, which includes the FTP-75 and the Supplemental Federal Test Procedure (SFTP or US06). The FTP cycle includes the following three phases: Cold Start, Transient, and after a 10-min hot soak period, Hot Start. Since the release of CFR 1066 guidelines for vehicle testing procedures, there are multiple approaches for varying the number of filters and phases to measure the equivalent FTP emissions. In essence, a combination of one, two or three filters can be used, and the relative weighting of the phases is 0.43, 1.00, and 0.57 for Cold Start, Transient, and Hot Start phases, respectively. The FTP test is 11.1 miles and has an average speed of 21.2 mi/hr. Figure 1.1(b) shows the US06 test schedule, which is a more aggressive test cycle to address shortcomings of the FTP cycle where a vehicle may meet the FTP standard but generate excessive emissions when driving under more aggressive off-cycle conditions. The total length of the US06 schedule is 8.01 mi, the average speed is 48.4 mi/hr, and the maximum speed is 80.3 mi/hr. The emissions standard for the US06 cycle for the LEV III program is currently defined

at 10 mg/mi, however ongoing negotiations with U.S. EPA may result in further modifications before the standards are implemented.

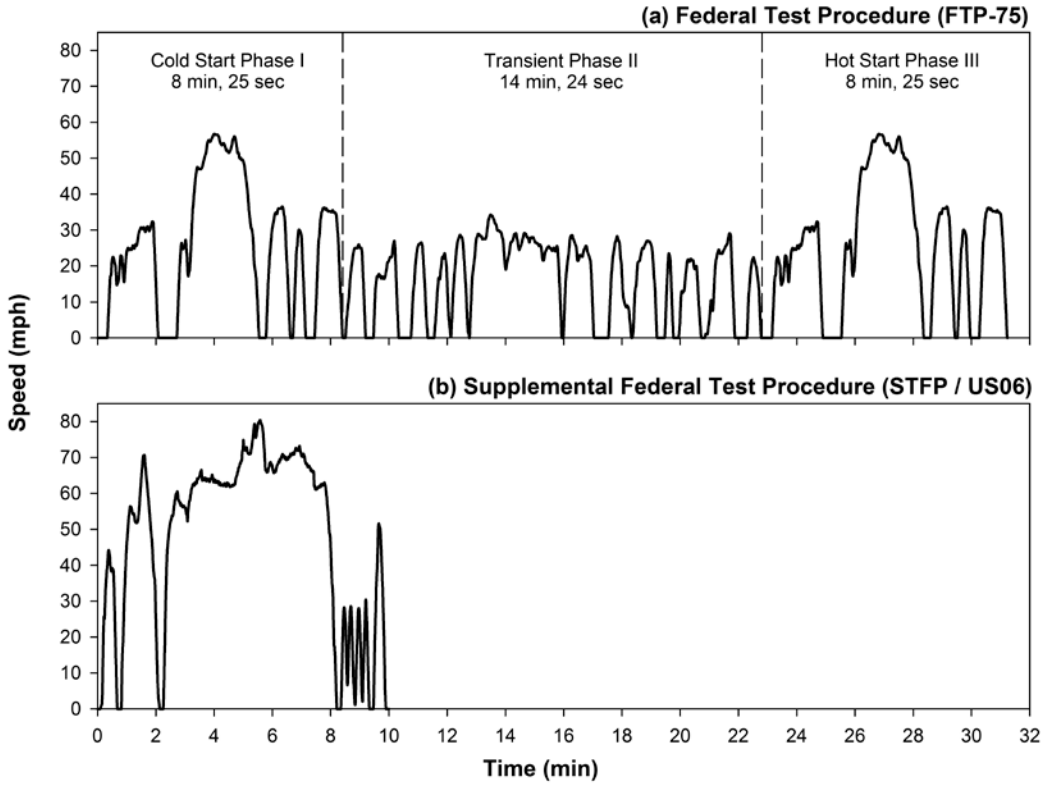

Figure 1.1. FTP and US06 test cycles used for certifying new LDVs.

1.2.2 Heavy-Duty Vehicles

Beginning in the 1980s, heavy-duty vehicles (HDV) began to be tested routinely using engine and chassis dynamometers. Federally, HDVs are defined by a gross vehicle weight rating (GVWR) greater than 8,500 pounds, but in California, they are defined by a GVWR greater than 14,000 pounds. California designates vehicles with a GVWR between 8,500 and 14,000 pounds as medium-duty vehicles, which are currently regulated alongside LDVs as part of the LEV III vehicle standards on a per-mile basis. The first PM emissions standard for HDVs was implemented for MY 1987 engines, which limited PM emissions to not exceed 0.6 g/bhp-hr over

the heavy-duty Federal Test Procedure (FTP). In contrast to the FTP-75 used for certifying LDVs on the chassis dynamometer, the heavy-duty FTP is conducted on an engine dynamometer, where engine speed (revolutions per minute) and torque (force-distance) are governed mechanistically rather than by a human driver that is commonly used for chassis certification. Similar to LDV certification, emissions are diluted using a constant volume sampler (CVS), and the same filter-based gravimetric method following specifications in 40 CFR 1065 are followed.

The latest emissions standards were adopted starting with MY 2007 engines, which limits PM emissions to 0.01 g PM/bhp-hr (CARB 2007). The adoption of the DPF as a control technology has resulted in dramatic emissions reductions of PM from diesel engines. Older engines retrofit with DPFs are over 98% effective in removing engine-out PM, and newer engines certified with DPFs over comply with the standard by more than 90%, based on evaluations conducted by ARB and the Southwest Research Institute (SwRI) (Khalek 2005; CRC 2009; Herner et al. 2009). The emissions reductions have also been observed during on-roadway measurement campaigns, such as by the ARB Mobile Measurement Platform that documented a 70% reduction in Black Carbon (BC), a surrogate for diesel PM, following the adoption of a regulation targeting Drayage Trucks frequenting the I-710 freeway in Los Angeles (Kozawa et al. 2014). Beginning with MY 2010 engines, even lower PM emissions were observed due to the adoption of Selective Catalytic Reduction (SCR) for NOx control, enabling leaner engine operation that lowers engine-out and tailpipe PM (CRC 2013). In addition, pollutant toxicity markers have declined as confirmed by multiple studies conducted by the ARB and other research groups based on human clinical studies (Lucking et al. 2011), animal models (McDonald et al. 2004; Tzamkiozis et al. 2010; HEI 2012), and *in vitro* cellular assays (Biswas

et al. 2009; Verma et al. 2010; Herner et al. 2011). Many of these studies discuss the removal of water-soluble organic compounds in the PM and gaseous phase by catalytic materials, resulting in the reduced cellular expression and biomarkers of toxicity.

Although California has the authority to issue regulations of HDVs that are at least as stringent as the federal standards, the state has been reluctant to issue separate standards because of the difficulty in enforcement given that trucks travel throughout the country and a large fraction of the vehicles operating within California are registered in other states. Nevertheless, the state has imposed some additional regulations to control emissions from HDVs in California, such as the 2008 Truck and Bus Regulation (On-Road Heavy-Duty Diesel Vehicles In-Use Regulation), which require the retrofit and eventually replacement of older equipment with newer and cleaner engines. Because the heavy-duty sector operates on a higher per-vehicle mileage basis, and the actual usable life of a truck is estimated at a median of 800,000 miles, the prevalence of older vehicle engines operating on the highways is greater than for the light-duty sector. The adoption of this rule was instrumental to achieve the emissions benefits associated with the 0.01 g/bhp-hr PM standard for heavy-duty engines, and was largely driven by the designation of DPM as a TAC in 1998 through the guidelines set forth in the Diesel Risk Reduction Plan (Lloyd and Cackette 2001). In contrast to the harmonization with federal programs on emissions standards for HDVs, the Truck and Bus Regulation requires trucks to meet regulation requirements within its jurisdiction regardless of the registered origin of the truck.

1.3 Scope of Work

One caveat to the emissions benefits of DPFs is that they periodically must be regenerated in order to maintain low engine backpressure by removing accumulated soot from the inner surfaces of the device. The certification process accounts for PM emissions during DPF regeneration by measuring the frequency of regeneration and the magnitude of PM emissions during the regeneration period. Nevertheless, the magnitude and exact frequency of regeneration will depend on multiple factors including thermal management strategies, catalytic substrate distribution, flow-through design, and other physical parameters such as DPF substrate pore size. Regeneration can be triggered passively while driving on the road as a result of exhaust temperature, or actively by applying heat through fuel injection into the DPF. Although the frequency and mass emissions are factored into the certification standards by the manufacturers, the quantity and physical characteristics of PM emissions emitted during a single regeneration have not been verified by regulatory agencies, and may present local source exposure concerns. Furthermore, the extent that real-world driving loads PM into the DPF and affects frequency or emissions of PM during regeneration has not been specifically evaluated. Control of total PM emissions from a fleet that is becoming increasingly equipped with DPF aftertreatment should focus on discrete high-emission events, such as DPF regeneration. Consequently, the research for heavy-duty vehicles will focus on the PM emissions during regeneration events from HDDTs.

Chapter 2 of this dissertation will investigate this critical knowledge gap by measuring PM mass and number emissions during parked active regeneration for a MY 2007 and a MY 2010 heavy-duty diesel truck. DPF regeneration is a discrete event that results in the emission of a disproportionate quantity of PM emissions. A better understanding of the emissions during DPF

regeneration will enable better quantification of the magnitude of these emissions, and will enable for more informed policy to be implemented to reduce emissions during these events, from both properly functioning and malfunctioning trucks that may need to regenerate more frequently. Although current PM emissions standards are defined on a mass basis, there is a growing body of evidence suggesting that other metrics, such as particle number, which provides a good indicator of ultrafine particle (UFP, <100 nm) concentration, are also linked to adverse health outcomes (HEI 2013). Heavy-duty engines equipped with DPFs have previously reported higher particle number emissions during regular operation (Vaaraslahti et al. 2004; Kittelson et al. 2006; Biswas et al. 2008; Swanson et al. 2009; Barone et al. 2010), but not during a discrete active DPF regeneration event with no useful work produced by the engine. Therefore, PM mass and number emissions will both be measured during parked active DPF regeneration. This work utilizes a novel ambient-dilution wind tunnel that uses ambient rather than filtered dilution air to mimic dilution under real-world scenarios.

Current ARB control strategies for reducing emissions from LDVs is through reducing the certification standard (from 10 mg/mi to 1 mg/mi over the FTP) to prevent anticipated emissions backsliding that is associated with the gasoline direct injection (GDI) engine technology as it replaces port fuel injection (PFI) conventional gasoline vehicles. The challenges associated with implementing this standard can be categorized as either (1) technology limitations to meet both PM and other standards such as greenhouse gas emissions reductions, or (2) measurement limitations using the existing gravimetric method at levels below 1 mg/mi over the FTP. The automotive industry has discussed the challenges of measuring at these levels (Maricq et al. 2011). ARB has already demonstrating the ability to measure PM emissions accurately below 1 mg/mi using data generated at multiple internal laboratories as well as at

external laboratories at the U.S. EPA (Hu et al. 2014). Nevertheless, additional demonstration is needed to ensure the LEV III regulations, specifically MY 2025 standard of 1 mg/mi, can be implemented without incident.

Prior to the ARB adopting the LEV III PM standards, several proposals considered including the European Union (EU) Particle Measurement Programme (PMP) solid particle number (SPN, >23 nm) standard as part of the regulatory package (CARB 2011b). ARB participated in a round-robin evaluation of a vehicle and measurement methodology, which determined the PMP methodology offered improved sensitivity and a very low detection limit relative to the gravimetric method (Ayala et al. 2008). However, prevailing issues were the lack of correlation and traceability to mass emissions, which are linked to the associations with adverse health impacts that are key drivers of mobile source regulation to reduce ambient PM concentrations.

Chapters 3 and 4 in this dissertation both support continued use of the gravimetric method by evaluating an alternative method that estimates PM mass by measuring particle size distribution (PSD) and applying an effective density function. The concept of estimating mass from particle size distribution was first discussed about a decade ago (Maricq and Xu 2004), and was more recently named as the Integrated Particle Size Distribution (IPSD) method for measuring real-time PM mass (Liu et al. 2009). The effective density functions for LDVs have largely explored light-duty diesel vehicles without DPFs, or early versions of GDI technology with a high degree of charge stratification and PM emissions compared to vehicles compliant with the LEV III PM standards (Maricq and Xu 2004; Olfert et al. 2007). The effective density functions were measured for five different LDVs with modern engine technologies, including for the first time a PFI conventional gasoline vehicle and DPF-equipped light-duty diesel vehicle.

The effective density measurement method selected for this study included a Differential Mobility Analyzer (DMA) in tandem with a Centrifugal Particle Mass Analyzer (CPMA), which offers better sensitivity at low PM emissions levels, but requires steady-state conditions. Then in Chapter 4, these effective density functions were applied to PSD measured by a fast-sizing spectrometer, the TSI Engine Exhaust Particle Sizer (EEPS) over a comprehensive dataset collected during FTP and US06 cycles. The results from these investigations help better understand the characteristics of PM emissions from light-duty vehicles, and the potential of new measurement approaches to control the health effects of PM emissions.

2 MEASURING PARTICULATE MATTER EMISSIONS DURING PARKED ACTIVE DIESEL PARTICULATE FILTER REGENERATION OF HEAVY-DUTY DIESEL TRUCKS

Published in Journal of Aerosol Science (2014, Volume 73, pp. 48-62)

DOI: 0.1016/j.jaerosci.2014.03.002

2.1 Abstract

Heavy-duty diesel trucks (HDDTs, >33,000 GVWR) are commonly equipped with diesel particulate filters (DPFs) to meet the California model year (MY) 2007 PM emissions standard. Particulate matter (PM) emissions were measured from nine parked active DPF regenerations of two HDDTs, a 2007 and 2010 MY, using a novel ambient-dilution wind tunnel. This work specifically evaluated PM mass emissions during regeneration by measurements from the following instruments: TSI DustTrak DRX 8533, TSI Engine Exhaust Particle Sizer 3090 (EEPS) and TSI Scanning Mobility Particle Sizer 3936L88 (SMPS), filters by gravimetric analysis, and for one test a Dekati Mass Monitor 230-A (DMM). Active regeneration by fuel injection upstream of the DPF began with the Soot Combustion Regime, where PM emissions had a count median diameter (CMD) of greater than 30 nm and some faint gray smoke was observed flowing from the tunnel. During brief moments of the Soot Combustion Regime, the DustTrak DRX reported more than half of the mass was >1 µm. As active regeneration continued, aftertreatment inlet temperature increased to >500 °C, beginning the Fuel Combustion Regime, defined conversely where the CMD of the emissions was <30 nm. Under both regimes, discrepancies were observed between EEPS and SMPS size distributions and improved agreement was attained after performing a post-hoc EEPS correction procedure. The accuracy of the DMM was equivocal; the average DMM emissions rate was within five percent of the

gravimetric filter, but the mass distribution was substantially shifted relative to SMPS and EEPS distributions. Uninterrupted parked active regeneration resulted in 13 g PM emissions from the 2007 MY and 1.8 g PM from the 2010 MY based on filter measurements. The PM mass emissions rates, based on measurements from real-time instruments, show that the contribution of Soot Combustion Regime to total regeneration emissions decreased from 75% to 5% between the 2007 and 2010 MY.

2.2 Introduction

Particulate matter (PM) emissions from mobile sources are a key regulatory priority for the California Air Resources Board (ARB) and the United States Environmental Protection Agency (U.S. EPA) (US) (Lloyd and Cackette 2001; EPA 2002). The PM emission standard for a 2007 model year (MY) or later heavy-duty diesel truck (HDDT, >33,000 pounds gross vehicle weight rating) is 0.01 g/bhp-hr; other regulated pollutants include carbon monoxide 15.5 g/bhp-hr, non-methane hydrocarbons 0.14 g/bhp-hr, and nitrogen oxides 0.20 g/bhp-hr (nitrogen oxide standard was not required until 2010). Engine operation modifications and exhaust aftertreatment devices such as the diesel particulate filter (DPF) and selective catalytic reduction (SCR) are key approaches to meet these stringent standards.

Periodically, DPFs must be regenerated to remove accumulated particulates such as soot and organic materials. Regeneration is initiated either actively by fuel injection upstream of the DPF or passively during aggressive engine duty cycles generating high exhaust temperatures. During regeneration, large quantities of PM are emitted, mostly as semi-volatile or sulfate materials (Kittelson et al. 2006; Cauda et al. 2007; Barone et al. 2010; Herner et al. 2011; Khalek et al. 2011). However, the scientific community has not reached consensus on the most appropriate

sampling method for new-technology vehicle emissions (Khalek et al. 2011; May et al. 2013). Moreover, DPF regenerations are intermittent, can be missed during dynamometer testing, and make accounting for their emissions during certification testing more challenging.

Real-time PM instrumentation has been successfully applied to vehicle emission studies measuring passive DPF regeneration. For example, Khan *et al.* (2012) compared various portable emissions measurement systems (PEMS) and showed strong correlation (R^2=0.78) between the Dekati Mass Monitor (DMM, 0 - 1.3 μm) and gravimetric measurements from a calibrated 1065-compliant mobile emissions laboratory. Another successful study, Liu et al. (2009), measured particle size distribution (PSD) using the TSI Engine Exhaust Particle Sizer (EEPS, 5.6-560 nm) and applied an effective density function from Maricq and Xu (2004) to calculate PM mass. However to the best of our knowledge, PM emissions have not been reported during parked active DPF regeneration where no useful work is produced by the engine. Many HDDTs persistently operate at light engine loads (e.g. inner-city buses and drayage trucks), do not initiate passive DPF regeneration, and therefore a parked active regeneration is conducted to remove accumulated PM deposits. Furthermore, many in-use HDDTs used for long-haul operation also may require an occasional parked active DPF regeneration. Therefore, the PM emissions during parked active DPF regeneration are expected to be observed from a variety of HDDT applications.

This chapter presents PM emissions during parked active DPF regenerations of a 2007 and 2010 MY HDDT measured using a novel ambient-dilution wind tunnel. The broad objective of this study is to evaluate PM emissions explicitly during regeneration without any applied engine load under controlled conditions using ambient air. The present objective is to evaluate the performance of the following PM instrumentation when challenged with ambient-diluted

regeneration emissions: TSI DustTrak DRX 8533, TSI Engine Exhaust Particle Sizer (EEPS, 3090), TSI Scanning Mobility Particle Sizer (SMPS, 3936L88), and Teflon-coated borosilicate filters with gravimetric analysis. For one regeneration, a Dekati Mass Monitor 230-A was included for direct mass measurements. This work classifies parked active DPF regeneration emissions into two distinct regimes defined by count median diameter (CMD) of the distribution. The characteristics, merits, and limitations of each real-time instrument are discussed.

2.3 Materials and Methods

2.3.1 Facility

Experimental work was conducted at the ARB Depot Park Facility located approximately 10 km southeast of downtown Sacramento, CA. Within the Depot Park Facility boundaries, there are several small private roads with sparse traffic and combustion sources. The impacts of transient local source emissions on test results were assumed negligible because no sudden increases in particle number concentration were observed during ambient monitoring and the study location was located greater than 500 meters from the nearest public roadway (Zhu et al. 2002a). It was assumed that the ambient dilution air was stable over the measurement period and represents a typical urban or suburban background. Although the contribution to measurements is quantified, no background correction was applied.

2.3.2 Testing Vehicles and Setup

Two Kenworth HDDTs were tested in this study; one was outfitted with a 2007 Cummins engine with a diesel oxidation catalyst (DOC) and a DPF (2007 MY), and another a 2010

Cummins engine with a DOC, DPF, and SCR aftertreatment system (2010 MY). Commercial-grade ultralow sulfur diesel fuel (< 15 ppm sulfur) was used during the testing of these vehicles. Prior to the study, the odometers read 391,000 miles and 18,600 miles for the 2007 and 2010 HDDTs, respectively. Aftertreatment equipment was neither replaced nor ash cleaned within one year of this study.

Figure 2.1 illustrates the routing of exhaust gases into the ambient-dilution wind tunnel. A circular steel deflection plate was affixed 50 cm downstream of and perpendicular to the exhaust transfer tube to induce rapid mixing to ensure complete mixing and maximum nucleation. Temperature measurements on horizontal and vertical traverses were made at various distances from initial mixing to ensure the mixture of exhaust gases and ambient air was homogenous at the sampling location (Dwyer 2013). The ambient-dilution wind tunnel flow used during this study of 9000 ft^3/min (CFM) resulted in a residence time of 7.2 seconds. A sampling probe facing upstream at the centerline of the ambient-dilution tunnel drew 6 CFM into a sample chamber. The sampling chamber intake was superisokinetic where tunnel flow was 2.85 m/sec and chamber intake flow was 1.40 m/sec. Sampling probe intake from the chamber ranged from subisokinetic to superisokinetic where chamber flow was 22 cm/sec and upstream-facing probe intake velocities ranged 15-210 cm/sec. Although aerosol sampling occurred under a range of anisokinetic conditions, the Stokes number was less than 10^{-3} for a 10-µm particle of unit density, indicating negligible impact on the sampling of the particle sizes observed during this study (Hinds 1999). During regeneration periods, exhaust flow was 290 and 250 CFM, and dilution ratio was 31 and 36 for the 2007 and 2010 MY, respectively. The greater dilution ratio of 36 for the 2010 MY compared to the ratio of 31 for the 2007 MY may have, to some degree, impacted the PM size distribution or concentration. However, the difference in dilution ratio is

expected to have a smaller effect than the difference of emissions between the two engines. A constant tunnel flow rate of 9000 CFM was used for this study; evaluation of tunnel flow rate and therefore residence time and dilution ratio, is beyond the scope of this work.

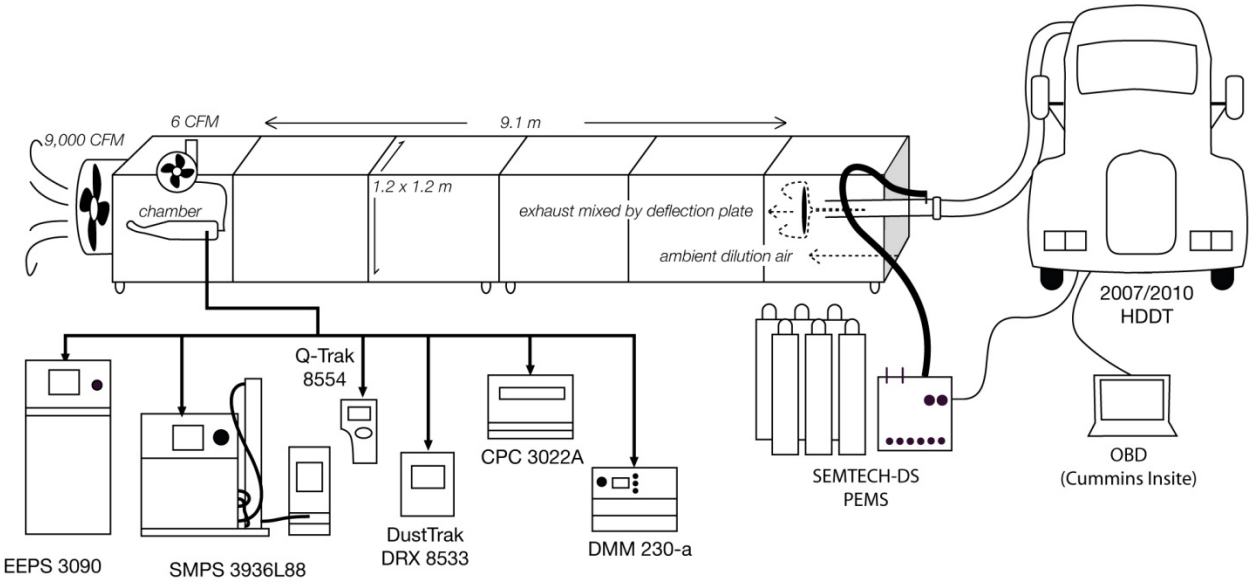

Figure 2.1. Experimental setup of the parked heavy-duty truck, ambient dilution tunnel, and instrumentation.

2.3.3 Instrumentation

The instrumentation in the study is described in detail in Table 2.1. On-board diagnostic (OBD) data were obtained from Insite Lite 7.5.0.234 (Cummins Inc., Columbus, IN, USA); this tool also enabled the "forced" parked active DPF regeneration when not otherwise permitted by the dashboard control. A PEMS, the SEMTECH-DS (Sensors, Inc., Saline, MI, USA) was used to measure CO_2 concentration and exhaust flow, which were used calculate dilution ratio based on total tunnel flow and mixed exhaust CO_2 measured from a TSI Q-Trak 8554. The Q-Trak also reported temperature and relative humidity of mixed exhaust. The real-time PM instrumentation included the TSI Engine Exhaust Particle Sizer 3090 (EEPS, TSI incorporated,

Shoreview, MN, USA), TSI Scanning Mobility Particle Sizer 3936L88 (SMPS), TSI DustTrak DRX 8533 (DustTrak), and Dekati Mass Monitor 230-a (DMM, Kangasala, Finland).

Table 2.1. Instrumentation measuring raw exhaust, diluted tunnel emissions, and engine parameters using OBD.

Device	Parameter	Detection Limits	Op. Temp	Location
SEMTECH-DS	CO_2, Exhaust Flow	0-200,000 ppm, N/A	0-45 °C	Raw Exhaust
Cummins INSITE	DPF Loading	N/A	N/A	OBD
TSI SMPS 3936L88	PSD (5.4-198 nm)	2 x 10^7 #/cm^3	10-35 °C	Chamber
TSI EEPS 3090	PSD (5.6-560 nm)	5.6 nm: 10^8 #/cm^3 560 nm: 10^6 #/cm^3	0-40 °C	Chamber
TSI CPC 3022A	PNC (7 nm-3 µm)	10^7 #/cm^3	0-35 °C	Chamber
TSI DustTrak DRX 8533	PM_1, $PM_{2.5}$, PM_{10}	>0.1 µm: 0.001-150 mg/m^3	0-50 °C	Chamber
TSI Q-Trak 8554	CO_2	0-5000 ppm	0-50 °C	Chamber
Dekati Mass Monitor 230-a	Mass 0.01-1.3 µm	1-5000 µg/m^3	5-40 °C	Chamber
Teflon-coated filters	Mass	1-µg resolution	Ambient	Chamber

2.3.4 Filter Gravimetric Analysis

Gravimetric filter media were 47-mm Pallflex Fiberfilm T60A20 (polytetrafluoroethylene-coated borosilicate glass fibers) manufactured by Pall (Port Washington, NY, USA). Sampling flow rate was 6 CFM, corresponding to an approximate filter-face velocity of 164 cm/s, and sample media was maintained at ambient-dilution exhaust temperatures ranging 18-38 °C. Comparability to 40 CFR 1065 compliant PM measurements is unclear due to larger filter-face velocities and the absence of any temperature control in this study. However, Bushkuhl et al. (2013) found gas-particle partitioning of measured PM within the limited temperature range and equilibrium was not discerned from test variability. PM collection onto filters commenced before the first ambient measurement lasting until the end of the second ambient measurement; no

independent ambient sample was collected. Sampling flows for filters and real-time instruments were drawn from the same sampling chamber manifold so that measurements were collected under identical dilution ratio and temperature conditions.

2.3.4.1 EEPS

The TSI EEPS 3090 measured a 32-channel PSD from 5.6 to 560 nm by classifying positive corona charged particles according to electrical mobility. The EEPS was developed by Johnson et al. (2004), and has been used for laboratory (e.g. Wang et al. 2006) and on-road (e.g. Kittelson et al. 2006) engine exhaust sampling studies because of its fast 10-Hz sampling resolution. However because unipolar charge accumulation may be greater for a particle of lower fractal dimension than of its mobility diameter equivalent sphere (Oh et al. 2004; Asbach et al. 2009), particle morphology can bias the size classification and reported size concentration. The accuracy of an EEPS-reported size distribution would be bolstered by quality assurance and quality control procedures. For this study, SMPS measurements were also collected (Section 2.3.3).

The detection column was cleaned following the basic procedure described in the manual twice during this study. This process involves using an acrylic cylinder and lint-free cloth to remove deposited PM from the electrode rings, followed by a zeroing of the electrical current readings. The zeroing procedure was performed a few additional times during the study; electrometer offsets were typically less than 15 fA, electrometer noise values (RMS) were less than 10 fA, and both were stable between successive zeroing procedures. The auxiliary column heater option was not used. Data collection was conducted using the TSI EEPS software release version 3.1.1.0 and the instrument was running firmware version MCU 3.04 DSP 3.01.

2.3.4.2 SMPS

The TSI SMPS 3936L88 measured a 100-channel PSD from 5.5 to 198 nm by classifying a bipolar charged distribution according to electrical mobility. Aerosol is neutralized to Boltzmann equilibrium, classified by a Differential Mobility Analyzer (DMA) with continuously varying voltage (Wang and Flagan 1990) on a two-minute time resolution. Particles are detected with a condensation particle counter (CPC) to produce a PSD using a software tool accounting for transfer functions and transport-time delays (Russell et al. 1995).

The TSI SMPS 3936L88 used for this study employed an Electrostatic Classifier (EC 3080), with a Long DMA 3081, and a Nano Water-Based Condensation Particle Counter (N-WCPC 3788). A 0.071-cm inlet impactor was used to remove particles of larger aerodynamic diameter capable of carrying multiple charges that could be mistakenly classified within the measurement range. The EC sheath flow rate was 18 L/min and N-WCPC aerosol flow rate was 0.6 L/min thereby achieving a sheath-to-aerosol flow ratio of 30 and a narrow transfer function between 5.5-198 nm. The TSI Aerosol Instrument Manager (AIM) Software Version was 9.0.0, using Diffusion Correction to correct for internal instrument losses and Multiple Charge Correction to attain an accurate size distribution within the electrical mobility range based on a typical Boltzmann charge distribution. Nanoparticle Aggregate Mobility Analysis was not used because fractal agglomerates were not expected and neither was primary particle size.

2.3.4.3 DustTrak DRX

The TSI DustTrak DRX 8533 combines photometric measurement for measuring fine particles ($PM_{2.5}$) with laser-based single particle sizing for reporting additional size fractions

(PM_1, PM_4, PM_{10}, and PM_{Total}). The total mass concentration is estimated by combining the signal from the 655-nm wavelength photometer and single particle laser pulse height signals. The result of using a dual-measurement approach is a fractionated and more sensitive PM mass measurement than previous DustTrak models, and measurement over a wider concentration range (Wang et al. 2009a). The instrument does not measure PM mass from ultrafine particles (UFPs, <100 nm) as they are undetected by the photometer. Consistent with calibration of previous DustTrak models, factory calibration is based on the density, refractive index, and shape factor of Arizona Test Dust (ATD, ISO 12103-1, A1). This work seeks to establish new relationships between the ATD calibration and ambient-diluted exhaust, similar to (1/2.4) calibration factor established by Yanosky et al. (2002) that is widely used in other vehicle emissions studies.

2.3.4.4 DMM

The DMM 230-A applies a positive corona charge to an influent aerosol stream, which is first classified by an electrical mobility channel followed by inertial impaction (Lehmann et al. 2004). The ratio of mobility and aerodynamic lognormal distributions is calculated for the mobility region (10-30 nm), and extended to larger sizes by applying a decreasing density function observed with increasing size for dry fractal soot agglomerates defined by Virtanen et al. (2002). When the majority of the total aerosol charge is detected by the mobility region, the instrument assumes a dominant nucleation mode and applies 1 g/cm^3 for all particle sizes. These procedures for measuring and applying density are both repeated at 1 Hz. Accordingly, the DMM is designed to accurately measure low and high PM mass concentrations for a wide range of particle sizes, and has been tested over the past decade in comparison to the traditional

gravimetric method (Khalek 2005; Mamakos et al. 2006; Khan et al. 2012). Data were collected using PC software version 1.2 rev 202, and daily cleaning and quality assurance procedures were followed according to the manual. The DMM was used in the present study only for test 3-A, the third initial regeneration event of the 2007 HDDT.

2.3.5 Procedure: Initial and Subsequent Regenerations

Before performing DPF regeneration, each HDDT was driven at low roadway speeds for up to thirty hours to accumulate material onto inner DPF surfaces without inducing a passive regeneration event. The parked active regenerations performed in this study were classified into two groups: Initial Regenerations and Subsequent Regenerations. Table 2.2 shows the five Initial Regenerations in this study (test IDs ending with "A"), which were performed on fully loaded DPFs. Initial Regenerations 1-A and 3-A were performed on higher levels of DPF loading than events 2-A, 4-A, and 5-A, which was indicated by a flashing dashboard indicator light and a data channel from the Insite OBD Tool. Four Subsequent Regenerations were measured (IDs ending with a "B, C, or D,"), which were initiated after the previous regeneration without any additional DPF loading.

All regeneration events followed the same protocol including the following order of measurements: ambient with engine off (ambient, 10 minutes), curb idle (idle, 10 minutes), regeneration (10-40 minutes), idle (10 minutes), ambient (10 minutes). Under this experimental design, measurements reflect the total mass flux of PM from ambient dilution air and from engine exhaust. The total Tunnel Emissions rate (g PM/hr) is reported for each phase of the test sequence rather than subtracting the ambient from total mass flux. This approach facilitates a simple evaluation of ambient-diluted engine emissions between phases. Unless indicated, the

contribution of PM from ambient dilution air was a negligible fraction of the Tunnel Emissions rate.

All regeneration events followed the same protocol including the following order of measurements: ambient with engine off (ambient, 10 minutes), curb idle (idle, 10 minutes), regeneration (10-40 minutes), idle (10 minutes), ambient (10 minutes). Under this experimental design, measurements reflect the total mass flux of PM from ambient dilution air and from engine exhaust. The total Tunnel Emissions rate (g PM/hr) is reported for each phase of the test sequence rather than subtracting the ambient from total mass flux. This approach facilitates a simple evaluation of ambient-diluted engine emissions between phases. Unless indicated, the contribution of PM from ambient dilution air was a negligible fraction of the Tunnel Emissions rate.

Table 2.2. List of parked active DPF regenerations and ambient dilution air parameters.

						Ambient Parameters		
ID	**Truck**	**DPF Loading State**	**Classification**	**Shutoff Method**	**Duration [sec]**	**Temp [°C]**	**RH [%]**	**$PM_{2.5}$ [µg/m^3]**
1-A	2007	Above Normal – Severe	Initial	Manual Abort	881	14.6	37.0	7.66
1-B	2007	Above Normal – Least Severe	Subsequent	Manual Abort	955	15.4	34.3	3.62
1-C	2007	Above Normal – Least Severe	Subsequent	Automatic	1200	11.3	49.9	32.4
1-D*	2007	Normal	Subsequent	Automatic	2411	14.4	36.1	41.2
2-A	2007	Above Normal – Least Severe	Initial	Automatic	1512	12.5	63.5	13.0
3-A	2007	Above Normal – Severe	Initial	Automatic	2415	34.0	9.7	4.21
4-A	2010	Above Normal – Least Severe	Initial	Automatic	2730	15.1	56.0	26.2
4-B*	2010	Normal	Subsequent	Automatic	1335	22.6	40.8	26.9
5-A	2010	Above Normal – Least Severe	Initial	Automatic	1000	19.8	17.7	9.33

*Forced parked active regeneration, initiated by on-board diagnostic (OBD) Insite Lite 7.5.0.234 tool.

2.3.6 Analyses

2.3.6.1 Tunnel and Sampling Line Losses

To minimize electrostatic sampling losses, conductive silicon tubing was used for all instruments except for the DMM where Tygon tubing was used per manufacturer specification (Liu et al. 1985; Timko et al. 2009). Measurements for all instruments were corrected for diffusional losses by multiplying measured particle number by the inverse of penetration, μ, defined below in Equation 2.1 (Hinds 1999):

$$\mu = D \, x \, L \, x \, Q^{-1} \qquad [2.1]$$

where D is the diffusion coefficient of the particles, L is the length of the tube, and Q is the volume flow through the sampling line. Because diffusional coefficient D is a function of particle size, SMPS and EEPS data were corrected individually by size channel, and DustTrak and DMM data were corrected individually at 1 Hz based on the CMD value of the EEPS distribution. Although actual corrections varied throughout the testing depending on the size distribution, the following approximate corrections were made for each instrument if all particles were 20 nm: 7% (SMPS), 2.1% (DustTrak), 1.3% (DMM), and 0.9% (EEPS). The calculated penetration of a 20-nm particle from the point of exhaust mixing with ambient air to the instrument-level sampling ports was greater than 99.7% (Hinds 1999). Therefore, particle losses to the inner walls of the ambient-dilution tunnel were negligible, and no correction was applied.

2.3.6.2 EEPS Zero Correction (C_1)

The upper detection limit of the EEPS (10^8/cm^3 at 5.6 nm, 10^6/cm^3 at 560 nm) was often approached during regeneration events due to high PM emissions. When measuring near the

upper detection limit, the TSI EEPS software reported zero particle counts for some groups of channels that should have reported positive values. The zeroes were observed similarly before and after EEPS electrometer cleaning, zeroing, and replacing corona charging needles, but not in PSD measured by the SMPS. A similar pattern is shown by Zheng et al. (2011) where channels of the EEPS distribution are zero adjacent to the peak also when measuring HDDT emissions. The cause of this phenomenon could be condensation of hygroscopic sulfates during these high-particle events that may have been prevented by using the column heater option (TSI 2011), or that the data inversion algorithm may have not properly accounted for irregularities when electrometers approached detection limits.

Channels with zero particle counts were assumed as measurement error because they corresponded to the channels immediately adjacent to the peak concentration where particle concentration was expected to be lower than peak concentration (10^7 #/cm^3), but higher than zero. Further, SMPS measurements did not report zero particle concentrations near the peak concentration. Therefore, it is likely the inversion algorithm used for converting charge on the 22 electrometers into a PSD performed poorly when the upper detection limit was approached or reached. The pattern of improper PSD measurement for high concentrations of engine exhaust particles was also observed in other studies, for example Figure 4 in Zheng et al. (2011) shows channels with zero particle counts, providing more support for TSI to improve its inversion algorithm, and for this work to correct for the missing data points.

Figure 2.2 shows a one-second average PSD measured during the Fuel Combustion Regime where the upper detection limit was reached. For each one-second observation, the CMD was calculated assuming a unimodal lognormal size distribution. The shaded panels shown in Figure 2.2 correspond to the remaining reported values from the TSI EEPS software. To the left of the

peak (smaller diameters), data were imputed using a linear least-squares regression based on reported data. To the right of the peak (larger diameters) a Junge power-fit distribution was used to impute missing data for the straight-line portion of accumulation mode particles, defined here as channels 10 nm greater than the CMD. Linear and power fit functions were applied for smaller and larger particles, respectively, because the range to the left of the peak (~30 nm), was typically less than the range to the right of the peak (~300 nm), and empirically have different shapes for combustion aerosols (Hinds 1999). The white outlined channels shown in Figure 2.2 correspond to the channels previously measured as zero that were imputed using this described fitting procedure.

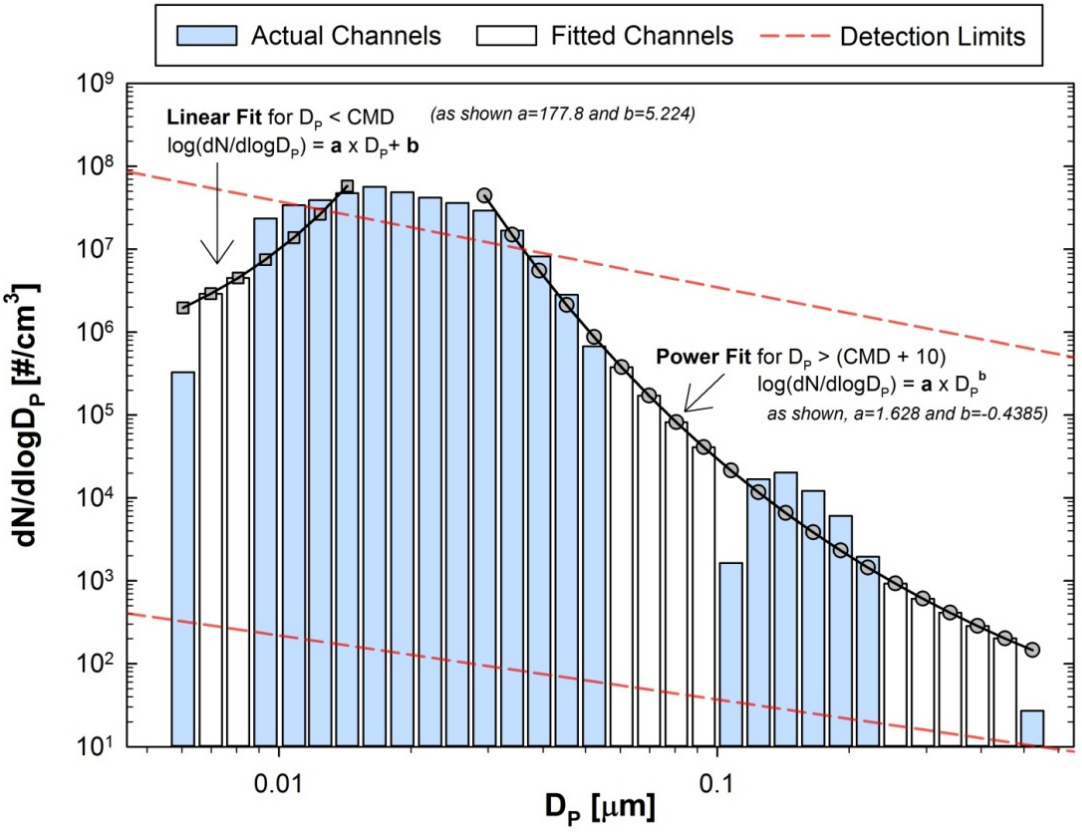

Figure 2.2. Illustration of the EEPS zero correction (C_1) by two fitting methods.

This correction procedure was applied all instances of zero-channel measurements during regeneration events, which increased integrated particle volume distributions by up to ~10% for any single distribution. The experimental maximum impact on estimating total regeneration emissions was 4.7% of uncorrected mass. Future studies should use a dilution ratio of at least 100 to preclude this measurement error. EEPS data that were corrected using this procedure are indicated as EEPS (C_1) in this work.

2.3.6.3 EEPS Correction Using SMPS Data (C_2)

The objective of this section is to generate a quantitative relationship between EEPS and SMPS measurements under four discrete Tunnel Emission phases: ambient, idle, and the Soot Combustion Regime and Fuel Combustion Regime during regeneration. The broad motivation of establishing these relationships is to compare the effects of measurement method (EEPS: corona charging + electrometer measurement, SMPS: bipolar charging + CPC detection) under these four discrete measurement conditions. Although highly time-resolved EEPS measurements have been shown comparable to the standard SMPS (Johnson et al. 2004), the instrument still presents a few limitations (Asbach et al. 2009). First, calibration checks using 100-nm polystyrene latex sphere standards showed the TSI Fast Mobility Particle Sizer (FMPS) 3091, which uses exactly the same hardware as the EEPS 3090, underestimated the CMD by 15%. Second, the FMPS distribution width, measured by geometric standard deviation (GSD), was consistently lower when measuring NaCl and consistently greater when measuring diesel soot particles. Oh et al. (2004) showed unipolar diffusion charging of TiO_2 agglomerates varied with fractal dimension, which suggests particle shape can have a significantly different impact on unipolar and bipolar particle charging which would need to be taken into account. Third, the number concentration of

particles greater than 100 nm appears to be underestimated by the EEPS (Johnson et al. 2003; Asbach et al. 2009). The specific motivation for this study, therefore, is to correct highly time-resolved EEPS data to an SMPS reference measurement.

PSD measurements from the EEPS and SMPS pooled from all tests according to the following groups: ambient, idle (~600 rpm), Soot Combustion Regime (CMD > 30 nm), and the Fuel Combustion Regime (CMD < 30 nm). Because the SMPS scans voltage in the DMA over a two-minute period and can only equal one value at a time, CMD values reported by the SMPS did not match the average EEPS for that given period. Thus for the Soot Combustion Regime, five two-minute SMPS measurements were manually selected to ensure the sampling interval where CMD values were within 10 nm.

The EEPS and SMPS distributions under each condition were fit to multimodal lognormal distribution curves using the DistFit 2009 software application (Chimera Technologies, Inc. Forest Lake, MN, USA). Equation 2.2 below can be used to generate ordinates (here, Y=dN/dlogD_p):

$$Y = \frac{1}{\sqrt{2\pi}}\left[\sum_i^n \frac{N_{tot,n}}{\ln GSD_n} \times e^{-0.5 \times \left[\frac{\ln D_p - \ln CMD_n}{\ln GSD_n}\right]^2}\right] \qquad [2.2]$$

where N_{tot}, *GSD*, and *CMD* are three constants derived by DistFit for the number of fitted peaks (n) required to reach the α=0.02 level. Distributions for this dataset with either unimodal or bimodal, and thus had a maximum of two sets of N_{tot}, *GSD*, and *CMD* for each of the fitted peaks (n) in the distribution. A second fitting was performed of the lognormal fit equations to obtain an SMPS-to-EEPS ratio that can also be expressed using Equation 2.2. The coefficients of N_{tot}, *GSD*, and *CMD* used to calculate the correction ratios are shown in Table 2.3. EEPS (C_1) data corrected using this procedure that is reported in this study is appended to read EEPS (C_1C_2).

The left column of Figure 2.3(a-d) shows EEPS (C_1) and SMPS data distributions (symbols) and their corresponding best-fit lines (solid black lines) determined by a unimodal or bimodal lognormal fit equation. The middle column of Figure 2.3(e-h) shows the ratio of the best-fit lines at the discrete EEPS measurement midpoint diameters (triangles), and the corresponding best-fit line of the SMPS-to-EEPS ratios (solid gray or red lines). The second lognormal fit was performed in order to express the SMPS-to-EEPS ratios as a function of diameter by applying coefficients in Table 2.3 using Equation 2.2

Table 2.3. Lognormal coefficients for deriving SMPS-to-EEPS ratios during DPF regeneration.

	Mode 1			**Mode 2**			**Mode 3**		
Condition	**N_{Tot}**	**CMD**	**GSD**	**N_{Tot}**	**CMD**	**GSD**	**N_{Tot}**	**CMD**	**GSD**
Ambient	8.19	51	4.38	--	--	--	--	--	--
Idle	3.63	21	2.36	4.01	383	2.36	31.6	1147	1.69
Regeneration Regimes									
Soot Combustion	1.21	70	1.25	1.69	148	1.28	--	--	--
Fuel Combustion	3.41	49	2.28	--	--	--	--	--	--

The right column of Figure 2.3(i-l) presents original SMPS and SMPS-corrected "EEPS (C_1C_2)" number and volume distributions. EEPS (C_1C_2) data agree well with original SMPS distributions, demonstrating the goodness of initial and secondary lognormal fit equations. No previous work has explored the impacts of ambient dilution, and therefore these results may be specific to the physical or chemical nature of mixing exhaust emissions from "new technology" 2007 and 2010 HDDTs with ambient PM in the Sacramento Valley region. In addition, application of the fit curves to other instrumental setups should be done with caution. For example, the of the TSI SMPS 3936L88 may not be applicable to SMPS systems using butanol-based CPCs because this study used a water-based CPC (model 3788) (Kulmala et al. 2007).

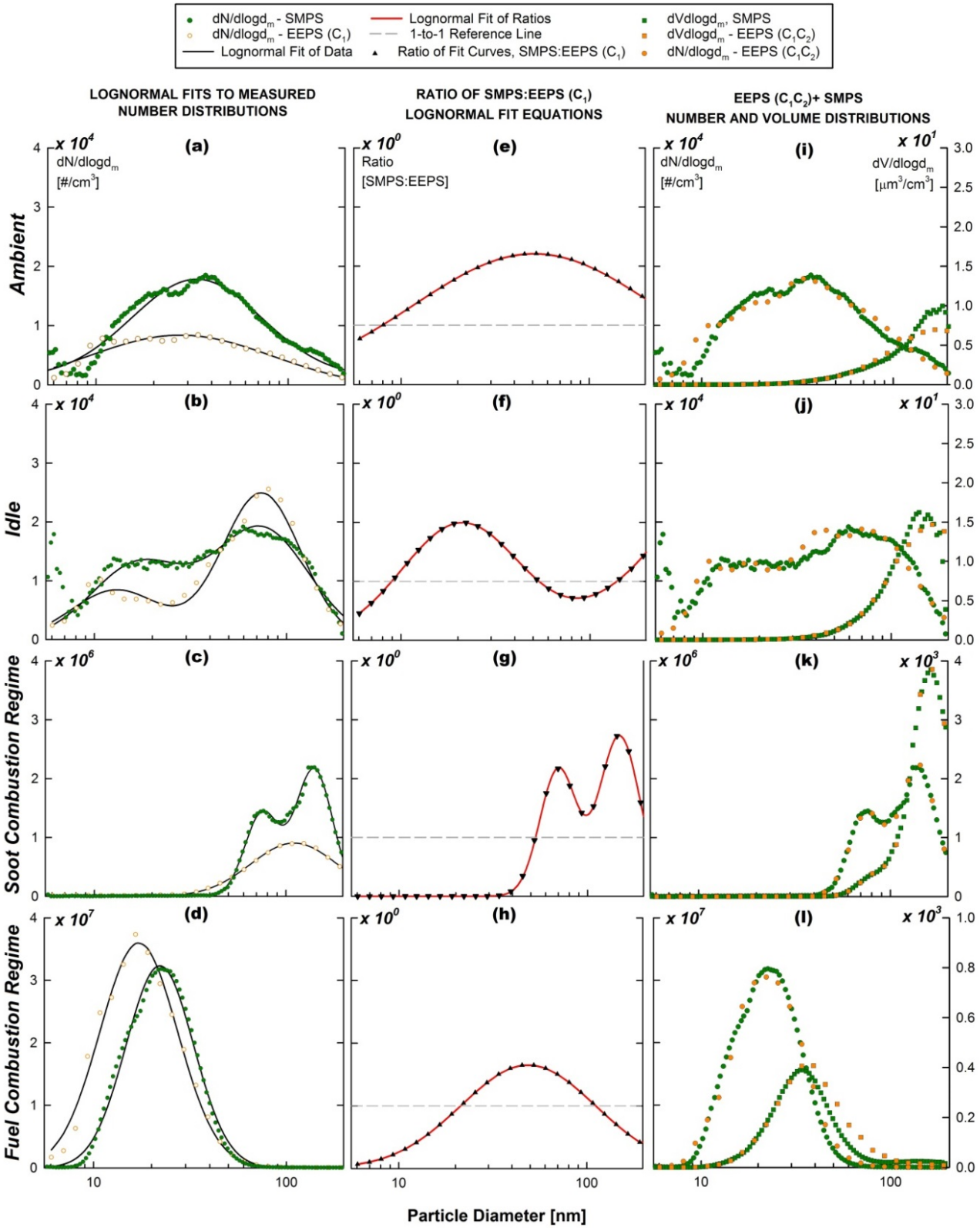

Figure 2.3. EEPS and SMPS distributions under four ambient-dilution conditions.

2.3.6.4 Calculating PM Mass from EEPS and SMPS

The EEPS and SMPS report PSD as the derivative of particle number with respect to size, dN/dlogD_p. The distribution of the derivative is converted to the spherical mobility-equivalent volume (dV/dlogD_p). PM mass is calculated by multiplying dV/dlogD_p and a particle effective density function defined in Equation 2.3 (Maricq et al. 2000; Liu et al. 2009), where D_p is electrical mobility diameter:

$$\rho_{eff} = 1.238 * exp(-0.0048 * D_p) \quad [2.3]$$

This exponential decay function was applied for all particles and decays sharply from 1.2 g/cm^3 for a 5.6-nm particle to 0.08 g/cm^3 for a 560-nm particle. This density was derived from both emissions of both direct-injection gasoline and diesel vehicles, and has been successfully applied to heavy-duty diesel engine emissions. Although the accuracy for active DPF regeneration emissions is unknown, the function is a valid reference that can be used to precisely measure PM mass.

2.4 Results and Discussion

2.4.1 2007 MY Heavy HDDT

2.4.1.1 Two Regeneration Regimes

Figure 2.4 shows a contour plot of the size distribution emitted during test 3-A, an Initial Regeneration of the 2007 HDDT. Within the first 500 seconds of regeneration (1200-1700 seconds of the test sequence), some faint gray smoke was observed leaving the tunnel, and the CMD of the distribution was between 100 and 200 nm. This may be due to oxidation of material from accumulated PM on inner DPF surfaces that reached their minimum activation energy

(Burtscher 2005; Matti Maricq 2007) as aftertreatment temperatures increased gradually and plateaued at temperatures above 500 ºC. Under this paradigm, materials emitted between 1300 and 1500 seconds of the test sequence were more volatile and abundant than those released later between 1500 and 1700 seconds of the test sequence. However, the material accumulated upon filter media was faint yellow; alternatively some of the emissions between 1200 and 1700 seconds could have been condensed engine oil downstream of the DPF. Although the composition remains unknown, this phase will hereafter referred to as the "Soot Combustion Regime", defined as whenever the CMD is > 30 nm during regeneration. Test 3-A was selected for discussion because it was uninterrupted from start to finish and the initial DPF loading was the greatest of the tests in the study. During this test, the Soot Combustion Regime accounted for 75% of the PM mass emissions of the parked regeneration based on an empirical combination of the real-time measurements. The remaining 25% of PM mass emissions were emitted after the Soot Combustion Regime.

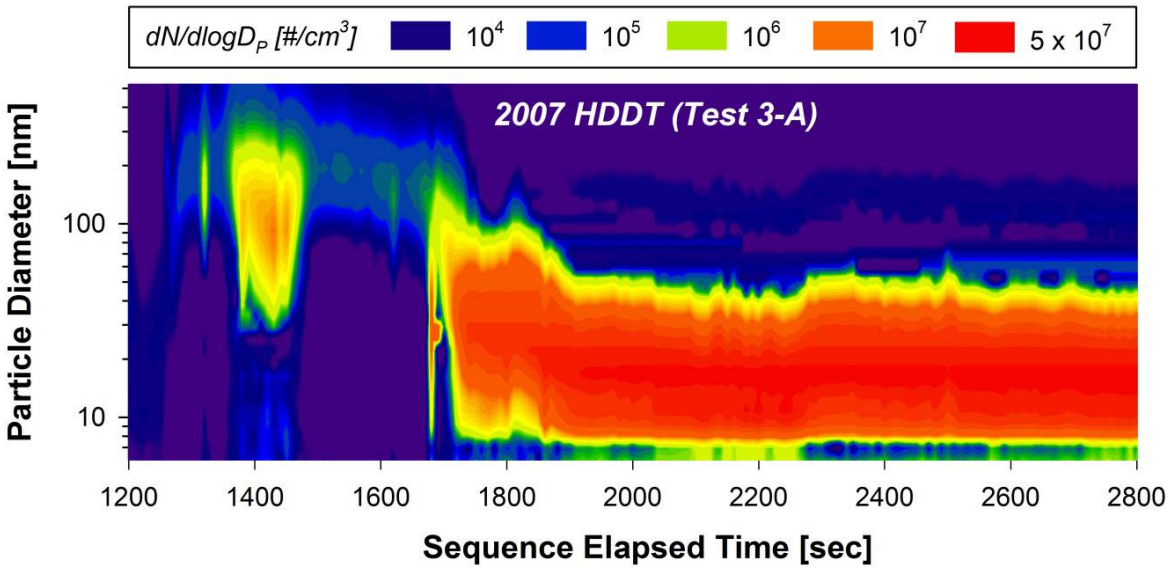

Figure 2.4. Contour plot showing EEPS (C_1) number-based size distributions during test 3-A, an Initial Regeneration of the 2007 HDDT.

Figure 2.4 shows that as active regeneration by fuel injection continued during test 3-A, CMD stabilized near 20 nm beginning around 1700 seconds of the test sequence. The CMD and GSD remained essentially unchanged for the remainder of the Initial Regeneration. Therefore for simplicity, whenever the CMD of the size distribution was < 30 nm, the DPF regeneration stage was defined as the "Fuel Combustion Regime." These emissions may have been due to the high-temperature catalytic conversion of SO_2 to SO_3 documented during DPF regeneration when applying engine load (Grose et al. 2006; Herner et al. 2011). However, the regeneration emissions with a CMD between 15-25 nm contrasts with emissions where CMD was < 10 nm observed during slow and gradual passive regeneration due to engine-generated heat (Herner et al. 2011).

2.4.2 Real-time PM Mass Emissions

Figure 2.5 presents the mass flux through the ambient-dilution tunnel (hereafter: Tunnel

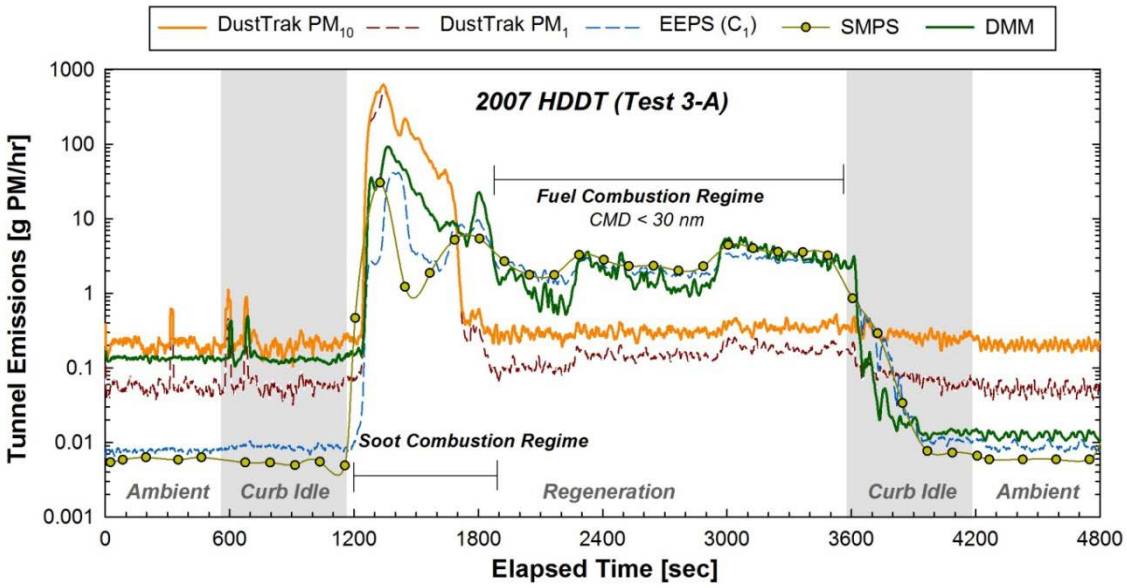

Figure 2.5. Tunnel Emissions over all sequence phases measured by EEPS (C_1), SMPS, DMM, and DustTrak during test 3-A, an Initial Regeneration of the 2007 HDDT.

Emissions, g PM/hr) from test ID 3-A measured by the EEPS (C_1, 5.6-560 nm), SMPS (5.4-198 nm), DustTrak PM_{10} and PM_1, and DMM (0.01-1.3 µm). Tunnel Emissions for all instruments remained unchanged from ambient to idle after engine cold-start (600 seconds) and from idle to ambient after turning the engine off (4200 seconds). The response of the instruments to the Soot and Fuel Combustion Regimes were dramatic and are described by each instrument in the following subsections.

2.4.2.1 DustTrak DRX

Within the Soot Combustion Regime, Figure 2.6 shows that DustTrak PM_{10} and PM_1 Tunnel Emissions peaked at 630 g and 480 g PM/hr and are much larger than measured by all other instruments. DustTrak size fractions are shown more clearly in Figure 2.6(a) where tunnel concentration is reported on a linear scale. At around 1280 seconds, tunnel PM was apparently ~40% larger than 1 µm, which is surprising because mechanical or extended atmospheric

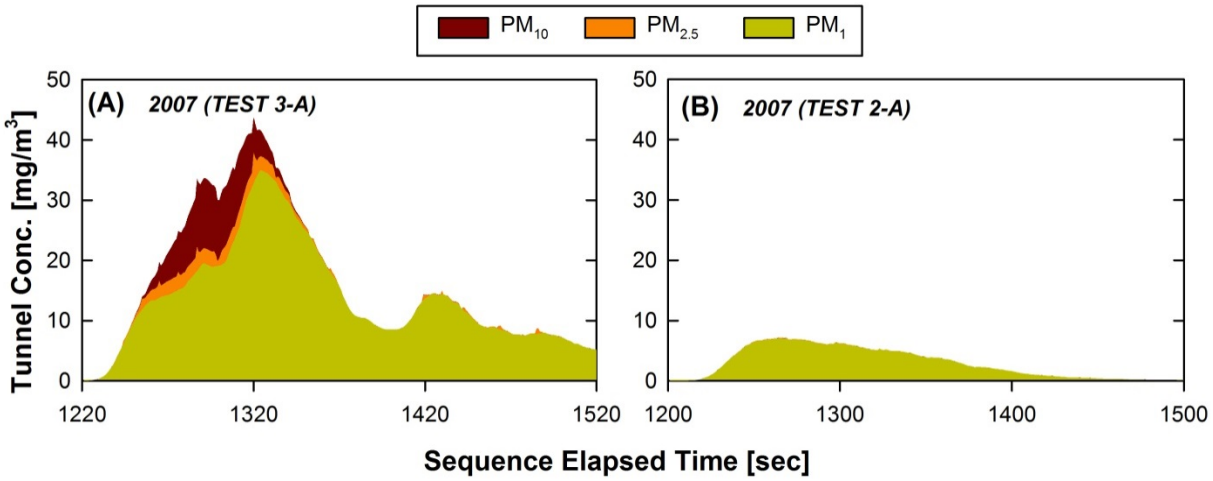

Figure 2.6. PM_1, $PM_{2.5}$, and PM_{10} concentrations simultaneously measured by the DustTrak during two Initial Regenerations of the 2007 HDDT: (a) test 3-A, and (b) test 2-A.

processing is typically required for generating PM in the fine and coarse size ranges (Harrison et al. 2000). This distribution with large particle sizes was only observed for regeneration events 1-A and 3-A where DPF loading was "Above Normal – Severe". Figure 2.6(b) shows all tunnel PM was smaller than 1 µm during test ID 2-A when DPF loading was "Above Normal – Least Severe".

Tunnel Emissions measured by the DustTrak were indistinguishable between the Fuel Combustion Regime during regeneration and the ambient phase. This was not surprising because the DustTrak does not measure ultrafine PM (<0.1 µm) that dominated the Fuel Combustion Regime. The low response of the DustTrak to ultrafine PM has been well-documented (Kinsey et al. 2006; Maricq 2013; Quiros et al. 2013) and this work illustrates how the instrument is useful but should be used with knowledge of its limitations.

2.4.2.2 SMPS and EEPS

During the ambient and first idle phases, the SMPS (5.4-198 nm) and EEPS (C_1, 5.6-560 nm) measurements agreed within a factor of two and remained nearly constant, but five to ten times lower than the DustTrak rates. However at the peak concentration reported during the Soot Combustion Regime, Tunnel Emissions peaked at the same rate (~35 g PM/hr) although the EEPS measures over a larger size range (5.6-560 nm) than the SMPS (5.5-198 nm). The emission of PM between 198-560 nm may have been negligible. Alternatively, particle concentrations measured by the two instruments may have differed by measurement principle.

Relative to each other during the Fuel Combustion Regime, both instruments reported parallel shifts at 1800, 2300, and 3000 seconds. The explanation for these observed fluctuations is unclear because fuel injection rates remained constant at 0.3 L/min over this period. After the

regeneration shut off during test 3-A, Tunnel Emissions reported by the EEPS and SMPS gradually declined during the idle phase to those observed during the initial ambient phase. According to Insite OBD data, engine exhaust and aftertreatment temperatures dissipated over five minutes (300 seconds) due to thermal inertia, consistent with emissions data. During both regimes, SMPS measurements confer adequate sensitivity to capture any transient shift in concentration reported by EEPS measurements.

2.4.2.3 DMM

The DMM (0.01 - 1.3 µm) supplemented the suite of PM instruments during test 3-A only. During the Soot Combustion Regime, the DMM measured a peak Tunnel Emissions rate of 80 g PM/hr, approximately six times lower than DustTrak PM_1, but two times larger than the EEPS and SMPS. Given that the DMM and DustTrak PM_1 upper cutoff sizes are closely matched, observed emissions differences indicate the density calculated and applied by the DMM was lower than the density inherent in the factory ATD-based DustTrak calibration.

During the Fuel Combustion Regime, the DMM also detected the definitive shifts in Tunnel Emissions at three time points reported by EEPS and SMPS measurements (at 1800, 2300, and 3000 seconds). The DMM also reported the Tunnel Emissions decreased an order of magnitude from 0.15 to 0.015 g PM/hr between the ambient phases before and after the regeneration. The corresponding concentrations of suspended mass were 10 and 1 $\mu g/m^3$, respectively, the latter of which is the lower detection limit of the DMM. The impacts of these fluctuations were trivial for measuring regeneration emissions at concentrations three orders of magnitude larger. Our data do not support use of the DMM for low PM mass measurement, a loose term defined here as any concentration below 10 $\mu g/m^3$.

2.4.3 Average Regeneration Emissions of the 2007 HDDT

2.4.3.1 Initial Regenerations

Figure 2.7 presents regeneration-average emissions from all tests conducted on the 2007 MY. Initial regeneration events shown in 5(a) all began in the Soot Combustion Regime where the magnitude of emissions positively correlated with the severity of DPF loading. For this comparison, EEPS (C_1C_2) data are presented where EEPS measurements were corrected to an SMPS equivalent. After grouping data by test sequence phase, the ratio of the lognormal fits of EEPS and SMPS measurements was computed and applied to EEPS (C_1) data to calculate the real-time SMPS equivalent. Using this approach, the size distribution is reported in terms of SMPS measurements but from higher time-resolved EEPS measurements. A comparison among

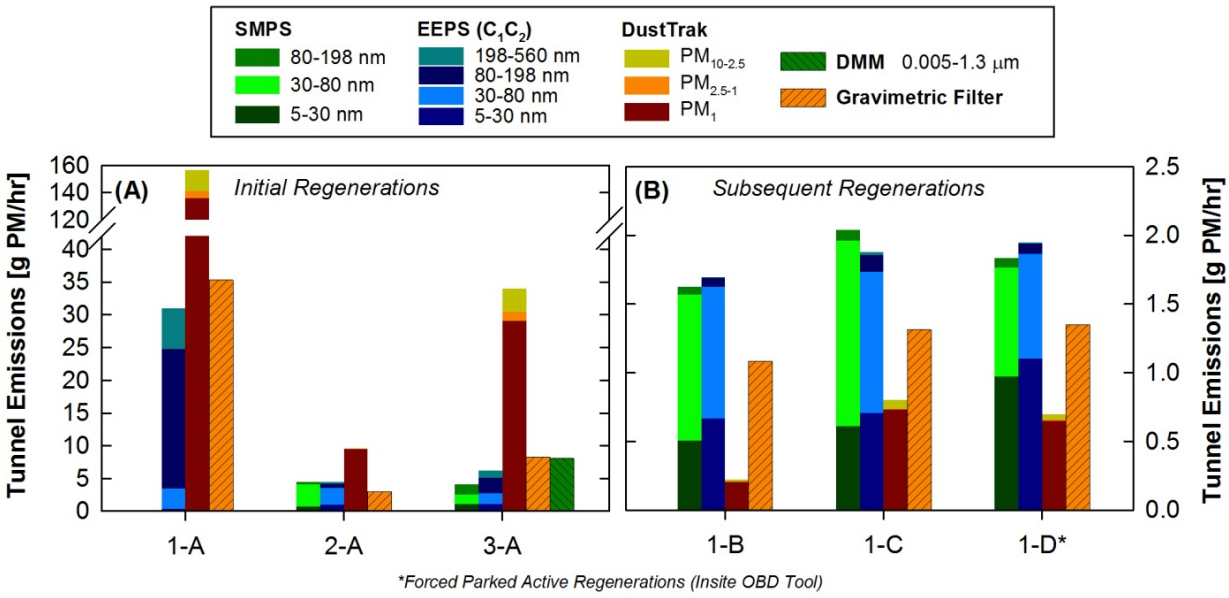

Figure 2.7. 2007 HDDT: Average Tunnel Emissions measured SMPS, EEPS (C_1C_2), DustTrak, DMM, and gravimetric filters during (a) Initial Regenerations and (b) Subsequent Regenerations.

EEPS, EEPS (C_1), and EEPS (C_1C_2) is presented in Section 3.3, and more details about the derivation of lognormal fit equations and corresponding correction equations are contained in Section 2 of Supplementary Data.

Test 1-A was initiated on an "Above Normal – Severe" DPF loading and resulted in the greatest Tunnel Emissions measured by all instruments: ~157 g PM_{10}/hr by the DustTrak, 35 g PM/hr by the gravimetric filter, and 31 g PM/hr by the EEPS. The average rate over the regeneration for test 1-A was disproportionately larger than for the other tests because test 1-A test was aborted immediately following the high mass emissions of the regeneration Soot Combustion Regime and therefore did not include lower mass emission rates that would have been observed in the Fuel Combustion Regime.

Test 2-A was initiated when the dashboard indicator light was solid but not flashing indicating an "Above Normal – Least Severe" DPF loading. As shown in Figure 2.6(b), the DustTrak classified all PM emissions as < 1 μm. The EEPS reported a negligible contribution of mass emissions for the 198-560-nm fraction, and because it is unlikely a second mass mode was present between 560 nm and 1 μm, these EEPS data show that virtually all Tunnel Emissions during test 2-A were from particles < 198 nm.

Test 3-A was initiated on a second "Above Normal – Severe" DPF loading where resulting average Tunnel Emissions rates of 34, 8.4, 8.1, 6.3, and 4.0 g PM/hr for the DustTrak PM_{10}, gravimetric filter, DMM, EEPS (C_1C_2), and SMPS, respectively. Similar to Test 1-A, the DustTrak size fractions indicated direct emission of PM in the fine and coarse fractions. Tunnel emissions measured by the EEPS and SMPS were typically within 10%, except the EEPS reported 50% more mass between 80-195 nm than the SMPS, and due to its larger size range reported about one-fifth of its total measured mass between 198-560 nm. The DMM reported 8.1

g PM/hr suggesting about one-quarter of the mass emissions (1.8 g PM/hr) were larger than 560 nm but below the upper measurement limit at 1.3 µm.

2.4.3.2 Subsequent Regenerations

Figure 2.7(b) shows the Subsequent Regenerations, where there were lower Tunnel Emissions, less intra-test variability among instruments, and less inter-test variability among regenerations. Tests 1-B and 1-C were initiated by a dashboard button, but test 1-D was a "forced" active parked regeneration that required using the Insite OBD tool. The emissions during this regeneration represent the result fuel injection into an already completely regenerated DPF. Tunnel Emissions rates measured by SMPS and EEPS (1.5-2 g PM/hr) were about 50% more than the gravimetric filter rate (1.0-1.5 g PM/hr) for Subsequent Regenerations 1-B, 1-C, and 1-D. For Subsequent Regenerations, the DustTrak *underestimated* Tunnel Emissions due to its limited response to ultrafine PM.

Based on DustTrak PM_{10} measurements of Tunnel Emissions during the ambient phases, dilution air contributions were 29%, 67%, and 96% of uncorrected particle mass flow through the tunnel for tests 1-B through 1-D, respectively. The successive increase in ambient contributions demonstrates two critical points. First, that although the Fuel Combustion Regime by our definition is where CMD remains < 30 nm, direct emissions of larger PM fractions were still observed. And second, that dilution air accounted for a dominant fraction of total mass flux through the tunnel. Therefore the ambient-dilution wind tunnel is a good tool for evaluating the effect of diluting exhaust emissions into ambient air, and underscores the importance of monitoring dilution air in engine exhaust testing studies.

2.4.4 2010 MY Heavy HDDT

2.4.4.1 Real-time PM mass emissions

Figure 2.8 presents a contour plot of the EEPS (C_1) distribution during test 4-A, an Initial Regeneration from the 2010 MY. PM mass emissions increased above ambient baseline levels ~300 seconds after initiating regeneration (1500 seconds), which was longer than the ~100 seconds observed for the 2007 MY (1300 seconds). For the 2010 MY, the Soot Combustion Regime was less pronounced in concentration and duration, and had lower peak CMD (40-50 nm) than the 2007 MY (100-200 nm). Furthermore, the Soot Combustion Regime for the 2010 MY only accounted for 5% of the total PM mass emissions, whereas 95% were emitted during the Fuel Combustion Regime. The Fuel Combustion Regime was similar between the two MYs where particle number concentrations exceeded 10^7 particles/cm^3, the CMD remained below 30 nm, and the observed nucleation possibly from the release of stored sulfur could be repressed for extended periods of time (Herner et al. 2011). Regardless of composition, particles 30 nm or smaller dominated, on a mass basis, the PM emissions during parked active regeneration of the 2010 MY truck.

Figure 2.9 presents Tunnel Emissions from the same Initial Regeneration shown in Figure 2.8 as measured by EEPS (C_1, 5.6-560 nm), SMPS (5.4-198 nm), and DustTrak PM_{10} and PM_1. Tunnel Emissions measured by all instruments (g PM/hr) remained essentially unchanged from ambient to idle upon engine cold-start (600 seconds). The response of the instruments during regeneration described below.

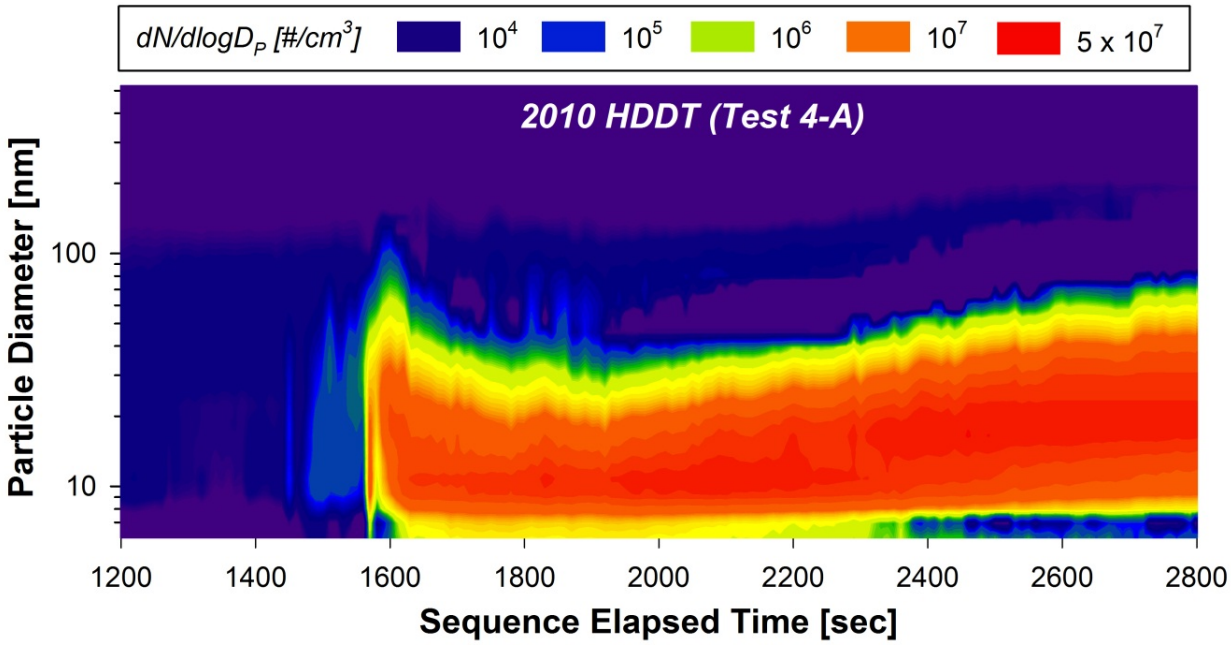

Figure 2.8. Contour plot showing EEPS (C_1) number-based size distributions during test 4-A, an Initial Regeneration of the 2010 HDDT.

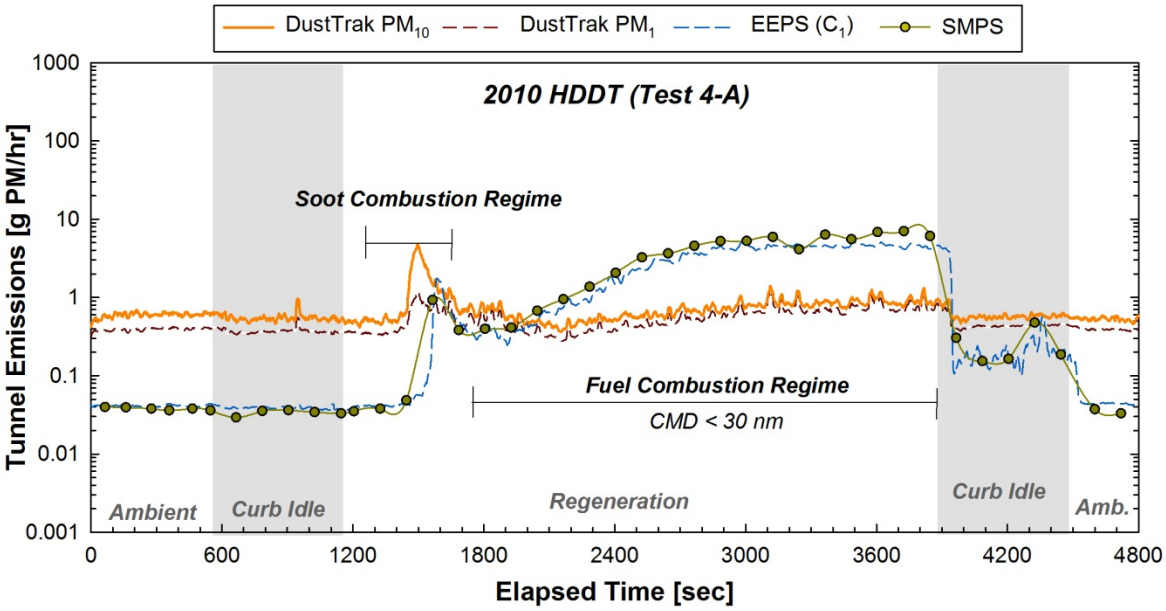

Figure 2.9. Tunnel Emissions over all sequence phases measured by EEPS (C_1), SMPS, and DustTrak during test 4-A, an Initial Regeneration of the 2010 HDDT.

2.4.4.2 DustTrak DRX

During the Soot Combustion Regime, the DustTrak PM_{10} Tunnel Emissions increased ten-fold relative to the ambient phase. The DustTrak emissions rate during test 4-A is shown on a linear scale in Figure 2.10(a) where 60% of PM was larger than one micron. Although a definitive increase of directly-emitted coarse PM was observed for during test 4-A of the 2010 MY, the measured tunnel concentration (0.25 mg/m^3, dilution ratio ≈ 36) was over one hundred times lower than the 2007 MY (40 mg/m^3, dilution ratio ≈ 31). There were no visible emissions leaving the tunnel during regeneration of the 2010 HDDT. Figure 2(b) shows the DustTrak did not measure PM from any size fraction during test 4-B, a forced parked active Subsequent Regeneration emitting strictly within the Fuel Combustion Regime.

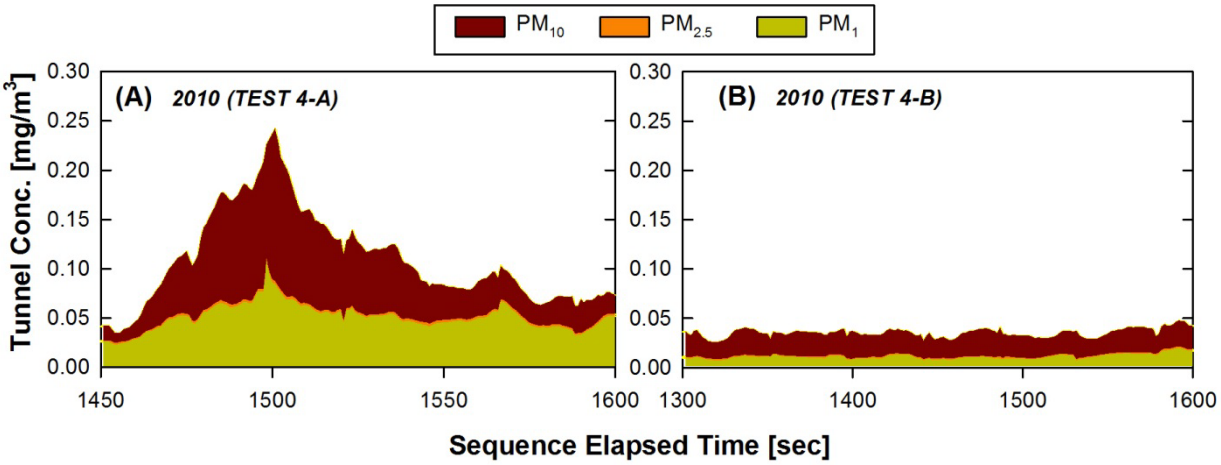

Figure 2.10. PM_1, $PM_{2.5}$, and PM_{10} concentrations simultaneously measured by the DustTrak during two regenerations of the 2010 HDDT: (a) test 4-A, and (b) test 4-B.

2.4.4.3 EEPS and SMPS

Figure 2.9 shows Tunnel Emissions measured by the SMPS and EEPS (C_1) tracked each other throughout test 4-A. During the Soot Combustion Regime, SMPS and EEPS (C_1) reported

~1.0 and ~1.8 g PM/hr respectively near 1600 seconds. These data suggest two distinct mass peaks were emitted: initially a coarse-fraction peak near 1500 seconds measured by the DustTrak followed by an ultrafine-fraction peak measured by EEPS and SMPS near 1600 seconds. Use of a standalone electrical mobility instrument (EEPS or SMPS) or a photometric instrument (DustTrak) would therefore have resulted in overlooking one of the two peaks observed within the Soot Combustion Regime. Tunnel Emissions during the Fuel Combustion Regime increased asymptotically from 0.5 g PM/hr with a CMD of ~12 nm to ~6 PM/hr with a CMD of ~24 nm. The increasing trend was also observed for test 5-A (not shown), and contrasts with the CMD remaining constant with time in the Fuel Combustion Regime of the 2007 MY.

2.4.5 Average Regeneration Emissions of the 2010 HDDT

Figure 2.11 shows average regeneration emissions for test 4-A: ~0.58 g $PM_{2.5}$/hr and 0.76 g PM_{10}/hr by the DustTrak, 1.6 g PM/hr by the gravimetric filter, 3.1 g PM/hr by SMPS, and 3.3 g PM/hr by EEPS (C_1C_2). The contribution of ambient PM to Total Emissions was <1% for EEPS and SMPS measurements, but as large as 73% for DustTrak PM_{10}. Therefore EEPS or SMPS measurements have negligible impact from ambient contributions but are highly responsive to measuring DPF regeneration emissions.

Test 4-B was a Subsequent *forced active* Regeneration on a completely regenerated DPF, and similar to every other Subsequent Regeneration, the Fuel Combustion Regime dominated. Tunnel Emissions measured by SMPS were about 50% greater than EEPS (C_1C_2) emissions that primarily arose from a discrepancy in measuring the 80-198 nm fraction. Ambient contributions to PM_{10} was 83%, indicating only 17% of emissions within its measurement range were from the HDDT.

Test 5-A also initiated on an "Above Normal – Least Severe" DPF loading, but the regeneration was terminated by the engine control module earlier than during test 4-A (after 1000 seconds of regeneration, see Table 2.2). The Tunnel Emissions measured by SMPS, EEPS (C_1C_2), DustTrak PM_{10}, and gravimetric filter were 0.6-0.7 g PM/hr. The values of EEPS and SMPS size fractions 5-30, 30-80, and 80-198 nm measured were within 10%, and the EEPS reported <1% of total Tunnel Emissions were from the 198-560-nm fraction. Based on DustTrak PM_{10} measurements, 66% of Tunnel Emissions were due to ambient dilution air. During this test, all methods showed agreement at average emissions between 0.6-0.7 g PM/hr, although filter values were expected to be the sum of ultrafine mass detected by the EEPS/SMPS and larger ambient PM detected by the DustTrak.

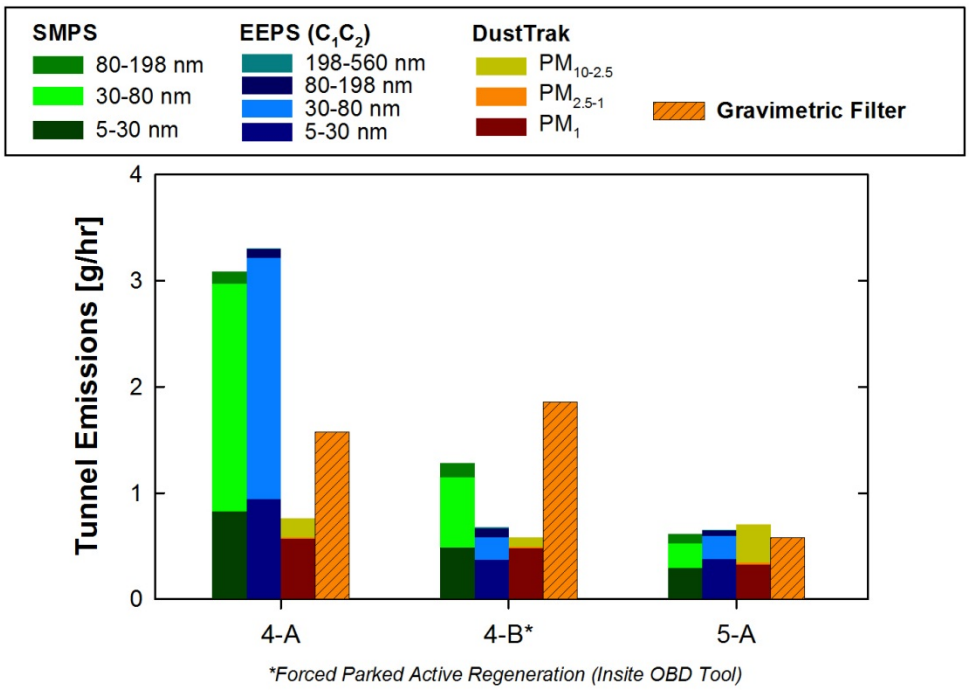

Figure 2.11. 2010 HDDT: Average Tunnel Emissions measured SMPS, EEPS (C_1C_2), DustTrak, and gravimetric filters during all regenerations.

2.5 Measuring Real-Time PM Mass

2.5.1 EEPS and SMPS

Figures 2.5 and 2.9 show Tunnel Emissions measured by the EEPS (C_1) were often lower than measured by the SMPS, especially during the Fuel Combustion Regime. Mass-based size distributions for test 3-A measured by the SMPS, EEPS (C_1), and DMM are plotted in Figure 2.12. Peak concentration at the mass median diameter (MMD) measured by the SMPS was 33% and 87% larger than measured by the EEPS for Fuel and Soot Combustion Regimes, respectively. Despite SMPS and EEPS agreement when measuring a laboratory-generated calibration aerosol, the impact of aerosol characteristics on measurement is substantial and has been previously discussed (Johnson et al. 2004; Oh et al. 2004; Asbach et al. 2009). Although a detailed discussion of the measurement principles is beyond the scope of this study, the bipolar charging and CPC detection of the SMPS is regarded as more accurate than the unipolar corona charging and electrometer detection of the EEPS. Therefore the relationship between SMPS and EEPS measurements was used to develop a novel post-hoc correction for EEPS data (Supporting Information, Section 2).

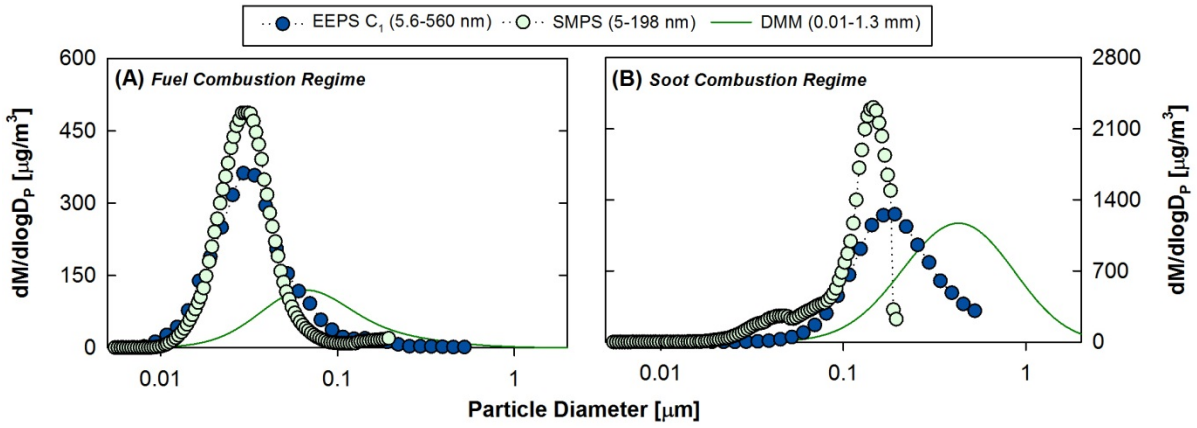

Figure 2.12. Mass-based particle size distributions during test 3-A measured by the EEPS, SMPS, and DMM during the (a) Fuel Combustion Regime and (b) Soot Combustion Regime.

Figure 2.13 presents the gravimetric-normalized ratios of Tunnel Emissions for uncorrected EEPS (reported), zero-corrected EEPS (C_1), and zero and the post-hoc, or SMPS-corrected, EEPS (C_1C_2) measured by each instrument divided by the respective gravimetric filter value. Viewing data as a ratio facilitates an easier comparison among instruments relative to a baseline reference. The EEPS (C_1) correction resulted in an increased emissions rate by 0.3 to 4.7% depending on the test. Therefore even if zeroes are reported in raw EEPS data, the majority of PM on a mass basis would still be reported. The EEPS (C_1C_2) correction induced more dramatic impacts on reported emissions; corrections changed measurements from 64% lower (test 1-D) to 140% higher (test 2-A) than the EEPS (C_1) Tunnel Emission rate. Better agreement was reached

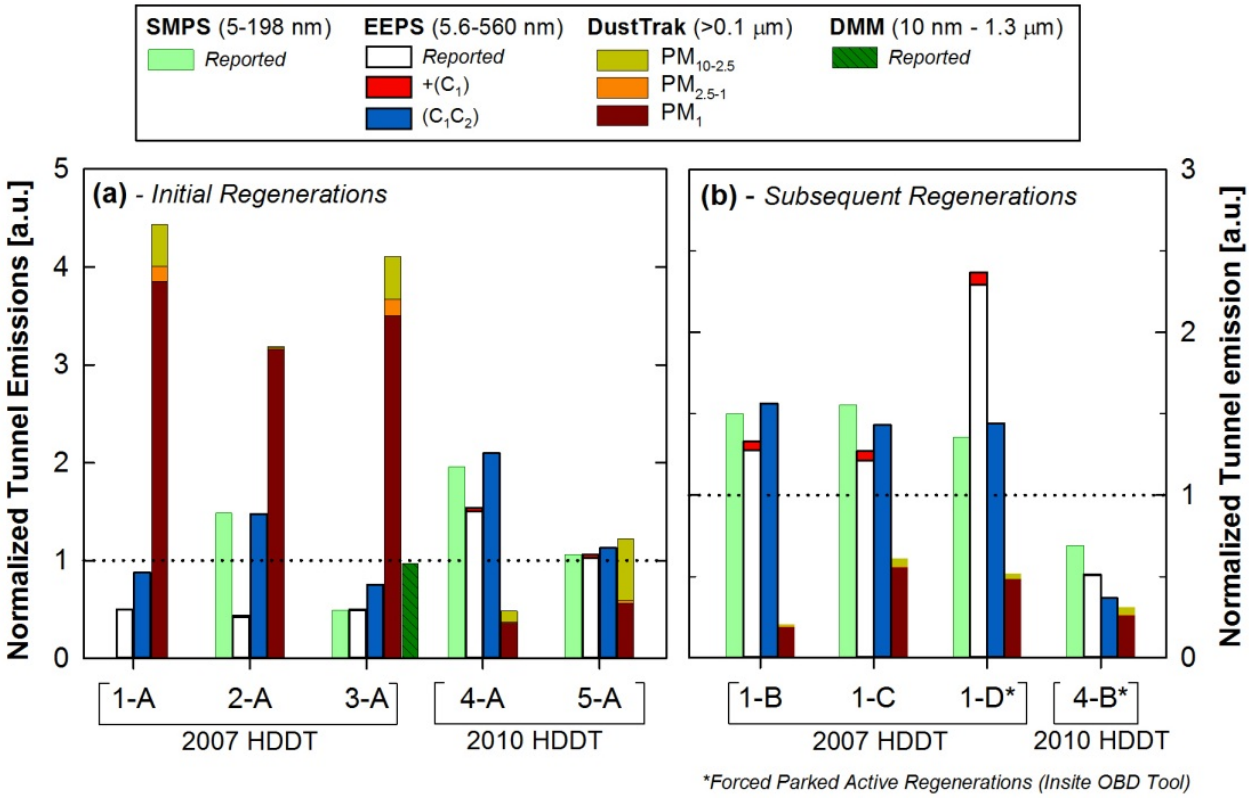

Figure 2.13. Tunnel Emissions normalized to gravimetric measurements for regenerations of the 2007 and 2010 HDDT during (a) Initial Regenerations and (b) Subsequent Regenerations.

between EEPS and SMPS Tunnel Emissions after applying the EEPS (C_1C_2) except for test 4-B where a larger discrepancy was observed.

Initial Regenerations resulted in gravimetric-normalized EEPS (C_1C_2) ratios ranging from 0.75 to 1.48 for the 2007 MY, and 1.14 to 2.08 for the 2010 MY. Subsequent Regenerations resulted ratios ranging 1.43-1.56 for the 2007 MY and 0.37 for the 2010 MY. Because filters collect particles of all sizes, these ratios are *underestimates* of the real differences between the applied effective density between 5.6 and 560 nm because the EEPS does not measure larger size fractions in the Tunnel Emissions. Selecting tests based on a smaller-size DustTrak distribution, the most reasonable gravimetric-normalized EEPS (C_1C_2) emissions ratios for the 5.6-560-nm range were approximately 1.5 for the 2007 HDDT, and 2.1 for the 2010 HDDT.

In summary, unless the manufacturer, TSI, provides an inversion matrix updated to address the observed discrepancies between EEPS and SMPS measurements shown in Figures 2.5, 2.9, and 2.13, our data support applying a post-hoc correction procedure for EEPS data. In addition, the accuracy of calculating PM mass from real-time SMPS or EEPS measurements of electrical mobility would most certainly be improved by refining the effective density function for an array of discrete new types of new technology PM.

2.5.2 DustTrak DRX

The merit and faults of the DustTrak DRX for DPF regeneration studies are clear: it qualitatively provides size distribution over a large size and concentration, but it fails to measure ultrafine PM and is factory calibrated to ATD that does not physically or chemically represent vehicle emissions. To improve its accuracy, Appendix B of the DustTrak DRX Operation and Service Manual specifies to collect PM onto an on-board filter using an inlet impactor for

derivation the photometric calibration factor for $PM_{2.5}$. Any calibration to a polydisperse aerosol with ultrafine PM will bias the calibration factor, however the bias is proportionally larger when measuring smaller size fractions. In this study, PM_{Total} was equivalent to PM_{10}, which resulted in an average gravimetric filter reference ratio of 3.91 for the 2007 MY. It is recommended that future studies to divide DustTrak reported values for all size fractions ($PM_{2.5}$, etc.) by 3.9 when measuring DPF regeneration that includes both a Soot and Fuel Combustion Regime.

2.5.3 DMM

The average mass-based distributions from test 3-A for the DMM are also shown for the Soot and Fuel Combustion Regimes in Figures 2.12(a) and 2.12(b). Because the DMM reports mass directly, the average distributions were derived from a reported MMD and geometric standard deviation (GSD) reported at each one-second interval. DMM distributions were skewed-right with lower peak concentrations than EEPS and SMPS distributions. Figure 10(a) shows MMD for the DMM was ~60 nm during the Fuel Combustion Regime where a constant 1-g/cm^3 density was likely applied all particle sizes. Figure 2.12(b) shows MMD for the DMM was ~600 nm during the Soot Combustion Regime, still a much larger and broader distribution than obtained from the EEPS and SMPS. During the Soot Combustion Regime, the instrument should have calculated and applied an effective density function based on the relationship of mobility and aerodynamic distributions and soot decay function described by Virtanen et al. (2002). The MMD of the distributions between the DMM, SMPS, and EEPS should have agreed better because the density functions applied are functionally similar: the Virtanen et al. (2002) function applied by the DMM and the Maricq and Xu (2004) function shown in Equation 2.3 and applied to EEPS/SMPS distributions. An evaluation of the density measurement approach employed by

the DMM shows the average density is typically reported within 15% (Rostedt et al. 2009), although the discrepancies shown in Figure 10 appear to be more of an error in measuring size distribution.

Figure 2.13 shows the Tunnel Emissions rate measured by the DMM for test 3-A agreed within five percent of the gravimetric reference using an undisclosed combination of reasonable algorithms to estimate particle density. The ostensible good agreement may be the result of the DMM having a relatively wide measurement range (0.01-1.3 μm) and high time resolution (1 Hz). However, rigorous testing would be required to demonstrate robust performance under a wide range of vehicle emissions. Furthermore, considering the discrepancy between the DMM size distribution and the EEPS or SMPS size distribution, the DMM should be tested alongside additional real-time instruments before used as standalone method for real-time mass measurement.

2.6 Discussion

This study measured ambient-diluted PM mass during parked active diesel particulate filter (DPF) regeneration of a 2007 and 2010 model year (MY) heavy-duty diesel trucks (HDDTs) using a TSI DustTrak DRX, TSI EEPS 3090, TSI SMPS 3936L88, DMM 230-A, and filters by gravimetric analysis. The strengths of each instrumental method are discussed; the principle limitation to measuring PM mass using the selected real-time methods is applying an appropriate particle density function. Gravimetric measurements indicated emissions from the 2007 MY were approximately an order of magnitude higher than the 2010 MY for initial regeneration events following equivalent treatments of on-road driving. The ten-fold reduction in PM mass emissions was largely due to a less dominant Soot Combustion Regime, which decreased from

75% to 5% of total regeneration emissions of the 2007 and 2010 MY, respectively. DustTrak emissions were divided by a factor of 3.9 to measure the proportion of the Soot Combustion Regime and SMPS measurements were used to measure the Fuel Combustion Regime. Applying this approach for test 3-A resulted in a mass apportionment of the two regimes to within five percent of those reported by the DMM.

Today in California, PM emissions during parked active regeneration represent an important category of PM emissions, even for on-road heavy-duty engines meeting the 2007 emissions standard (0.01 g PM/bhp-hr). The comparability between PM emissions from parked active DPF regeneration versus other approaches for DPF regeneration is not entirely clear. In some cases, DPF regeneration may be initiated during on-road operation, either actively or passively. This study shows a sharp reduction trend in PM emissions during a discrete parked active DPF regeneration between the 2007 and 2010 MY. However, many factors influence engine-out PM emissions entering the DPF, the management of accumulated soot on inner surfaces, and total PM emissions over longer periods including non-regeneration periods.

The ambient-dilution wind tunnel used in this study is a useful tool for evaluating the controlled real-world dilution of exhaust gases. Particle number, count median diameter, and geometric standard deviation were not impacted by the incidental ranges of dilution air temperature, relative humidity, and ambient particulate characteristics. However, the observed count median particle diameter between 15 and 25 nm during the Fuel Combustion Regime was larger than 10 nm as reported by Herner, et al. (2009) during DPF active regeneration where useful work was being produced by the engine and measurements were conducted using filtered laboratory air. On a mass basis, the contribution of ambient dilution air to tunnel mass flux (Tunnel Emissions) was substantial, sometimes exceeded the contribution from exhaust

emissions. Therefore, dilution air should be always monitored under the present experimental setup. Future work could evaluate the interaction between ambient dilution air characteristics and regeneration emissions under higher dilution ratios, residence times, or newer HDDT models.

3 PARTICLE EFFECTIVE DENSITY AND MASS DURING STEADY-STATE OPERATION OF GDI, PFI, AND DIESEL PASSENGER CARS

3.1 Abstract

Particle effective density is an important physical property of vehicle exhaust, and is required for estimating particulate matter (PM) mass emissions using the Integrated Particle Size Distribution (IPSD) method. This study included measurements of particle effective density of five light-duty vehicles with PM emissions below the Low Emission Vehicle (LEV) III PM standards of 1 or 3 mg/mi (0.62 and 1.86 mg/km) using the Differential Mobility Analyzer (DMA) – Centrifugal Particle Mass Analyzer (CPMA) approach. Test vehicles included two gasoline direct injection (GDI) vehicles without particulate filters, and for the first time reported in the literature, two port-fuel injected (PFI) vehicles and a turbocharged direct injection (TDI) light-duty diesel vehicle with a diesel particulate filter (DPF). The particle effective density functions generally resemble previous work on GDI and diesel engines without particulate filters but, for many size ranges, the PFI and TDI vehicles produced emissions with higher particle effective densities than GDI vehicles. Good linear correlation was found between the gravimetric and IPSD methods when applying the new particle effective density functions to size distribution measured by the TSI Engine Exhaust Particle Sizer (EEPS, 5.6-560 nm, R^2 = 0.84); however, the IPSD method underestimated gravimetric mass by 64%. When using a TSI Aerodynamic Particle Sizer (APS, 0.54-2.5 μm) to measure the contribution of larger particles, underestimation bias was virtually eliminated and the correlation improved dramatically (R^2 = 0.96). Even stronger correlation between IPSD and gravimetric methods was achieved when

using a Scanning Mobility Particle Sizer (SMPS, 8.7-365 nm) and the APS (R^2=0.97). A procedure for correcting EEPS measurements using the SMPS is presented and evaluated.

3.2 Introduction

Exposure to particulate matter (PM) is associated with increased cardiopulmonary morbidity and mortality (Pope and Dockery 2006) and is influenced by mobile source emissions (Lloyd and Cackette 2001; EPA 2002; Hill et al. 2009). The California Air Resources Board (ARB) recently adopted the Low Emissions Vehicle (LEV) III regulations which, by 2025, will reduce the light-duty vehicle PM emission standards for the Federal Test Procedure (FTP) from 10 to 3 and ultimately to 1 mg/mi (6.2 to 0.62 mg/km). Recently, ARB and U.S. EPA demonstrated measurement of PM emissions below 1 mg/mi (0.62 mg/km) using the existing filter-based gravimetric method (Hu et al. 2014). However, alternative measurement approaches are still of great interest to better understand the characteristics of PM at very low levels.

One alternative method for PM mass measurement is the Integrated Particle Size Distribution (IPSD) method, a phrase first used by Liu et al. (2009) referring to the general method for estimating PM concentrations from particle size distribution and effective density. Defined as mass divided by electrical mobility equivalent volume (Kelly and McMurry 1992), particle effective density enables rapid conversion between number and mass distributions, or between mobility and aerodynamic diameters, without assuming bulk density or morphology. Several studies have reported particle effective density of both gasoline and diesel engines (e.g. Ristimäki et al. 2002; Park et al. 2003; Maricq and Xu 2004; Van Gulijk et al. 2004; Virtanen et al. 2004b; Zelenyuk et al. 2005; Olfert et al. 2007; Barone et al. 2011). The majority of them show particle effective density decreases as a function of particle size, in general agreement with the power fit model for fractal aerosols using a mass-mobility scaling exponent (Sorensen 2011).

However, to the best of our knowledge, only one study has evaluated gasoline direct injection (GDI) emissions (i.e. Maricq and Xu 2004), and no previous studies have measured particle effective density from port-fuel injected (PFI) gasoline or light-duty diesel vehicles equipped with a diesel particulate filter (DPF). Therefore, redefining the particle effective density functions over the breadth of current vehicle technologies is needed to properly evaluate IPSD.

Kelly and McMurry (1992) first measured effective density of laboratory aerosol using a Differential Mobility Analyzer (DMA) and an inertial cascade impactor. Subsequently, several studies used a DMA placed upstream of an Electrical Low Pressure Impactor (ELPI, Keskinen et al. 1992; Ahlvik et al. 1998; Maricq et al. 2000; Maricq and Xu 2004) providing real-time aerodynamic size distribution for a given DMA set point. A DMA has also been operated as part of a Scanning Mobility Particle Sizer (SMPS) in parallel to, rather than in series with, an ELPI for making density measurements more quickly by fitting size distributions (Ristimäki et al. 2002; Virtanen et al. 2002; Virtanen et al. 2004a). A DMA has also been placed upstream of an Aerosol Particle Mass Analyzer (APM, Ehara et al. 1996) and Centrifugal Particle Mass Analyzer (CPMA, Olfert and Collings 2005), which both classify according to mass to charge ratio using two rotating concentric cylinders to balance electrostatic and centrifugal forces. McMurry et al. (2002) used a DMA and APM to measure the effective density of atmospheric aerosol, and the approach has been subsequently applied to characterize engine exhaust particles (e.g. Park et al. 2003; Barone et al. 2011). Later, the CPMA was designed to improve the transfer function of the APM by using slightly different angular velocities for the two rotating cylinders (Olfert and Collings 2005; Olfert et al. 2006). There are other methods for measuring particle effective density, such as using a DMA and Single Particle Laser Ablation Time-of-flight Mass Spectrometer (SPLAT, Zelenyuk et al. 2005). However, the system measures vacuum

aerodynamic diameter and has low (<0.1%) detection efficiencies for particles below 50 nm (Zelenyuk et al. 2009) and is not commercially available. The Dekati Mass Monitor (DMM, Lehmann et al. 2004) uses yet another approach by combining one mobility with six aerodynamic channels measuring size distribution to estimate particle effective density in real time. The DMM is used widely to measure PM mass, but density values are not reported but are used to directly report mass concentration based on a unimodal size distribution, mass median diameter, and geometric standard deviation (GSD), which have all shown to largely deviate from accepted reference methods (Mamakos et al. 2006).

This study used the DMA-CPMA method to measure particle effective density from two gasoline direct injected (GDI-1 and GDI-2) and two port fuel injected (PFI and PFI-E85) gasoline vehicles, and one turbo direct injection (TDI) light-duty diesel vehicles on a chassis dynamometer. Because the DMA-CPMA approach requires several minutes to complete each measurement, steady-state testing was conducted. The primary objective of this study was to determine particle effective density functions that can be used to evaluate the capability of IPSD to estimate PM mass emitted from light-duty vehicles meeting the LEV III standards. A secondary objective is to compare size distributions measured by the TSI Engine Exhaust Particle Sizer (EEPS, 5.6-560 nm) and SMPS (8.7-365 nm). The SMPS is regarded as the reference method for measuring size distribution; however, it requires one to two minutes to complete a scan, and therefore the EEPS was developed to measure transient particle size distributions. Therefore, SMPS-to-EEPS ratio is calculated under controlled steady-state conditions, and is used to correct EEPS measurements. Finally, this study also aims to measure the contribution of larger particle sizes using a TSI Aerodynamic Particle Sizer (APS, 0.54-2.5

μm), in order to compare total suspended real-time mass with the filter-based gravimetric standard method.

3.3 Methods

3.3.1 Laboratory, Instruments, and Quality Assurance

All data were collected at ARB's Haagen-Smit Laboratory (HSL) in El Monte, CA in one of the light-duty test cells equipped with a 48-inch single-roll electric chassis dynamometer, a constant volume sampler (CVS), and sampling systems meeting certification requirements defined by 40 CFR 1066 (U.S. EPA 2012). A cyclone upstream of all PM sampling was used to remove particles larger than 2.5 μm, an optional requirement listed in the CFR.

Figure 3.1 shows the instrumentation and sampling setup. The real-time PM instrumentation included two (Units A and B) TSI Engine Exhaust Particle Sizers (EEPS 3090, 5.6-560 nm, Firmware MCU 3.11 DSP 3.02, TSI Inc., Shoreview, MN, USA) both operating with a 1-sec sampling interval, a TSI Scanning Mobility Particle Sizer 3936L88 (SMPS, 8.7-365 nm) operating at a two-minute time resolution (upscan 100 sec, downscan 20 sec), a TSI Aerodynamic Particle Sizer 3321 (APS, 0.54-19.81 μm) operating at a five-second time resolution, and the DMA-CPMA setup with the TSI Long DMA (model 3081, Shoreview, MN) and Cambustion CPMA (Cambustion Ltd, Cambridge, United Kingdom).

The CPMA was calibrated by the manufacturer immediately prior to the study where angular velocity and voltages were within 3% and 5%, respectively, of relevant international standards, indicating good system functionality for classifying particle mass (Symonds et al. 2013). The overall uncertainty of the method may be up to 9.4% (Johnson et al. 2013); however, the actual uncertainty of particle effective density measurement has been shown to be about 3% (Olfert et

al. 2006). To verify proper system function, dioctyl sebacate (DOS) spheres were generated to compare measured density with the bulk density (0.917 kg/m^3) for spherical laboratory particles. DOS aerosol was generated using a 0.05% volume solution DOS in HPLC-grade 2-propanol at 18 PSI using a triple-jet nebulizer (BGI model MRE CN24/25, Waltham, MA) and a dilution ratio of 300. The ranges of calculated densities agreed with reference material density, where COV ranged between 1.6-10.1%, for all sizes except at 30 and 55 nm which resulted in more substantial underestimation. Evaporation of DOS in the CPMA after DMA may have been most pronounced at 30 and 55 nm because of the increased vapor pressure described by the Kelvin effect for smaller particles with stronger surface curvatures. Importantly, the accuracy and precision of the DMA-CPMA remained constant and no performance drift was observed over the duration of the test program.

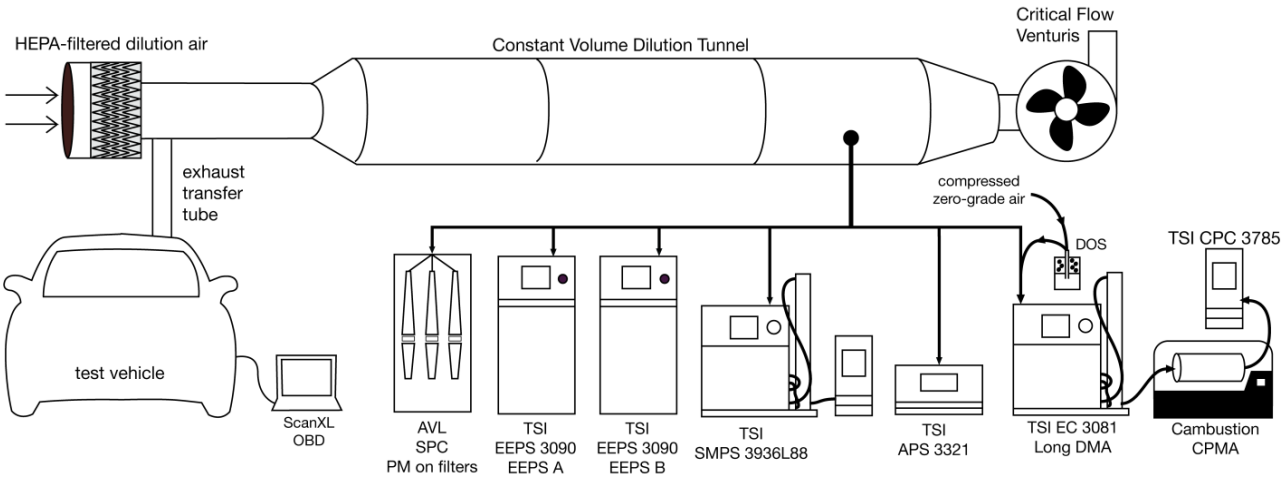

Figure 3.1. Laboratory and instrument setup during steady-state emissions testing for effective density measurement.

Prior to the study, the SMPS and the DMA used with the CPMA were challenged by particles with diameters between 30 and 240 nm that were selected by a third reference DMA.

The reference DMA was calibrated to standard polystyrene latex (PSL, Thermo Fisher Scientific, Waltham, MA, USA) spheres and was not used for experimental measurement. The average size discrepancy between reference and challenge instruments was 2% for the DMA used in tandem with the CPMA and 4% for the DMA used for the SMPS, suggesting good calibration of sample flows from the CPC and the sheath flows controlled by the TSI electrostatic classifier units. The two CPCs were checked daily for leaks by ensuring a zero reading when measuring particle-free air. Similarly, the two EEPS were challenged for verification using the reference DMA; depending on particle size, error between 5 and 40% was calculated for either unit. The discrepancy between DMA and EEPS sizing is of notable concern and is discussed as a key objective of this paper. EEPS electrodes were cleaned prior to the study using the provided acrylic cylinder and lint-free cloth, and charging needles were cleaned using forceps. Each day before testing, the units were warmed up for at least one hour, the electrometers were zeroed, and electrometer offset and noise values were recorded; the cleaning procedure was repeated once for both instruments during the study using the acrylic cylinder when offset readings exceeded the 20-fA threshold. The response of the two EEPS was averaged, although during a few tests only one instrument reported usable data.

PM mass was measured using the regulatory method by collection onto 47-mm Teflon filters (2-µm pore size, Whatman) heated to 47±5 °C at a filter face velocity of approximately 90 cm/s using an AVL Smart Sampler (model SPC 478). Filters were handled and weighed following ARB Standard Operating Procedure for the Determination of Particulate Matter (PM) Mass Collected On Filters (SOP NO. MLD145), which has specifications for charge neutralization, buoyancy correction, temperature and humidity control, and an ISO Class 6 weigh room (CARB 2012b). Quality control and assurance checks were performed on the laboratory CVS and PM

sampling equipment on a weekly basis to ensure compliance with 40 CFR parts 86 and 1066 standards for regulated pollutants (U.S. EPA 2001; U.S. EPA 2012).

3.3.2 Vehicles and Testing Conditions

Table 3.1 describes the five vehicles tested by engine size, type, PM emission rates over the FTP, key emission control technologies, and mileage. Two late model year vehicles with GDI engines were selected to evaluate particle effective density as a function of smaller engine size (2.0 L, GDI-1) to larger engine size (3.6 L, GDI-2). Two vehicles with PFI engines were evaluated, one operating on standard fuel (PFI), the other a Flex-fuel engine operating on commercially available E-85 (PFI-E85). The fifth vehicle (TDI) was operated on ultralow sulfur diesel and was equipped with a diesel oxidation catalyst, DPF, and selective catalytic reduction system. The TDI was procured and tested with low accumulated mileage (< 320 km), which

Table 3.1. Vehicles used to measure density and PM mass using IPSD over steady-state cycles.

ID	Fuel	Model Year	Make/ Model	Engine	CA Emissions Level	Emissions Technologies	PM FTP mg/mi (/km)	Mileage (10^3) km
GDI-1	E10	2013	Ford Focus	2.0-L GDI	SULEV II	TWC	0.99 (0.61)	49.2
GDI-2	E10	2014	Chevrolet Traverse	3.6-L GDI	ULEV II	TWC	2.02 (1.23)	23.1
PFI	E10	2012	Chevrolet Malibu	2.4-L PFI	ULEV II	TWC	0.29 (0.18)	43.4
PFI-E85	E85	2008	Chevrolet Impala	3.5-L PFI	ULEV II	TWC	0.10 (0.06)	92.1
TDI	ULSD	2013	Volkswagen Passat	2.0-L TDI	ULEV II	DOC, DPF, SCR, EGR, TC	0.11 (0.07)	0.32

PFI=port fuel injection, GDI=gasoline direct injection, TDI=turbo direct injection, TWC=three way catalyst, DOC = diesel oxidation catalyst, DPF=diesel particulate filter, SCR=selective catalytic reduction, EGR=exhaust gas recirculation, TC=turbocharger.

implies that the repression of stored sulfur from catalyzed after treatment may be more limited compared to vehicles later during useful life, and therefore effective density values may differ as a function of vehicle age (Swanson et al. 2009; Herner et al. 2011; Zheng et al. 2011).

Table 3.2 lists the operating conditions of each test vehicle by engine power (kW). Each power target is labeled with the percentile (%) of time the FTP test demands a vehicle power less than the value, which was calculated using target dynamometer coefficients and the FTP speed-time trace. In this paper, all parameters are reported relative to work at the engine (target coefficients), which is the sum of the dynamometer power (set coefficients) and internal mechanical resistance. Vehicle wheel speeds ranged from 40-120 km/h, and a simulated road grade between 0 and 2.5% was applied to obtain desired engine power and torque parameters. A 15-minute warm-up period preceded each 75-minute test to warm up the engine, catalyst, exhaust manifold, and exhaust transfer tube. Each condition was repeated between two to four times, resulting in over 60 hours of data collected in the study.

Figure 3.2 illustrates the two testing configurations used in this study: steady-state with constant speed (SS), and steady-state with a simulated transient (ST) operation. During ST operation, the driver was instructed to modulate the accelerator every six seconds to vary the wheel speed within a ± 3 km/h range of the target driving speed. Experimental data indicate peak acceleration typically ranged between 5 and 6 km/h-sec (3.1 and 3.8 mi/h-sec) during ST operation. This approach was used to introduce some aspects of transient operation such as changes in the injected fuel quantity and spark timing while maintaining the same average power as SS operation. Furthermore, the ST operation generated higher particle concentrations for lower loads of the PFI and TDI vehicles. At the point of density measurement, sufficient axial dispersion had occurred so that particle concentrations were constant. Although effective density

Table 3.2. Test conditions for each vehicle defined by engine power (kW), engine torque (N•m), engine speed (rpm), and percentile of power demanded during an FTP test.

GDI-1	*SS*	*SS*	*SS*		
Power (kW),	6.5 (48%)	16 (89%)	30 (99.5%)		
Torque (N•m)	40	81	107		
Speed (rpm)	1550	1900	2650		
Dilution Ratio	13.3	8.6	5.5		
exponent, $\boldsymbol{D_m}$	2.44 ± 0.06	2.45 ± 0.08	2.32 ± 0.07		
constant, ***c****	5.90 ± 1.78	6.32 ± 2.22	11.2 ± 3.65		
GDI-2	*SS*	*SS*	*SS*	*SS*	*SS*
Power (kW)	9.0 (42%)	9.0 (42%)	26 (91%)	26 (91%)	51 (99.7%)
Torque (N•m)	67	33	188	100	180
Speed (rpm)	1250	2600	1350	2500	2650
Dilution Ratio	10.1	7.7	5.8	5.2	6.3
exponent, $\boldsymbol{D_m}$	2.52 ± 0.00	2.40 ± 0.01	2.47 ± 0.05	2.40 ± 0.04	2.29 ± 0.08
constant, ***c****	4.52 ± 0.37	6.22 ± 0.47	5.46 ± 0.90	7.12 ± 1.14	17.3 ± 6.27
PFI	*ST*	*ST*	*SS*		
Power (kW)	5.4 (32%)	14 (78%)	18 (88%)		
Torque (N•m)	35	89	110		
Speed (rpm)	1500	1500	1500		
Dilution Ratio	9.4	6.9	8.0		
exponent, $\boldsymbol{D_m}$	2.68 ± 0.06	2.45 ± 0.08	2.67 ± 0.08		
constant, ***c****	2.23 ± 0.67	6.95 ± 2.71	2.47 ± 1.07		
PFI-E85	*ST*	*ST*	*SS*		
Power (kW)	6 (40%)	16 (84%)	16 (84%)		
Torque (N•m)	38	120	120		
Speed (rpm)	1500	1300	1300		
Dilution Ratio	10.4	6.5	7.8		
exponent, $\boldsymbol{D_m}$	2.52 ± 0.07	2.42 ± 0.10	2.39 ± 0.03		
constant, ***c****	3.77 ± 1.32	5.89 ± 3.00	7.33 ± 1.01		
TDI	*SS*	*SS*	*ST*	*Regeneration*	
Power (kW)	12 (87%)	16 (93%)	16 (93%)	16 (93%)	
Torque (N•m)	100	100	100	100	
Speed (rpm)	1150	1550	1550	1500	
Dilution Ratio	5.6	6.8	6.3	6.8	
exponent, $\boldsymbol{D_m}$	2.96 ± 0.04	2.59 ± 0.02	2.59 ± 0.07	2.68 ± 0.03	
constant, ***c****	1.71 ± 0.34	3.88 ± 0.33	7.86 ± 2.60	2.44 ± 1.10	

***** Following the exponential decay function in the following form given by Equation 3.4. Fitting using the mass-mobility scaling exponent are reported as average plus one standard deviation.

measured during ST operation may exhibit some characteristics of transient operation induced during certification test cycles, it does not account for some conditions such as the brief enrichment period following a cold-start, or emissions during deceleration periods.

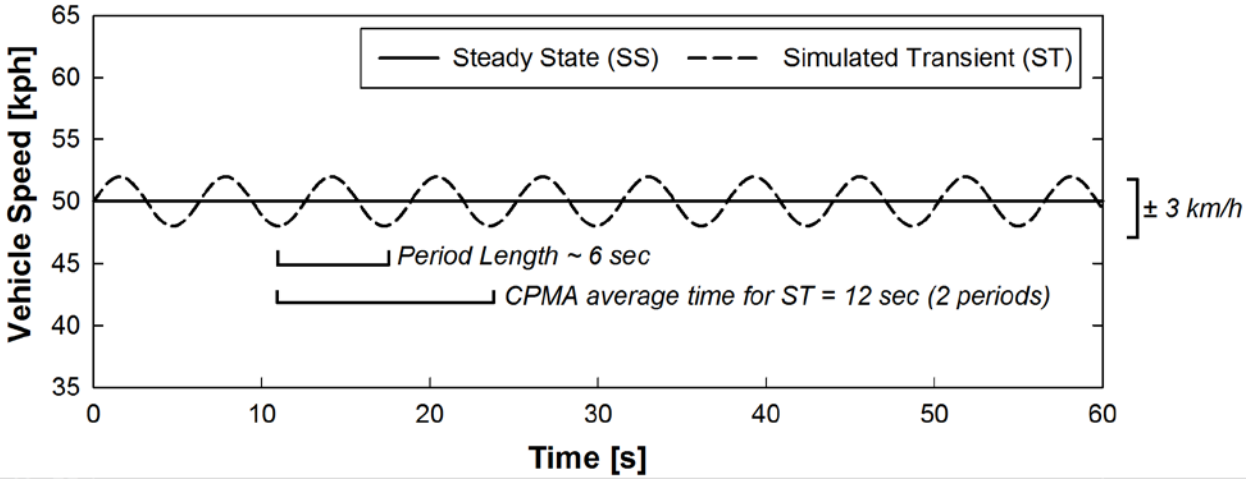

Figure 3.2. Comparison of steady-state (SS) and Transient Throttling (ST) operations at 50 km/h.

3.3.3 DMA-CPMA Operation and Analysis

Effective density was determined at seven set points between the lower boundary of interest and upper detection limit, at 30, 55, 90, 140, 210, 270, and 350 nm. The CMPA was operated with a constant transfer function, with a resolution parameter R_m between 5 and 10 (the inverse of the full width half maximum of the transfer function normalized by the mass set point), and with an averaging time of 4 seconds for SS operation, and 12 seconds for ST operation (Figure 3.2). When using a CPC 3785 aerosol flow rate of 1.0 L/min and collecting between 15 to 30 points per scan, each scan required 8 to 12 minutes. The first and last CPMA scans were made at the same DMA set point to verify density did not change for that size over the 75-minute test

sequence. In some cases, insufficient signal was generated (< 1.00 particles/cm^3 reaching the CPC 3785) and no measurement was completed.

Average particle mass was determined from CPMA spectra as shown in Figure 3.3(a), where multimodal lognormal fitting was conducted using DistFit 2009 (Chimera Technologies, Inc. Forest Lake, MN, USA) to calculate the average particle mass of all peaks corresponding to only particles carrying a single charge, $m_{p,i}$, for each DMA set point, *i*. The influence of doubly charged particles was removed by calculating the ratio of particle mass and concentration between doubly and singly charged particles transmitted by the DMA. This process involved determining the ratio between particle mobility diameter (d_p) carrying *i* and *i*+1 charges, which is a proportionality adapted from the definition of electrical mobility according to Hinds (1999) as shown in Equation 3.1:

$$\frac{d_{p,i+1}}{d_{p,i}} \propto \frac{C_{c,i+1}}{C_{c,i}} * \frac{n_{i+1}}{n_i} \qquad [3.1]$$

where *n* equals the number of charges, and C_c is the Cunningham slip correction factor. The ratio between the mobility equivalent volumes was used to calculate the ratio of the peaks as a function of CPMA mass set point. In addition, the relative concentration of doubly charged particles was calculated from the SMPS size distribution, and the positive charging efficiency of soot particles reported by Maricq (2008). This approach enabled both mass and concentration to be used to identify and remove the influence of doubly charged particles exiting the DMA that could influence results from the CPMA scan. This approach is similar to those described and implemented by Olfert et al. (2007) and Wang et al. (2010) for estimating the doubly charged particle fraction, the latter of which has been adopted as an ISO standard (ISO/DIS 27891) for particle number measurement.

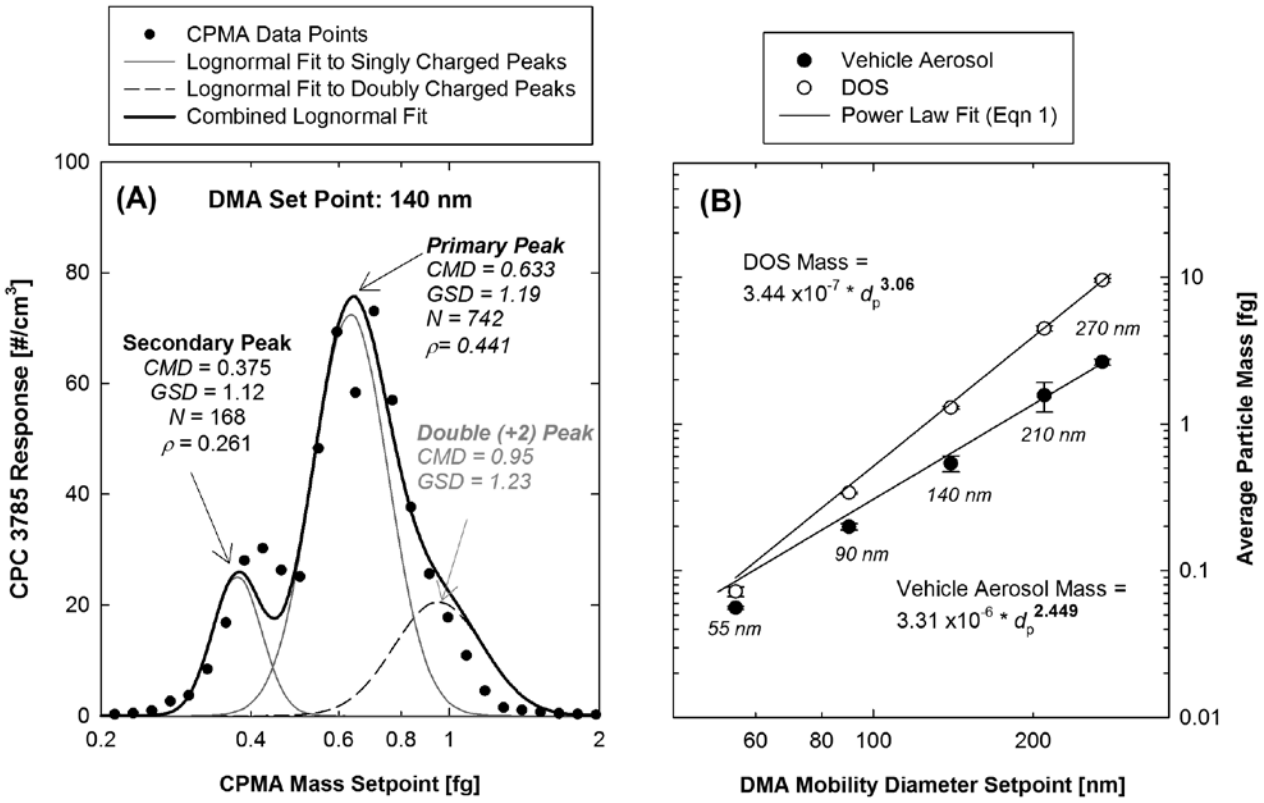

Figure 3.3. Lognormal fitting to calculate average CPMA mass, and power-law fitting to determine mass-mobility exponent for calculating effective density.

3.3.3.1 Accurate Measurements at Low Concentrations

Maricq and Xu (2004) discussed the challenge of measurement particle effective density from PFI vehicles because concentrations are generally too low to be quantified using the DMA-ELPI method. When using the DMA-CPMA method, sufficient measurement signal was generated even for very dilute particle concentrations in CVS dilution air (200-500 #/cm^3) by using the TSI water-based CPC (model 3785, d_{50}=5 nm, Shoreview, MN) which provided 0.01 particles/cm^3 readability due to the highly sensitive laser optics and good counting statistics. Instead, the bigger challenge was distinguishing vehicle and dilution air signals at low concentrations. Whenever the vehicle emissions signal was less than five times higher than

background, a separate CPMA scan was completed for the dilution air. Typically, background particle density was ~1.2 g/cm^3 irrespective of size, and peaks were clearly distinct from vehicle aerosol densities (~0.3-0.8 g/cm^3).

3.3.3.2 Particle Mass-Mobility Scaling Exponent and Effective Density

Schmidt-Ott et al. (1990) determined the mass of a particle, m_p, as a function of its mobility diameter d_p, mass constant b, and its mass-mobility scaling exponent D_m assuming primary particle density is constant, as expressed by Equation 3.2:

$$m_p = b * d_p^{D_m} \qquad [3.2]$$

The mass-mobility scaling exponent expresses the change of particle mass with respect to mobility diameter according to nanoparticle aggregate theory of primary particle spherules (Lall and Friedlander 2006; Sorensen 2011).

Particle effective density, ρ_{eff}, is defined as the particle mass m_p divided by the mobility equivalent spherical volume. Equation 3.3 shows the adapted equation for particle effective density from previous studies (e.g. Skillas et al. 1998; McMurry et al. 2002; Park et al. 2003; Olfert et al. 2007):

$$\rho_{eff} = \frac{m_p}{\frac{\pi}{6} d_p^3} \qquad [3.3]$$

Equations 3.2 and 3.3 then are combined to express particle effective density (g/cm^3) as a function of a new constant c (= 6b/π, a.u), mobility diameter d_p (nm), and mass-mobility scaling exponent D_m as shown in Equation 3.4:

$$\rho_{eff} = c * d_p^{D_m - 3} \qquad [3.4]$$

In order to properly determine the mass-mobility scaling exponent, agglomerates should have a reasonable number of monomers enabling an infinite number of conformations. Therefore, measurements at 30 nm were excluded from the fitting procedure used to obtain D_m, because the agglomerate size approaches within a factor of two primary particle diameter, which ranges between 10 and 25 nm for engine exhaust (Wentzel et al. 2003; Maricq and Xu 2004). Fitted values of D_m depend on flow regime, which in this study spanned the transition and continuum regimes (Sorensen 2011). Therefore, in order to compare D_m among operating conditions enabling a variable number of density measurements at unique DMA set points, this analysis is limited to the same five DMA set points between 55 and 270 nm inclusive. Table 3.2 reports fitted D_m according to Equation 3.2 and calculated c according to Equation 3.4 for each test condition using Pearson's least-squares regression.

Typically, fractal dimension is used to characterize the change of mass with size for a truly fractal agglomerate comprised solely of primary particle spherules. However, vehicle emissions contain solid primary particle spherules that are agglomerated during combustion and semi-volatile materials that condense onto solid particle cores during dilution and cooling. Therefore, the fitted mass-mobility scaling exponent characterizes the change of total particle mass (and density) with size. This approach is useful for defining effective density functions that can be used to estimate suspended PM mass.

The selection of an appropriate fitting method to the power law function is important because it determines the relative weighting of each mass point. The least squares regression used in this study minimizes total residuals, and because particle mass spanned about two orders of magnitude, greater weight is placed on larger particle sizes (DMA set point = 270 nm) than on smaller particle sizes (DMA set point = 55 nm). Some early vehicle exhaust studies (e.g.

Ristimäki et al. 2002; Virtanen et al. 2002) used a method to weight particles by relative number abundance in the distribution; therefore reported fractal dimension (actually mass-mobility scaling exponent) weighted more heavily the smaller nucleation mode particles. Other fitting methods would be able to equally weight each point. However, this study used the least squares regression to allow larger particles to carry more weight because of their larger mass contribution when evaluating the IPSD method.

3.3.3.3 EEPS vs. SMPS

Particle size distribution (PSD) was measured over SS and ST conditions using an SMPS and two different units of the same EEPS model. The EEPS is carefully calibrated by the manufacturer using traceable PSL aerosol. However, its performance is uncertain particularly when measuring fractal engine exhaust containing a mixture of several chemical compounds (Oh et al. 2004; Asbach et al. 2009; Kaminski et al. 2013; Zimmerman et al. 2014). The EEPS does not adapt its inversion routine to account for differences in particle charging due to particle morphology. Therefore, EEPS and SMPS distributions were compared over a breadth of engine technologies and a wide range of engine conditions. The Differential Mobility Spectrometer (DMS500, Cambustion Ltd.) does account for particle morphology effects on particle charging by calibrating the instrument with soot and PSL but it was not tested here. In order to use the SMPS (Wang and Flagan 1990) as a reference size distribution instrument, proper transport and instrument response times need to be calculated and incorporated into a calibrated DMA and CPC (Russell et al. 1995). Bimodal fits were derived according to the same methodology described in Section 2.3.6.3, and applying the same lognormal equation presented in Equation 2.2.

3.4 Results

3.4.1 Particle Mass-Mobility Scaling Exponent and Effective Density

Figure 3.3(a) shows the lognormal fitting procedure used to determine average particle mass of 140-nm particles selected by the DMA during the 16-kW test of the GDI-1 vehicle. In this case, the CPMA scan reported three peaks: a primary peak centered at 0.633 fg with ρ_{eff} = 0.441 g/cm^3, a secondary peak centered at 0.375 fg with ρ_{eff} = 0.261 g/cm^3, and a doubly charged peak centered at 0.95 fg that was subtracted from the distribution before calculating average mass. In many cases, only two peaks were observed, a primary peak and its doubly-charged equivalent.

Fitting, using the power law described by Equation 3.2, determined mass-mobility scaling exponents as illustrated in Figure 3.3(b). One standard deviation of the measurement of each size is shown in the error bars. In Figure 3.4, symbols represent measured data points, and best fit lines represent the fitting according to the power law model following Equation 3.4. The fitted values for D_m and c are listed in Table 3.2 by engine operating condition.

3.4.1.1 GDI-1 and GDI-2

The effective densities for GDI-1 and GDI-2 are plotted in Figures 3.4(a) and 3.4(b), respectively. The emissions from GDI-1 had similar particulate effective density among all operation conditions, decreasing from ~0.7 g/cm^3 at 30 nm to ~0.2-3 g/cm^3 at 350 nm. In contrast, the particle effective density of GDI-2 particulate emissions was higher at 55 nm (~0.9 g/cm^3) during 51-kW SS operation compared to all other conditions. However, particle effective density for 51-kW operation converged with other conditions for 270 nm and larger. When operating GDI-2 at higher engine speeds but maintaining constant power, particle effective density decreased between 10-20% for all sizes, and average mass-mobility scaling exponent

decreased from either 2.52 (9-kW) or 2.47 (26-kW) to 2.40, resulting in lighter and less compact particles.

The effective densities of exhaust emissions from GDI-1 and GDI-2 were similar for smaller particles at 30 nm (0.65-0.8 g/cm^3) and also for larger particles at 350 nm (0.2-0.3 g/cm^3), despite differences in engine size (2.0-L versus 3.6-L) and PM emissions rates over the FTP cycle (0.99 versus 2.02 mg/mi (0.61 and 1.23 mg/km)). However, the mass-mobility scaling exponent of the emissions decreased to ~2.3 as power approached 100% of the calculated FTP maximum for both GDI-1 (30 kW) and GDI-2 (51 kW). The mass-mobility scaling exponents were significantly lower during these 100% FTP tests than any other GDI test when applying a two-sided Rank Sum Test for $\alpha = 0.05$. It is possible that due to higher exhaust temperature, catalyst efficiency increased thereby reducing emissions of high molecular weight hydrocarbons and semi-volatile compounds to fill the soot void space. Up to this point, density measurements can be grouped as: (i) gasoline GDI, which thus far includes the average of GDI-1 and GDI-2 emissions, and (ii) the average of the 30-kW operation of GDI-1 and 51-kW operation of GDI-2, both operating at ~100% of FTP, hereafter, gasoline GDI FTP-max.

3.4.1.2 PFI and PFI-E85

Figure 3.4(c) shows the effective densities measured from the gasoline PFI vehicle; these are the first reported densities from PFI engines in the literature. The trend of all the PFI density functions is similar to those from GDI emissions; namely, density decreases with increasing particle size from ~0.6-0.7 g/cm^3 at 30 nm to ~0.2-0.3 g/cm^3 at 350 nm for all conditions. However, important subtleties for PFI emissions are apparent from a careful analysis of the fitted

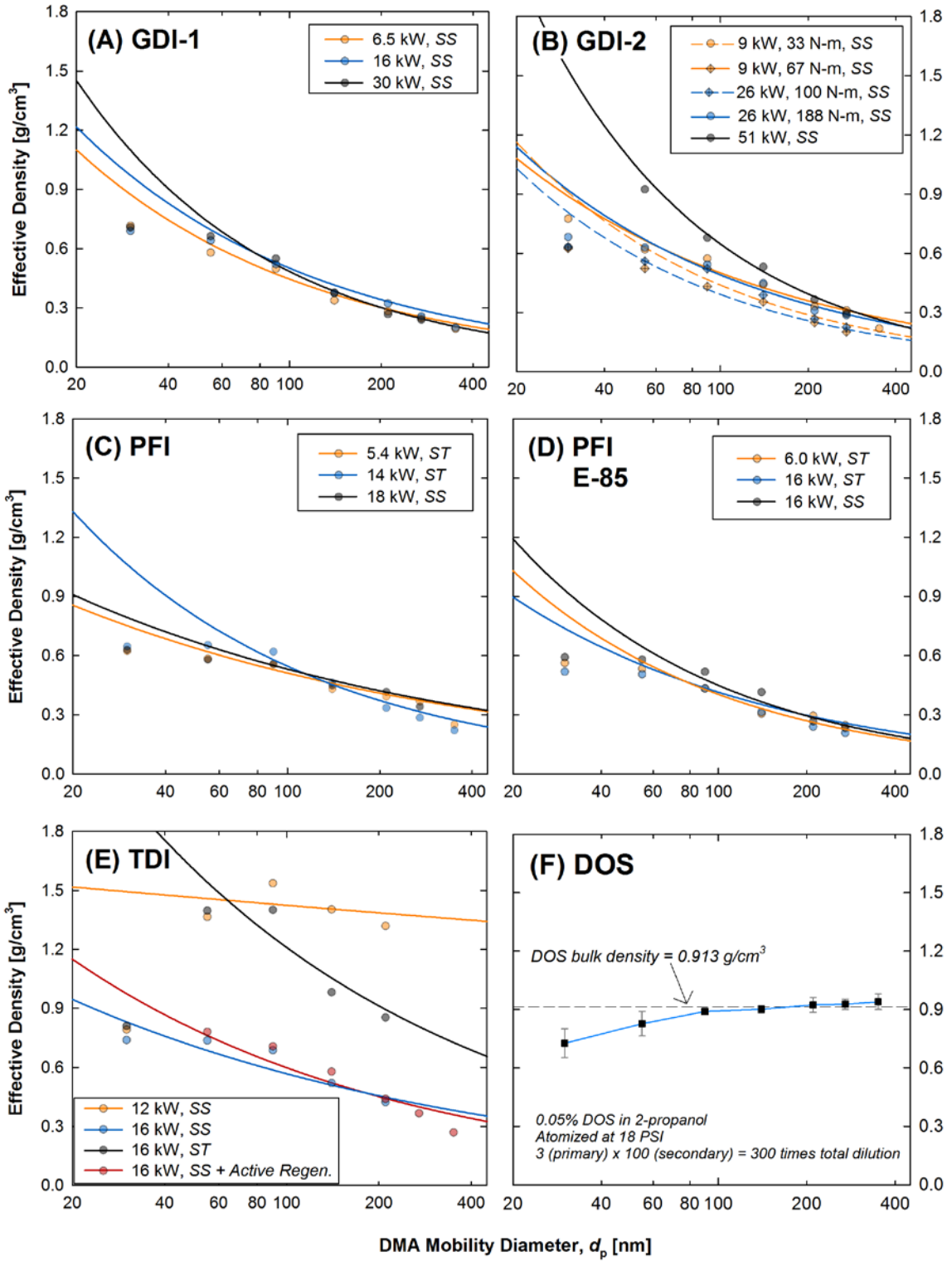

Figure 3.4. Fitted particle effective density functions and raw data points by condition as a function of electrical mobility diameter for (a-e) the five light-duty vehicles and (f) the atomized DOS.

mass-mobility scaling exponents. ST operation under lower load (5.4 kW) or SS operation under high load (18-kW) resulted in significantly higher ($\alpha = 0.05$, two-sided Rank Sum Test) mass-mobility scaling exponents (d_m=2.68 and 2.67, respectively) than during 14-kW ST operation (d_m=2.45). These emissions from PFI engines are more spherical than GDI emissions, suggesting less soot formation as a result of homogenous fuel mixing during combustion. The instantaneous high loads elicited during 14-kW ST operation may have induced more heterogeneous fuel mixtures, which increased soot formation, resulting in the lower mass-mobility scaling exponent. Therefore a third new category of particle effective density will be defined: (iii) PFI gasoline, the average of the 18-kW SS and 5.4-kW ST conditions.

Figure 3.4(d) shows the effective densities measured from the PFI-E85 vehicle were lower than the PFI gasoline vehicle for all sizes. However, the trends between the two vehicles were similar. Nucleation mode particles measured at 30 nm were roughly equivalent to the effective densities measured at 55 nm, between 0.5 and 0.6 g/cm^3, and particle effective density was a decreasing function of particle diameter reaching 0.2-0.3 g/cm^3 at 270 nm. Unlike the PFI gasoline particle effective density functions, the calculated density curves from the PFI-E85 were not a strong function of operation condition, where mass-mobility scaling exponent of vehicle exhaust from the PFI-E85 ranged from ~2.4-2.5. Although the PFI-E85 vehicle does not use direct fuel injection, the mass-mobility scaling exponent was more comparable to GDI emissions, and the particle effective density function was lower than PFI and GDI emissions. Therefore, its particle effective density function is grouped into a fourth category (iv): PFI-E85, the average of 6-kW ST, 16-kW ST, and 16-kW SS operations.

3.4.1.3 TDI

Figure 3.4(e) presents the effective densities calculated from the TDI vehicle, also the first time in the literature particle effective density has been measured downstream of a DPF. For two of the three conditions (12-kW SS and 16-kW ST), effective densities were dramatically greater than for all other conditions; the effective densities ranged between 0.9 and 1.6 g/cm^3 between 30 and 210 nm. During 12-kW SS operation (87% of FTP), the mass-mobility scaling exponent was 2.96 ± 0.04, indicating nearly spherical particles. The high mass-mobility scaling exponent suggests the DPF effectively removes fractal-like soot, where remaining particles are solid refractory particles or those formed by nucleation of higher molecular weight semi-volatile materials downstream of the DPF as has been shown in heavy-duty applications (e.g. Kittelson et al. 2006; Biswas et al. 2008), . Under an increased vehicle load during 16-kW SS and 16-kW ST operation (92% of FTP), mass-mobility scaling exponent decreased to ~2.6, possibly due to the passage of fractal soot agglomerates due to diminished DPF filtration efficiency or higher engine soot production. However, particle effective density remained higher during ST operation (0.9-1.4 g/cm^3) than during SS operation (0.3-0.8 g/cm^3) at the same power output.

An active DPF regeneration was triggered automatically by the engine control module for an approximate 10-20 minute period during each of the 16-kW SS test cycles in this study (approximately every 320 km). The active regeneration event was characterized by an increase in oxidation catalyst temperature from 270 to 490 °C, which resulted in CVS particle number concentration increasing by two to three orders of magnitude. Interestingly, active regeneration occurred during the 16-kW SS operation and produced a particle effective density which is nearly equivalent to our observation during the 16-kW SS operation without active regeneration.

3.4.1.4 Literature Comparison

3.4.1.4.1 Gasoline Vehicles

As presented in the previous section, particle effective densities for gasoline vehicles are grouped into four relevant and statistically significant groups: (1) gasoline GDI, defined by all measurements from GDI-1, GDI-2 except those denoted hereafter, (2) gasoline GDI FTP-max, defined by arithmetic mean density measured 30-kW SS operation of GDI-1 and 51-kW SS operation of GDI-2, (3) gasoline PFI, defined by the arithmetic mean of the 5.4-kW ST and 18-kW SS operation, and (4) PFI-E85, defined by the arithmetic mean of all three test conditions of the vehicle. Table 3.3 presents these parameters for calculating particle effective density using mass-mobility scaling exponent and the defined constant in Equation 3.4.

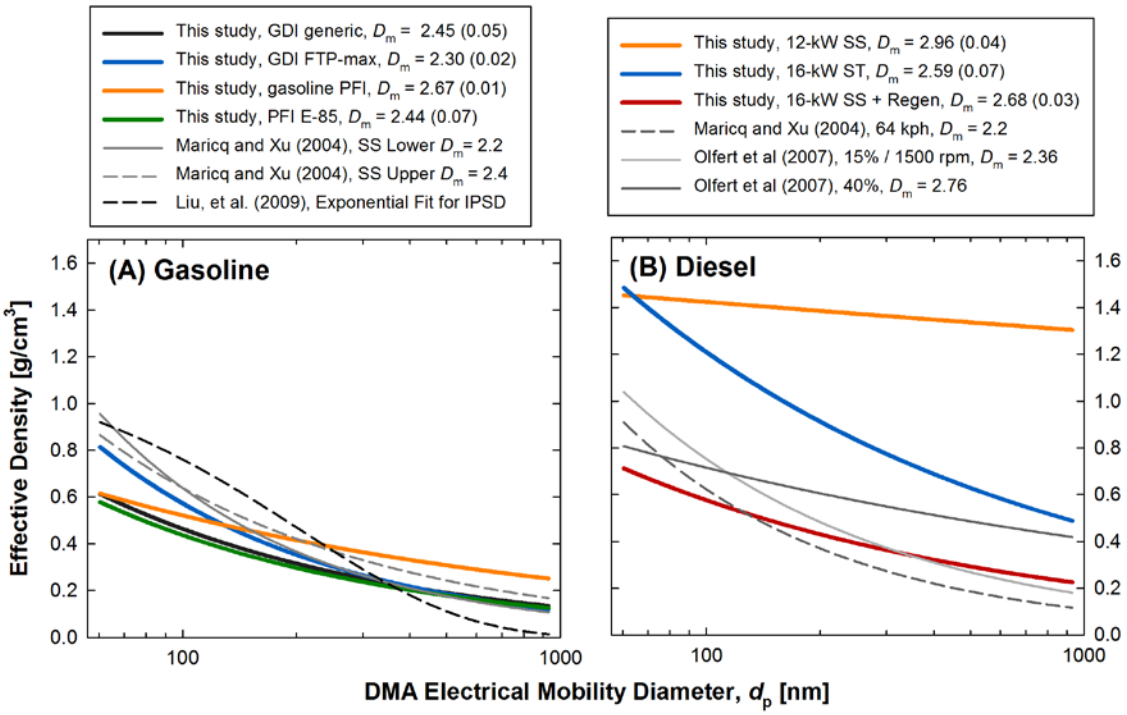

Figure 3.5. Consolidated density functions for (a) gasoline and (b) diesel vehicles in this study compared to other selected studies.

Table 3.3. Coefficients for average gasoline particle effective density functions in Figure 3.5(a).

	(i) Gasoline GDI	**(ii) Gasoline GDI FTP-max**	**(iii) Gasoline PFI**	**(iv) Gasoline PFI-E85**
exponent, $\boldsymbol{D_m}$	2.45 ± 0.05	2.30 ± 0.02	2.67 ± 0.01	2.44 ± 0.07
constant, $\boldsymbol{c}$	5.95	14.3	2.35	5.97

The widely recognized evaluation of gasoline particle effective density was conducted by Maricq and Xu (2004) using a Direct Injection Spark Ignition, or DISI vehicle, which is now known as GDI. The authors reported a mass-mobility scaling exponent of 2.3±0.1 using the DMA-ELPI method for a range of operating conditions. The curves shown in Figure 5(a) for gasoline emissions were plotted using mass-mobility scaling exponents of 2.2 and 2.4 while *c* was determined iteratively until the value calculated for 60 nm equaled the graphically presented data in the literature. All measurements of emission from gasoline vehicles in this study show a lower density at 55 nm (0.6-0.8 g/cm^3) than those reported by Maricq and Xu (2004). The density at larger particle sizes closely matches for all conditions (gasoline GDI, gasoline GDI FTP-max, and gasoline E85) except for gasoline PFI, which demonstrated a higher mass-mobility scaling exponent and therefore greater particle effective density for larger sizes.

Figure 3.5(a) also plots the density function, which Liu *et al.* (2009) presented as an exponential fit to Maricq and Xu (2004) data. The exponential fitting process provides a smooth transition between the flat density function of nucleation-mode particles to the power law decay empirically fit to larger fractal-like particles. However, the exponential fit model deviates from measured data at larger sizes and underestimates the particle effective density, whereas the power fit law provided good fit to experimental data up to 350 nm. This underestimation provides some explanation of the underestimation of PM mass for our initial evaluation of the IPSD method (Li et al. 2014).

3.4.1.4.2 Diesel TDI

Figure 3.5(b) presents particle effective density measured for the TDI diesel equipped with a DPF and the data compared to other diesel engines without a DPF. Olfert et al. (2007) demonstrated higher DOC temperatures at high engine loads promotes homogenous nucleation of sulfate (SO_2 to SO_3 conversion), which condenses onto fractal agglomerates and increases mass-mobility scaling exponent: d_m=2.76 at 40% compared to d_m =2.36 at 15% load of the same light-duty diesel vehicle. Maricq and Xu (2004) reported d_m = 2.3 from testing of another light-duty diesel vehicle at 64 and 112 km/hr, which ostensibly did not result in loads high enough to result in nucleation and condensation of sulfate because mass-mobility scaling exponent did not increase substantially when increasing vehicle load. Our measured effective densities and mass-mobility scaling exponents were in agreement with previous evaluations only for the 16-kW SS operation, where density decreased from ~0.8 to 0.3 g/cm^3 between 55 and 270 nm according to d_m=2.59. The effective densities measured during 12-kW SS and 16-kW ST operation were notably higher than any previous evaluation, beginning around 1.4 g/cm^3 at 55 nm and decreasing according to d_m = 2.96 ± 0.04 and d_m = 2.59 ± 0.02, respectively. The high particle effective density measured during 12-kW SS and 16-kW ST operations were not due to hydrated sulfate, because DOC temperature was only sufficiently high to promote SO_2 to SO_3 formation during active regeneration, which resulted ironically in the lowest effective densities equivalent to 16-kW SS operation.

3.4.2 Evaluation of IPSD Over Steady-State Cycles

3.4.2.1 Derivation of SMPS-to-EEPS ratios

Figure 3.6(a) shows the lognormal fitting procedure used to quantitatively relate EEPS and SMPS size distributions. A bimodal fit was applied to each distribution in order to segregate the smaller nucleation mode particles (diameter 10-30 nm) from the larger accumulation mode particles (diameter >30 nm) that are expected to have different physical properties producing measurement bias between the two instruments. Figure 3.6(b) shows the SMPS-to-EEPS ratios for each vehicle, averaged over all operating conditions evaluated. The ratios were impacted by operating condition, most especially TDI emissions. The average for each vehicle is presented, and the average of all the vehicles is shown by the thick solid black line. The average of all test

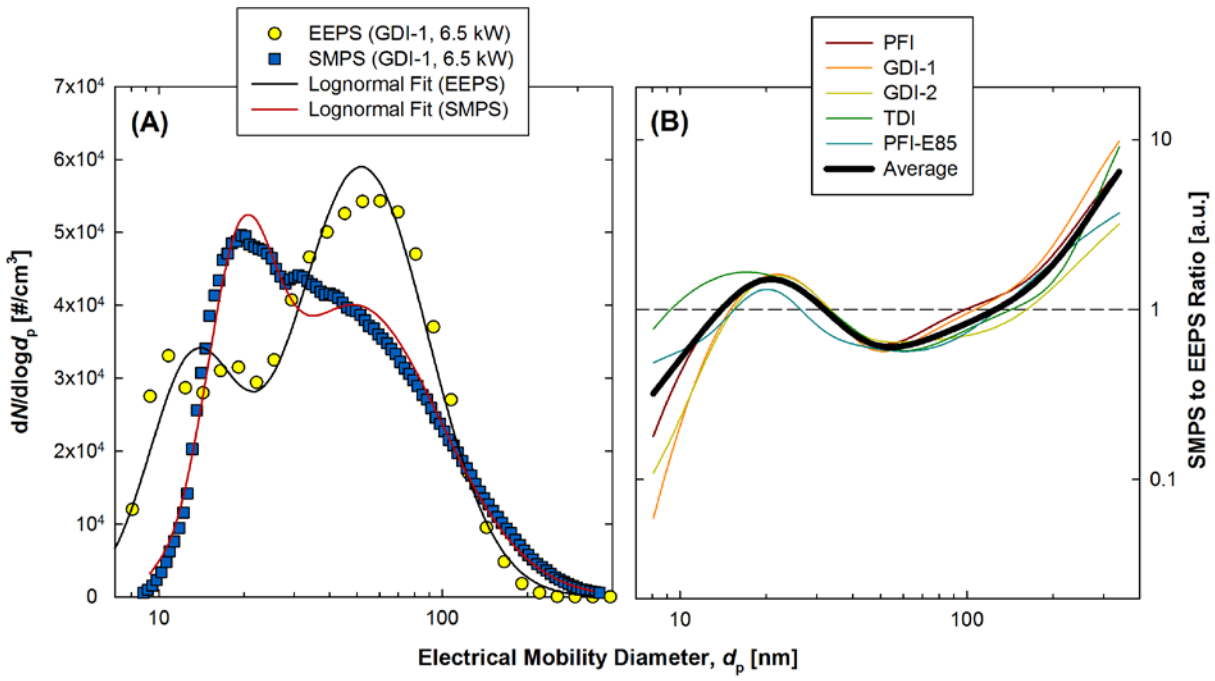

Figure 3.6. (a) The bimodal fitting approach for comparing the size distributions measured by the SMPS and the EEPS, and (b) the average SMPS-to-EEPS ratios as a function of mobility diameter.

conditions can be quantitatively expressed using Equation 2.2 and the following inputs derived from the data N_1=0.99 N_2=1.9 N_3=20 GSD_1=1.5 GSD_2=3.0 GSD_3=1.9 CMD_1=19 CMD_2=56 and CMD_3=750.

Based on the study-average function, the EEPS overestimated particle concentrations from 20 to 100 nm, and underestimated smaller and larger particles. These results are strikingly similar to a recent evaluation by Zimmerman et al. (2014) who reported EEPS overestimation at 20 and 120 nm relative to the SMPS when measuring diesel exhaust. The underestimation of larger particles between 100 and 560 nm is important, for these particles contribute greater particle mass than smaller particles, and therefore this issue would need to be addressed when applying IPSD. Therefore, the five functions shown in Figure 3.6(b) were applied to correct EEPS data to evaluate the improvement by correcting to an SMPS equivalent.

3.4.2.2 Size Distributions

Figure 3.7 presents the mass distributions based on corrected EEPS, SMPS, and APS distributions during two selected tests. For graphical purposes only, the mobility and aerodynamic diameters were combined using a similar approach discussed by Khlystov et al. (2004) using particle effective density functions measured in this study to convert aerodynamic distributions to a mobility diameter equivalent using Equation 3.5:

$$\rho_{\mathrm{e}}(d_{\mathrm{p}}) * d_{\mathrm{p}}^2 * C_{\mathrm{c}}(d_{\mathrm{p}}) = \rho_0(d_{\mathrm{a}}) * d_{\mathrm{a}}^2 * C_{\mathrm{c}}(d_{\mathrm{a}}) \qquad [3.5]$$

where d_{p} is the mobility diameter as previously defined, d_{a} is the aerodynamic diameter, C_{c} is the Cunningham slip correction factor as a function of respective diameter, and ρ_0 is unit density according to the definition of aerodynamic diameter.

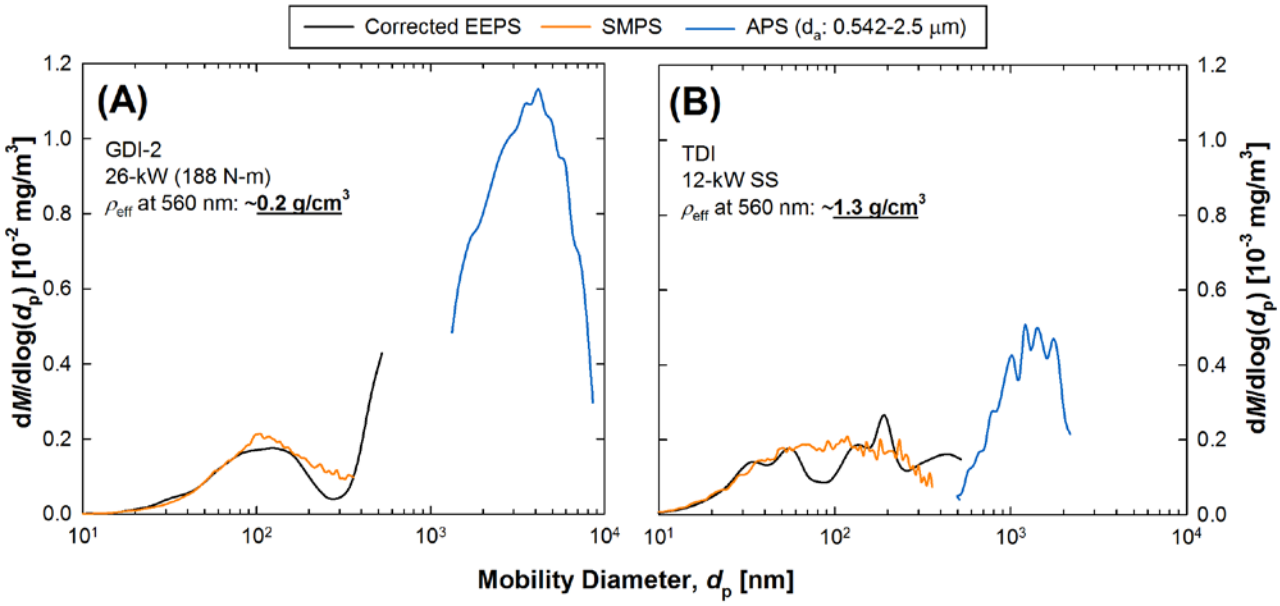

Figure 3.7. Particle mass distributions shown from the corrected EEPS, SMPS, and APS where particle effective density is (a) less than 1 g/cm^3 and (b) greater than 1 g/cm^3 at 560 nm.

Figure 3.7(a) presents size distributions measured by the EEPS and APS during 26-kW (188 N•m) operation of GDI-2. In this case, particle effective density at 560 nm (~0.2 g/cm^3) was lower than unit density (1.0 g/cm^3), and the APS range (d_a=0.54-2.5 μm) becomes extended to 1,300-8600 nm when converted into mobility diameter. This illustrates a gap between measurement ranges and that some PM is not sampled by either measurement approach. For other conditions as shown in Figure 3.7(b) for the 12-kW SS operation of the TDI diesel vehicle, particle effective density at 560 nm (1.2-1.3 g/cm^3) is larger than unit density, and the referenced APS range is condensed to 510-2,200 nm on a mobility scale. In this scenario, there is a theoretical small overlapping measurement range. Therefore for simplicity, the contribution of larger particles is calculated by the sum of the aerodynamic fraction measured by the APS between 0.54 and 2.5 μm, and the mobility fraction measured by the EEPS or SMPS.

Accordingly, the conversion of aerodynamic diameter to mobility diameter with Equation 3.6 is merely to graphically illustrate the overlap or gap in the measurement ranges shown in the figure.

3.4.2.3 Correlation with gravimetric method

Gravimetric filter samples were collected to evaluate the IPSD method over SS and ST cycles using (a) uncorrected EEPS data, (b) corrected EEPS data, and (c) SMPS data shown in Figure 3.8. Uncorrected EEPS data show the best correlation to gravimetric data (R^2=0.84), followed by SMPS (R^2=0.79) then corrected EEPS data (R^2=0.67). However, the IPSD method persistently underestimated gravimetric PM mass by 50-64% as shown by the slope of the black dashed lines in each panel. When considering the contribution of larger particles between 0.54 and 2.5 µm in aerodynamic diameter measured by the APS (ρ_0 = 1 g/cm^3, by definition), bias was virtually eliminated between gravimetric and IPSD methods using corrected EEPS + APS distributions (slope = 1.031) and SMPS + APS distributions (slope = 1.029). Good fit was achieved when combining either corrected EEPS or SMPS with APS measurements (R^2=0.96 and 0.97); however, visual scatter in the low measurement range (<0.3 mg/mi / 0.18 mg/km) was greater for the corrected EEPS data shown in Figure 3.8(b) compared to the SMPS data shown in Figure 3.8(c). Nevertheless, corrected EEPS data showed reduced measurement bias against the gravimetric method compared to the uncorrected data (slope = 1.031 versus 0.892), suggesting some measurement improvement when applying the empirically derived correction ratio.

No positive or negative residuals were observed in the correlation between the gravimetric and IPSD methods down to at least 0.01 mg/mi (0.006 mg/km) as shown in Figure 3.8(c) for the SMPS + APS. This suggests filter loadings were dominated by particle-phase emissions during the 75-minute steady-state tests conducted in this study, and is consistent with IPSD tunnel blank

calculations. The suspended mass contributions in the dilution air affecting IPSD detection limit were calculated based on SMPS (constant ρ_{eff} = 1.2 g/cm^3) and APS (unit density) data during tunnel blank procedures, resulting in a calculated suspended mass concentration of ~0.6 µg/m^3, which equates to 0.014 ± 0.010 mg/mi (0.0087 ± 0.0062 mg/km) over the SS and ST sequences. Nevertheless, gaseous adsorption may still impact filter measurement variability, especially during transient FTP certification tests that are of shorter duration (~32 min for a three-phase test).

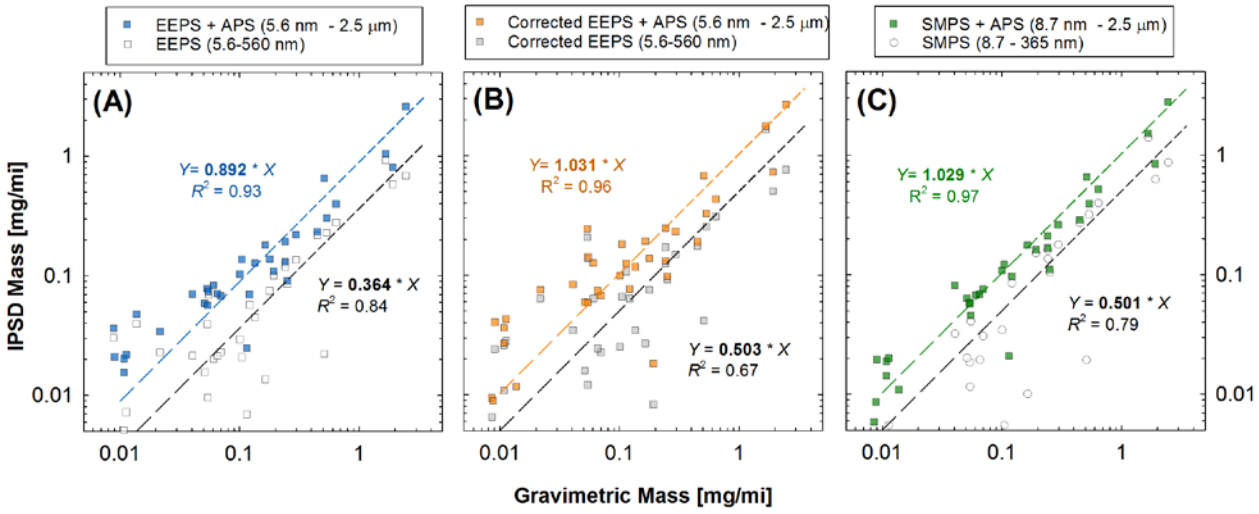

Figure 3.8. Correlations between IPSD and gravimetric mass during steady-state cycles using (a) the EEPS and APS, (b) the EEPS with correction and APS, and (c) the SMPS and APS.

3.4.2.4 Size Fraction Mass Contributions

Figure 3.9 presents the size fractional contributions during the steady-state and single FTP tests by the following delineations: mobility diameters of 5.6-100 nm, 100-340 nm, and 340-560 nm based on corrected EEPS data, and aerodynamic diameters between the nominal 560 nm and the 2.5 µm APS. The average filter-based PM emissions factors for each cycle are indicated above each column for reference.

The smallest size fraction (5.6-100 nm) indicates the mass contribution from ultrafine PM, which contributed less than 25% of total mass in most cases. This fraction was substantially greater (~65%) during 51-kW SS test of GDI-2, where a dominant nucleation mode was observed. The ultrafine PM mass contribution was less than 5% for all tests conditions of the PFI-E85, including the single FTP test. Otherwise, there was no trend associated between operating conditions or vehicle engine load and the contribution from ultrafine PM.

The largest size fraction (560 nm – 2.5 µm) measured by the APS varied dramatically between 2% and 80%. There was variability between the two GDI vehicles evaluated over steady-state cycles; the fractional contributions ranged 10-40% for GDI-1 and 25-72% for GDI-2. The largest fraction was observed for the 16-kW ST operation of the PFI-E85 vehicle. The contribution of larger particles was minimal from the DPF-equipped TDI diesel vehicle, even during active regeneration, in contrast to our previous work for heavy-duty diesel regeneration (Chapter 2). However, the larger particles were observed during 16-kW ST operation, where the removal efficiency of the DPF may have declined during higher bursts of exhaust flow. This observation is consistent with the decreased mass-mobility scaling exponent observed

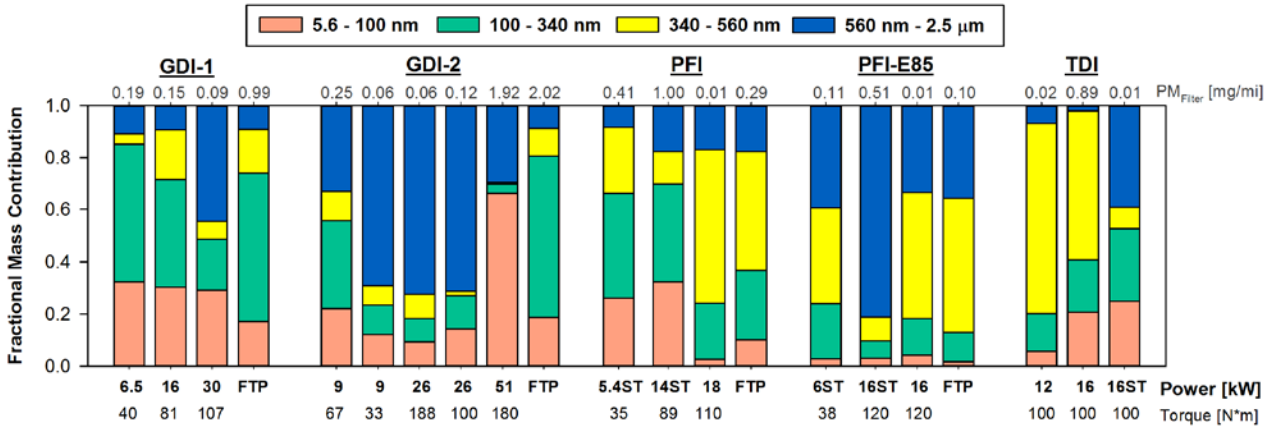

Figure 3.9. Size fractional mass as measured by corrected EEPS data for steady-state and transient conditions.

from the density function. During each of the single FTP tests, the fractional contribution of larger PM beyond the EEPS measurement range ranged between 9 and 35%.

3.5 Discussion and Conclusion

The effective densities of the four gasoline vehicles tested in this study (i.e. two GDI, a PFI, and a flex-fuel PFI operating on E85) were largely consistent with the first evaluation of GDI emissions made by Maricq and Xu (2004). These results suggest gasoline particle effective density functions may continue to remain robust to evolving emissions reduction strategies, and can be used for accurately measuring mass emissions from future generations of vehicles that are not equipped with gasoline particulate filters. Each particle effective density function is summarized by a power law model (Equation 3.4) and coefficients used to fit measured data between 55 and 270 nm are listed in Table 3.3. The dataset of gasoline density functions is reduced into four summary functions: gasoline GDI, gasoline GDI FTP-max, gasoline PFI, and gasoline PFI-E85. Particle effective density functions measured from the TDI vehicle are reported as measured, and defined by the four conditions listed in Table 3.2.

These particle density functions can be applied to measure PM mass emissions from size distributions measured between 55 and 270 nm. Measured data for larger sizes (i.e. 350 nm) fit to the power law model well, and therefore, the parameters can be used to estimate particle effective density for larger mobility diameters. For smaller particles, effective density typically plateaus, and in some cases, increases between 30 and 55 nm. Further investigation could help better understand this increase; for example a thermodenuder could be used to examine the influence of organic and sulfate concentrations on particle effective density and mass-mobility

scaling exponent. Therefore, as a general rule, the authors recommend using the calculated value at 55 nm for smaller particles.

The TDI vehicle was procured immediately prior to the test program and underwent typical testing preparation procedures. The accumulation and release of sulfur compounds has been documented to occur during field aging of diesel aftertreatment devices (Swanson et al. 2009; Herner et al. 2011). Therefore, the future release of hydrated sulfate during active regeneration periods where DOC temperature was sufficiently high may result in elevated particle effective density (~1.5 g/cm^3) for nucleation mode particles (Zheng et al. 2011). Although our density functions were measured near these values, during active regeneration periods when catalyst temperature was sufficient to promote sulfate nucleation, lower density functions were measured. Therefore, caution should be exercised when applying these particle density functions to vehicles with higher quantities of accumulated mileages, such as during the useful life period. Moreover, additional evaluation of diesel passenger cars equipped with advanced aftertreatment is needed to better understand the influence of vehicle operating condition on particle effective density and mass-mobility scaling exponent because TDI particle effective density varied considerably by operating condition based on our measurements.

The comparison of particle effective density between SS and ST operation could indicate the impact of transient operation on effective density. As presented in discussion of PFI density in Figure 3.4(c), the combination ST operation and high engine load (14-kW, 78% of FTP) appeared to result in some degree of heterogeneous fuel mixtures as evidenced by the lower mass-mobility scaling exponent during this condition. The mass-mobility scaling exponent calculated during the 14-kW ST operation of the PFI gasoline vehicle resembled that of the GDI gasoline generic function (D_m=2.45). Thus, transient driving conditions during an FTP

certification test could result in PFI particulate emissions resembling the density and mass-mobility scaling exponents closer to those from GDI vehicles. The gasoline and diesel functions defined in this study could be used to develop a density matrix for each point in the FTP speed-time trace.

Good linear correlation was found between the gravimetric and IPSD methods when applying the new particle effective density functions to size distribution measured by the EEPS (R^2 = 0.84); however, the IPSD method underestimated gravimetric mass by 64%. When using the APS to measure the contribution of larger particles between 0.54-2.5 μm aerodynamic diameter, measurement bias between the methods was lowered to less than 3%, and fit improved dramatically (R^2 = 0.96). Even stronger correlation between ISPD and gravimetric methods was achieved, with little measurement bias when using the SMPS instead of the EEPS with the APS (R^2=0.97). The good agreement of IPSD and gravimetric methods has previously been shown by Liu et al. (2012), but our results indicate that approximately half of PM mass lay within the SMPS range (8.7-365 nm). Liu et al. (2012) configured their SMPS to measure particles over a wider range, 15-660 nm, and in addition, calculated PM mass between 10 and 1000 nm by applying a lognormal fit equation. In principle, this fitting method should be valid; however, the actual measurement of size distributions provides a better measure of particulate mass than estimation by lognormal fit models.

In Figure 3.6, SMPS and EEPS size distributions are compared using lognormal fitting curves over all the SS and ST cycles in this study. As a proof of concept refining the EEPS inversion method, EEPS data were corrected to an SMPS equivalent using these empirically derived equations. Measurement bias between IPSD and gravimetric methods was reduced using the corrected versus uncorrected EEPS; however, increased scatter was observed for tests

emitting less than 0.3 mg/mi (0.18 mg/km). Future work could evaluate the Cambustion DMS, which is commercially available and has been calibrated directly using fractal-like vehicle PM. The contribution of larger particles measured by the APS could be further evaluated using a Dekati ELPI to measure smaller and larger particles up to 10 µm using a single aerodynamic distribution. However, similar to the EEPS, both the DMS and the ELPI utilize electrometer signals to calculate concentration, and therefore may still be fundamentally limited by a high detection limit and a biased response depending on calibration method.

In summary, this work presents particle effective density functions from two late model year GDI vehicles, and for the first time, two PFI vehicles, and a diesel passenger car equipped with a DPF. Over the SS and ST cycles measured, gravimetric and IPSD methods exhibited excellent agreement for steady-state emissions over the emission ranges evaluated ($R^2 > 0.96$). Virtually no measurement bias was observed between the methods when combining measurements from an EEPS or SMPS with an APS to capture particle emissions up to 2.5 µm. These data underscore the importance of defining measurement size range when performing real-time PM measurement. Moreover, these results are based on the measurement of steady-state emissions, and the IPSD method should be fully evaluated over transient test cycles, such as the FTP and US06.

4 MEASURING PARTICULATE EMISSIONS OF LIGHT DUTY PASSENGER VEHICLES USING INTEGRATED PARTICLE SIZE DISTRIBUTION (IPSD)

4.1 Abstract

The California Air Resources Board (ARB) recently adopted the Low Emission Vehicle (LEV) III particulate matter (PM) standards, which requires, among other limits, vehicles to meet 1 mg/mi over the Federal Test Procedure (FTP). One alternative measurement approach evaluated to support implementation of the LEV III standards is Integrated Particle Size Distribution (IPSD), which reports suspended PM mass using size distribution and effective density. IPSD was evaluated using size distribution and gravimetric filter data from over 250 tests from 34 vehicles at ARB's Haagen-Smit Laboratory (HSL). IPSD mass was persistently lower than gravimetric mass by 57-75% over the FTP tests and 81-84% over the Supplemental FTP (US06) tests. The limited size range of the TSI Engine Exhaust Particle Sizer (EEPS, 5.6-560 nm) appears to be the key contributor to the negative bias, precluding the adoption of IPSD as a standalone measurement method for PM. Nonetheless, the covariance of the methods among repeat tests of vehicles with emissions greater than the tunnel background level (0.17 mg/mi) indicates emissions variability does not originate from measurement uncertainty. The correlation between suspended and filter-based mass measurements provides additional information to better understand gravimetric measurement variability at or below the LEV III standards.

4.2 Introduction

Chronic exposure to ambient particulate matter (PM), a mixture of natural and anthropogenic solid and semi-volatile constituents, is associated with increased cardiopulmonary morbidity and

mortality (Pope and Dockery 2006; Brook et al. 2010). Exposure to primary PM from mobile sources has been well characterized (Fenger 1999; Zhu et al. 2002b; Westerdahl et al. 2005; Gauderman et al. 2007; Hu et al. 2012; Choi et al. 2013; Quiros et al. 2013), and has been linked directly to adverse health outcomes (Lloyd and Cackette 2001; EPA 2002; Hill et al. 2009). Over the past decades, the California Air Resources Board (ARB) has implemented several mobile source control programs resulting in widespread emission reductions (May et al. 2014), and recently ARB adopted new PM standards for the Low Emissions Vehicle (LEV) III standards as part of the Advanced Clean Cars program. Beginning with MY 2017 and MY 2025, the current 10 mg/mi PM standards will decrease to 3 mg/mi and 1 mg/mi, respectively, over the Federal Test Procedure (FTP) (CARB 2012a). The LEV III PM standards also include other requirements over the Supplemental FTP (US06) test cycle as well as in-use emissions limits.

One objective of the LEV III package was to reduce the PM emissions standard to control emissions backsliding. Over compliance with the current PM standard may have dissipated as gasoline port-fuel injection (PFI) technology is replaced with gasoline direct injection (GDI) technology that offers greenhouse gas emissions benefits (Chase et al. 2000; CARB 2011b; Maricq et al. 2011; Liang et al. 2013). Although most PFI vehicles would have already complied with a 1 mg/mi standard, the measurement precision at these low levels has not been thoroughly investigated. Since the adoption of the LEV III standards, ARB and the U.S. Environmental Protection Agency have begun evaluating gravimetric measurement capabilities of PM emissions below 1 mg/mi using the existing filter-based gravimetric method defined in 40 CFR Parts 86, 1065, and 1066 (Hu et al. 2014). Nevertheless, ARB has continued to evaluate several alternative measurement approaches to better understand variability observed at emission levels below 1 mg/mi and to investigate potential lower-cost measurement approaches. Furthermore, although

California vehicle PM emission standards and health impacts have thus far been defined on a mass basis, a growing body of evidence suggests health effects are also associated with alternative metrics such as particle number and surface area (Wichmann et al. 2000; Donaldson et al. 2001; Sager and Castranova 2009; HEI 2013). Other alternative methods ARB is evaluating to determine PM measurement feasibility include the solid particle number (SPN, >23 nm) standard adopted by the European Union (Ayala et al. 2008), and the so-called "AVL" method that combines a composite filter measurement of PM with a real-time metric such as black carbon to apportion PM to the various phases of the FTP (Bushkuhl et al. 2013; Kamboures 2015).

Another alternative method for PM mass measurement is Integrated Particle Size Distribution (IPSD) (Liu et al. 2009). IPSD uses a measurement of real-time particle size distribution (PSD), where number distribution is converted into a volume distribution assuming spherical particles, and then volume is then converted into mass by applying a size-resolved particle effective density function (Maricq and Xu 2004; Oh et al. 2004; Asbach et al. 2009; Swanson et al. 2010; Sorensen 2011; Kaminski et al. 2013; Zimmerman et al. 2014). The IPSD method has previously exhibited reduced variability and a good one-to-one relationship with gravimetric mass measurements when characterizing emissions from heavy-duty diesel trucks (Liu et al. 2009; Liu et al. 2012). Effective density of particulate emission of light-duty gasoline vehicles has been measured by Maricq and Xu (2004), and the work in Chapter 3 sought to determine effective densities for GDI and PFI gasoline vehicles, and a light-duty diesel vehicle (LDD) with a diesel particulate filter (DPF). Hereafter, all diesel vehicles will be referred to as LDD and they will be assumed to be equipped with a DPF unless otherwise specified.

Our initial hypothesis was that real-time size distributions could be used to calculate PM mass more rapidly, cost effectively, and accurately than using existing measurement procedures. We test this hypothesis using a comprehensive dataset including 168 FTP and 87 US06 tests, from 34 different vehicles that included PFI, GDI, and LDD technologies. Size distributions were all measured between 5.6 and 560 nm using the TSI EEPS to calculate cycle-average PM emissions (M_{IPSD}) for comparison with CFR-compliant gravimetric filter measurements (M_{GRAV}). Second, this work evaluates trends in total particle number and surface area emissions derived from EEPS size distributions, which are compared to gravimetric PM.

4.3 Methods

4.3.1 Test Cycles Evaluated

Testing was conducted at the ARB Haagen-Smit Laboratory (HSL) in El Monte, CA. Data were collected in three of the light-duty test cells that were each equipped with a 48-inch single-roll electric chassis dynamometer, a constant volume sampler (CVS), and a PM sampling system that meets requirements defined by 40 CFR 1065 (CFR 2011). Each test included gravimetric filter sampling using Teflon media downstream of a cyclone (cutoff 2.5 µm). A detailed description of the test cells and typical operational procedures can be found in Hu et al. (2014). An FTP certification test includes a cold-start Urban Dynamometer Driving Schedule (UDDS) and a hot-start UDDS weighted by 0.43 and 0.57, respectively. This study included both three-filter and two-filter tests as defined in CFR Part 1066.801(b) options 1 and 2, respectively (U.S. EPA 2012). Tunnel blank filters were collected regularly, but subtraction was not conducted for this evaluation to avoid introducing uncertainty associated with blank-subtraction methods. US06 tests were measured using a single filter following an initial US06 test and 90-sec hot soak

period. In total, 168 FTP tests and 87 US06 tests were completed, and additional information including vehicle make, model, year, and mileage are listed in Tables S1 and S2 in Supporting Information. Test fuels included both certification- and commercial-grade gasoline containing between 0 and 10% ethanol, and only commercial-grade ultralow sulfur diesel was used (< 15 ppm sulfur).

4.3.2 EEPS Size Distribution Measurement and Correction

The TSI EEPS was used to measure particle size distribution between 5.6 and 560 nm, and because testing was conducted in three test cells concurrently over a period of a few years, four different physical units were used, running firmware versions between 3.05 and 3.11. The EEPS uses a unipolar diffusion and field charger that generates a positive corona to induce a high degree of charge onto particles, which are then classified using 22 electrodes providing size distribution over 32 channels (Johnson et al. 2004). The manufacturer-recommended maintenance procedures were followed, including regular cleaning of the electrode surfaces, using an acrylic cylinder and a lint-free cloth, and charging needles using forceps. A small portion of routine laboratory PM mass and size distribution data were rejected because of invalid PM sampling criteria (e.g. filter temperature violation) or size distribution errors (e.g. EEPS flow or charger needle voltage errors). The EEPS has been widely used to measure transient PSD (Kittelson et al. 2006; Wang et al. 2006), but it has been shown to underestimate the concentration of fractal-like exhaust particles with diameters greater than 100 nm relative to an SMPS reference (Asbach et al. 2009; Jeong and Evans 2009; Wang et al. 2009b; Xue et al. 2014; Zimmerman et al. 2014). To correct for this discrepancy, EEPS size distributions were multiplied by the average SMPS-to-EEPS ratio measured during the steady-state operation of

five light-duty vehicles under low and high loads determined in Chapter 3. Figure 4.1 shows an example of this correction, which results in about a ten percent increase in PM mass when applied to the size distributions measured during this project. In this case, the SMPS provides a more accurate reference size distribution when proper transport and instrument response times are calculated between a calibrated DMA and CPC. Refer to Chapters 2 or 3 for more details on the correction procedure.

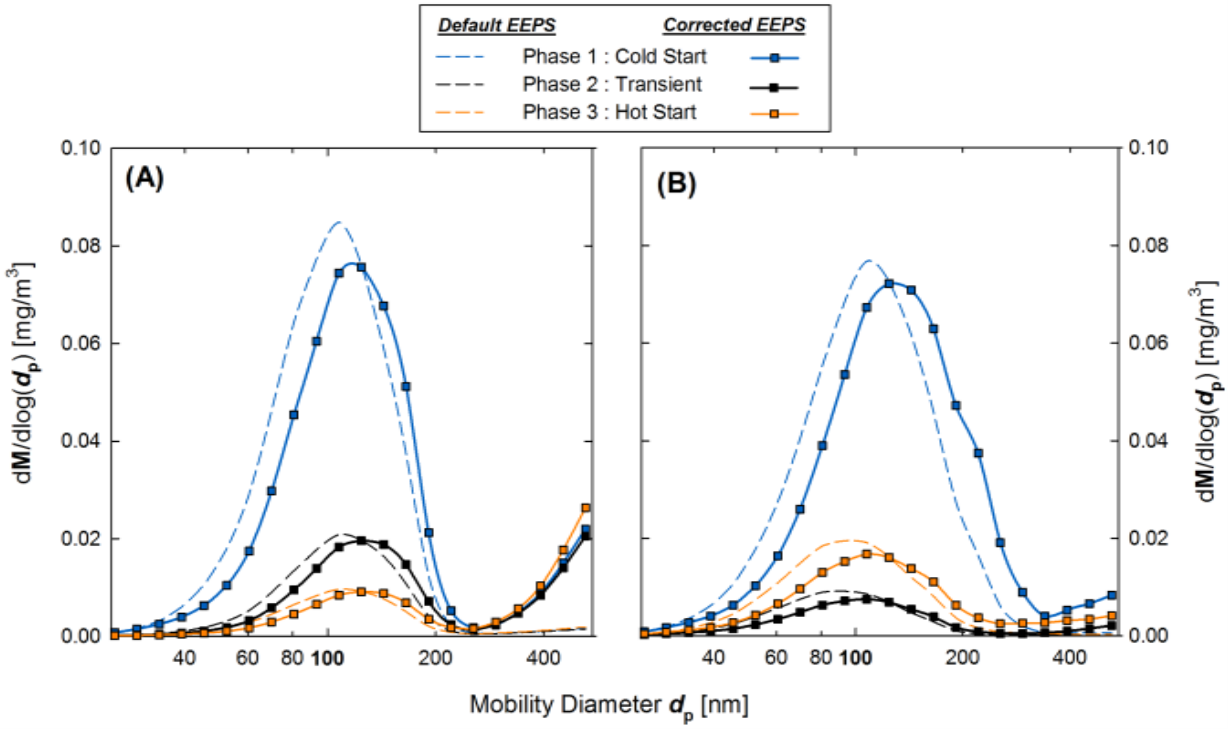

Figure 4.1. Mass distributions for a selected PFI and GDI vehicle test.

The corrected data in Figure 4.1 show the development of a second mass mode that was not observed before applying the correction. As indicated by several previous studies and the steady-state evaluation in Chapter 2, the EEPS underestimates size distribution relative to the SMPS, and this bias increases with increasing particle size. Accordingly, the correction

increases the largest size bin (centered at 523 nm) by a factor of 13.9, which may vary between EEPS units. Henceforth, the development of a second mode with mass median diameter (MMD) centered above the EEPS measurement range should be verified with an instrument with a larger measurement range.

4.3.3 Calculating IPSD Mass, Surface Area, and Number

Size distributions were used to calculate three moments, or parameters, of IPSD, which included the following: total number (N_{IPSD}); active surface area (SA_{IPSD}) by weighting mobility diameter (d_p) by an exponent of 1.4 (Jung and Kittelson 2005); and, particle mass (M_{IPSD}) following Equation 4.1:

$$M_{\mathrm{IPSD}} = \sum_i [\rho_{\mathrm{eff},i} * \left(\frac{\pi}{6} {d_{\mathrm{p},i}}^3\right) * n_i] \qquad [4.1]$$

where $\rho_{eff,i}$ is the effective density, d_p is the mobility diameter, and n_i is the measured number concentration for size bin i. IPSD calculations were derived from EEPS measurements of diluted vehicle exhaust, whereas gravimetric measurements and CVS parameters are reported at standard conditions (T=293.15 K and P=1013 mbar). The EEPS measurements were corrected to standard conditions using the proportionality of pressure (P), volume, and temperature (T) following the ideal gas law, which experimentally resulted in an average 3.0 ± 0.6% and 7.1 ± 2.0% increases for real-time calculations for the FTP and US06 tests, respectively.

Figure 4.2 presents the effective density functions used in this study, which were calculated by the power fit law presented in Equation 4.2:

$$\rho_{\mathrm{eff}} = c * d_{\mathrm{p}}^{D_{\mathrm{m}}-3} \qquad [4.2]$$

where effective density (g/cm^3) is a function of electrical mobility d_p (nm), a constant c (dimensionless), and mass-mobility scaling exponent (D_m). The transition from the effective

density of nucleation-mode to larger accumulation-mode particles, which typically dominate the size distributions of vehicular emissions, is described well by an exponential fit model (Liu et al. 2009; Swanson et al. 2010). However, deviation from experimental data is observed with increasing particle size, and therefore the power fit law expressed in Equation 4.2 is more appropriate for reporting particle mass emissions by IPSD. The density of smaller particles is assumed equivalent to the calculated value at 55 nm, which generally fits measured data shown in Chapter 3 and in Maricq and Xu (2004), and agrees with the empirical approach for calculating coefficients c and D_m based on fractal aggregate theory (Sorensen 2011). The effective density functions are generally robust to engine load for PFI and GDI vehicles, but

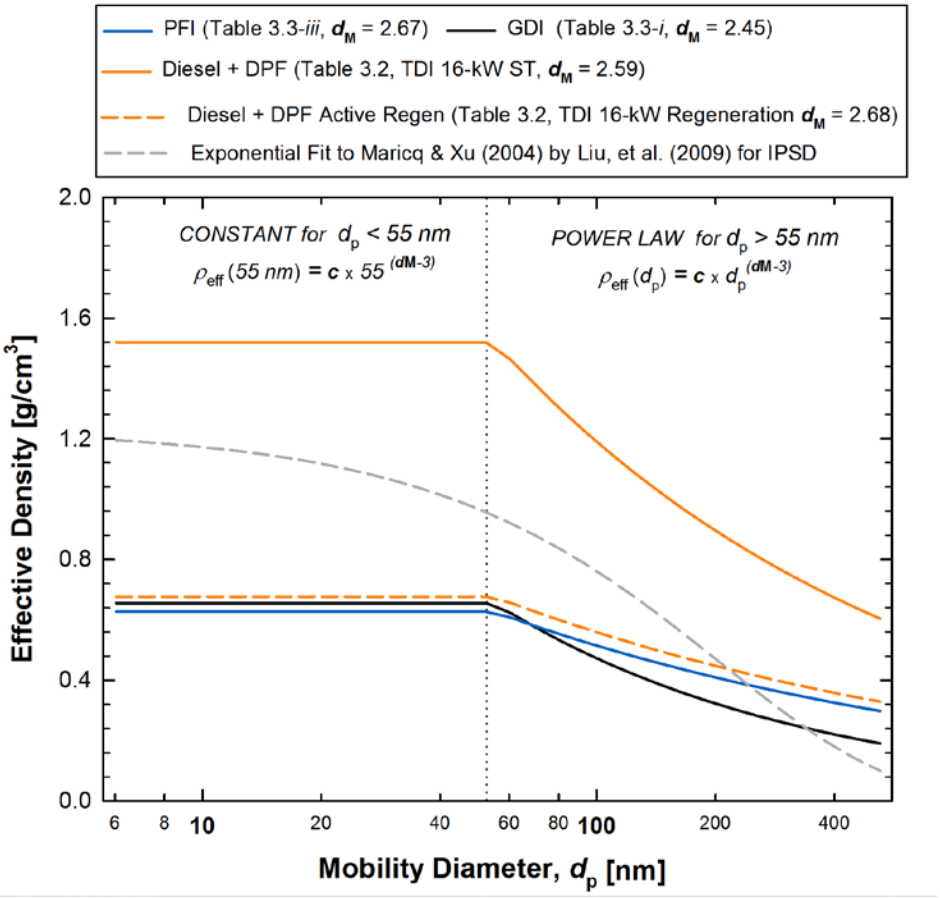

Figure 4.2. Particle effective density functions applied to the FTP and US06 test cycles.

differs more for LDD vehicles (Chapter 3). However, even for LDD vehicles, static effective density functions were used for all time points in the transient cycle because time-resolved functions had a negligible impact on final mass. Density functions were applied based on vehicle technology rather than test cycle, except for one US06 test of a LDD that included an active DPF regeneration as shown in Figure 4.2. The density functions derived in Chapter 3 of this dissertation were developed explicitly for their application to FTP and US06 data in this paper.

4.4 Results and Discussion

4.4.1 Real-Time PM Mass and Size Distribution

Figure 4.3 presents real-time and cumulative IPSD mass for the following selected tests of each engine technology: one PFI (2011 Nissan Altima, M_{GRAV} = 0.99 mg/mi), one GDI (2010 Volkswagen Jetta, M_{GRAV} = 1.69 mg/mi), the same GDI retrofit with a prototype gasoline particulate filter (GPF) (M_{GRAV} = 0.22 mg/mi), and one LDD (2013 Volkswagen Jetta Tdi, M_{GRAV} = 0.11 mg/mi). The first acceleration of the FTP resulted in the maximum emissions rate for gasoline vehicles, especially for the GDI vehicle that produced emissions peaking around 0.4 mg/sec. The first 45 seconds of the phase includes three distinct accelerations, during which about 25% and 55% of cumulative PM was emitted from the PFI and GDI vehicle, respectively. Figure 4.4 shows these two vehicles were each tested multiple times and a similar cold start trend was observed during each repeat test. Elevated cold start emissions for GDI vehicles have been widely reported (Samuel et al. 2010; Zhang et al. 2010; Maricq et al. 2013; Li et al. 2014), and

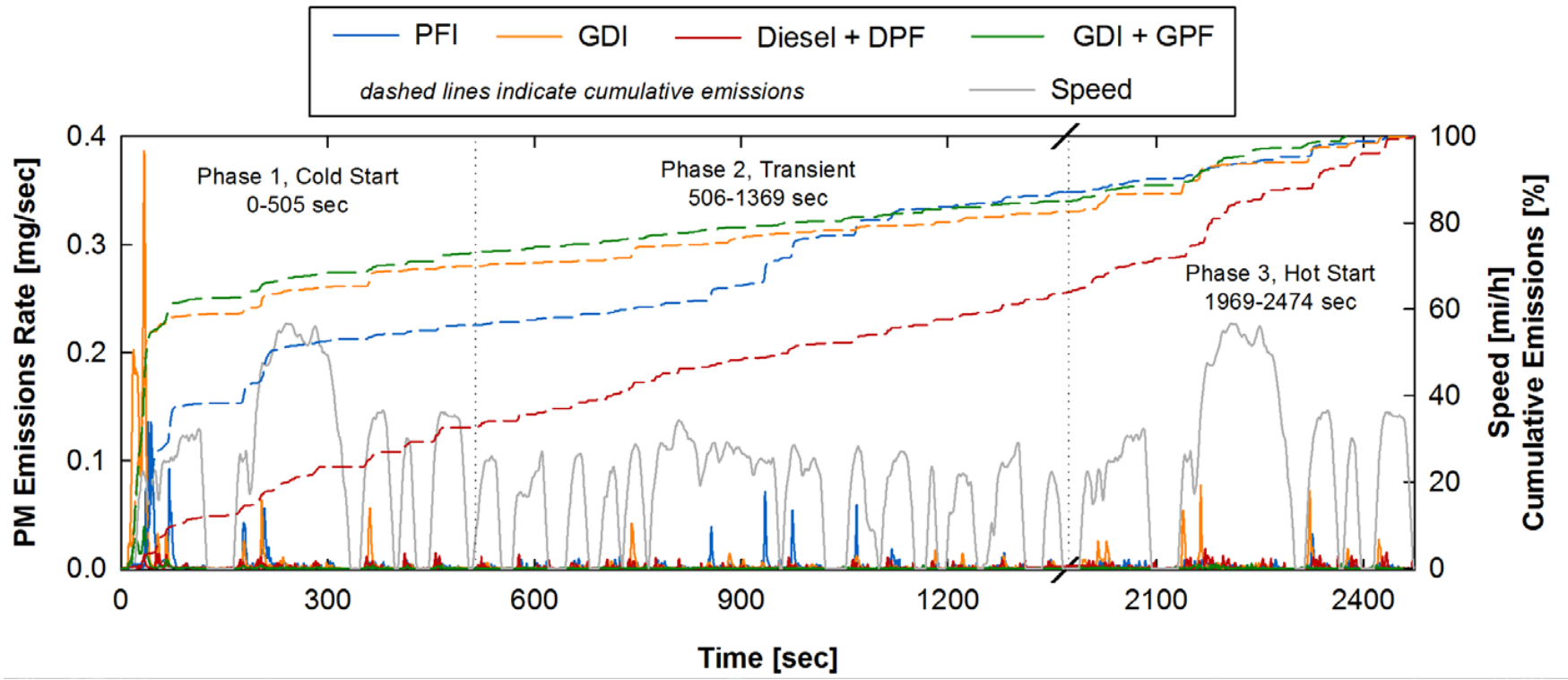

Figure 4.3. Real-time and cumulative PM emissions over three-phase FTP cycles for four LDV technologies.

this phenomenon is attributable to cylinder wall and piston surface wetting before temperatures are sufficient for rapid evaporation. Although PFI emissions typically produce lower PM emissions following cold start, due to the injection of premixed fuel, Figure 1 shows that real-

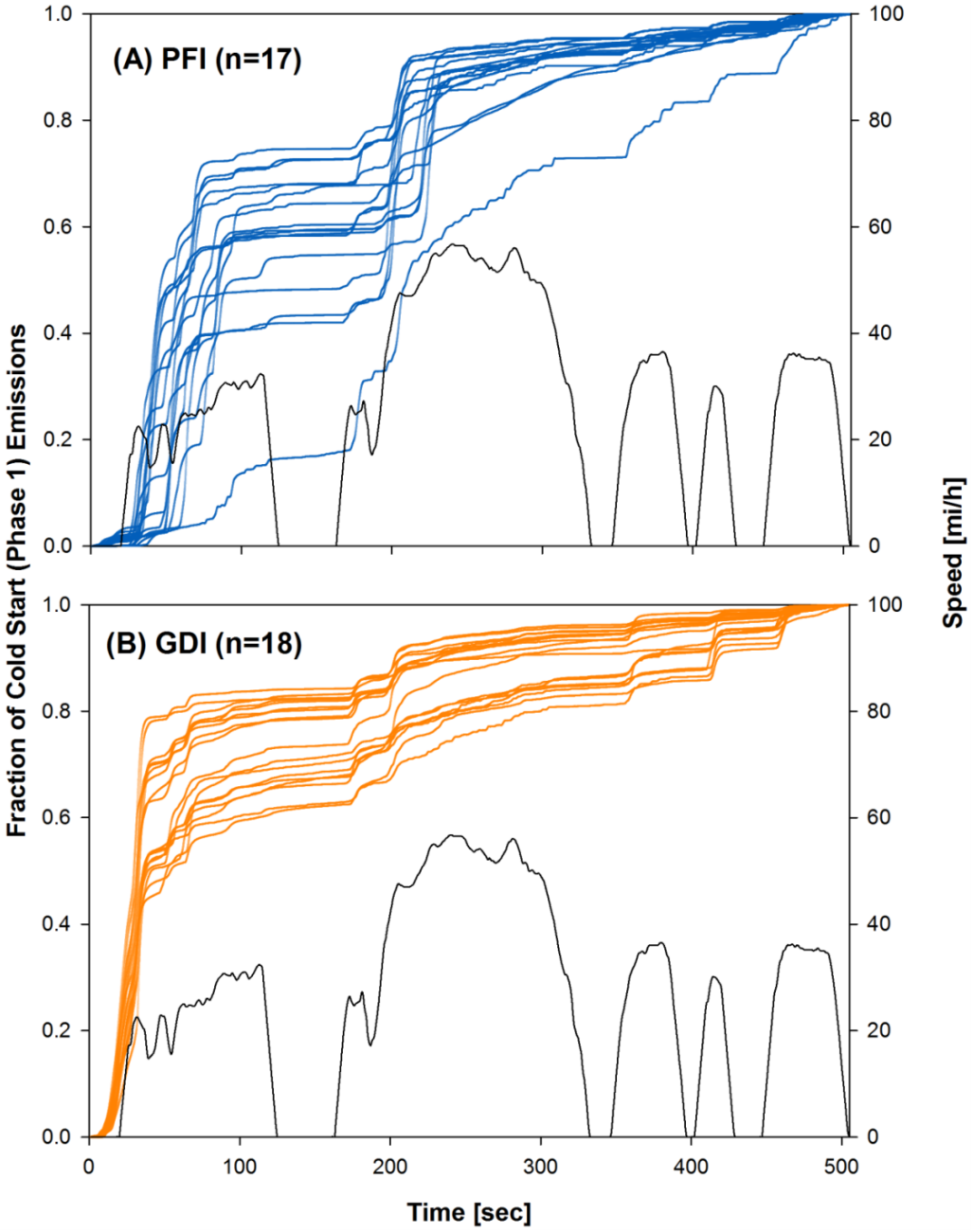

Figure 4.4. Comparison of PM mass emissions during Phase 1 for repeat tests of a PFI and GDI vehicle.

time emissions, in some instances, can be higher, such as during the successive accelerations during the Transient Phase between 800 and 1100 seconds. In contrast to the gasoline vehicles, the LDD emitted at a near constant rate over the FTP, which is consistent with unfiltered diesel emissions (Maricq et al. 1999). The impact of emission following engine cold-start can be assessed by calculating the ratio between phases 1 and 3 because the driving traces are identical. The study-average average and standard deviations of the ratios, without considering any flow weighting, were 5.9 ± 2.0 for GDI, and 2.7 ± 0.9 for PFI, and 1.8 ± 1.9 for LDD.

Figure 4.3 also illustrates the PM emissions reductions associated with either a wall-flow DPF or GPF. When equipped with the GPF, PM emissions were reduced by 87% relative to the test without the GPF. Fill state, or soot loading on the inner filter surfaces strongly impacts removal efficiency; Chan et al. (2014) showed a removal efficiency range of 73-88% for BC comparing an empty to filled GPF. The fill state of the GPF on the GDI was unknown at the time of testing. Importantly, the cumulative PM emissions of the GDI with and without the retrofit GPF were nearly identical, even during cold start conditions, indicating the removal efficiency was a constant percentage of engine-out PM upstream of the GPF.

Figure 4.5 shows the phase-average MMD and geometric standard deviation (GSD) of emissions from each of the vehicles shown in Figure 4.3. Annotations indicate the MMD and GSD (in parentheses) for the primary peak of each phase; the primary and secondary peak lognormal parameters are listed in Table 4.1. The emissions from gasoline vehicles were consistent among phases, and MMD and GSD ranged between 112-132 nm and 1.40-1.59, respectively. The peak concentration and width of the primary peaks were larger for the GDI (~0.1 mg/m^3 and GSD ~1.51-1.59) than PFI vehicle (~0.08 mg/m^3 and GSD ~1.40-1.44). However, the both GSDs were smaller than the value of 1.8 that is generally regarded as

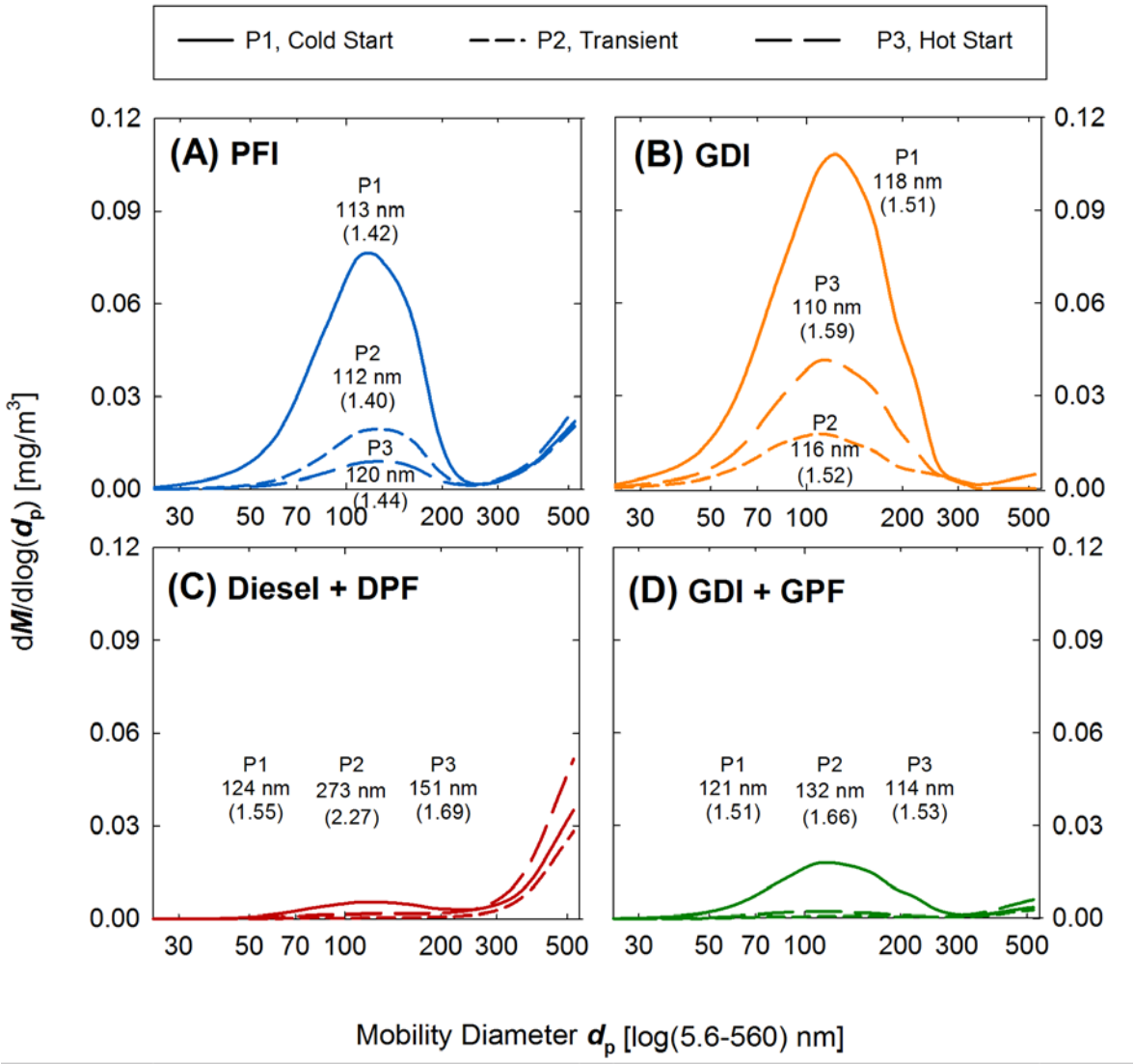

Figure 4.5. Particle mass distributions by phase for four LDV vehicle technologies.

universal for GDI emissions (Maricq et al. 2013). The MMD of the diesel vehicle ranged between 124-273 nm with a GSD between 1.55 and 2.27. The diesel vehicle exhibited the strongest bimodal distribution, but MMD of the second peaks were centered at a diameter larger than the TSI EEPS measurement range. The certainty of fitting parameters to the secondary peaks and their contribution to overall PM mass is uncertain based on fitting a curve to only a fraction of the total data. Importantly, data suggest particle mass emissions from light-duty

Table 4.1. Lognormal fitting parameters corresponding to tests presented in Figures 4.3 and 4.5.

	MMD_1 (nm)	GSD_1	N_1 (mg/m^3)	MMD_2 (nm)	GSD_2	N_2 (mg/m^3)
PFI						
P1	113	1.42	0.0679	554	1.28	0.0139
P2	112	1.4	0.0170	620	1.37	0.0188
P3	120	1.44	0.0083	698	1.44	0.0327
GDI)						
P1	118	1.51	0.1111			
P2	110	1.59	0.0200			
P3	116	1.52	0.0437			
Diesel + DPF						
P1	124	1.55	0.0061	777	1.5	0.0578
P2	273	2.27	0.0014	658	1.38	0.0290
P3	151	1.69	0.0025	698	1.44	0.0647
GDI + GPF						
P1	121	1.51	0.0190	516	1.19	0.0016
P2	132	1.66	0.0011	615	1.38	0.0025
P3	114	1.53	0.0025	651	1.42	0.0066

vehicles exhibit a bimodal distribution, which could be improperly quantified from direct-mass reading instruments such as the Dekati Mass Monitor (DMM, Kangasala, Finland) (Lehmann et al. 2004) that assumes a unimodal distribution when making real-time density and mass calculations. Based on the results during steady-state testing in Chapter 3, it is possible that up to 40% of mass emitted during an FTP test could originate from particles with diameters larger than the 560-nm mobility cutoff of the TSI EEPS. The Cambustion DMS 500 (Cambustion Ltd, Cambridge, UK) offers a larger size range that spans up to a 1000 nm upper size cutoff, and may be a more suitable choice for measuring size distributions used to calculate PM mass during light-duty vehicle tests on the chassis dynamometer. Future evaluations of the IPSD method need to consider the contribution of particles larger than the EEPS measurement range. The TSI Aerodynamic Particle Sizer (APS, 0.54-19.81 μm) offers a wide measurement range and high time resolution that would be suitable for this purpose. However, the conversion between

aerodynamic and electrical mobility diameter requires knowledge of the effective density function, and there is the potential for a gap or measurement overlap when combining its measurements with a TSI EEPS.

4.4.2 Defining Detection Limits

Background PM concentrations were previously determined of the sampling systems at HSL was 0.17 mg/mi (Hu et al. 2014). The FTP tunnel blank procedure can be used similarly to the IPSD detection limit. When applying a constant effective density of 1.2 g/cm^3 to tunnel blank size distributions with total particle concentrations around ~900 #/cm^3 the IPSD background contribution was 0.012 mg/mi. These concentrations were greater than the theoretical EEPS number detection limit of 170 #/cm^3 calculated for a 1874-sec averaging period (the duration of an FTP test) using the RMS noise values provided by TSI generated from five EEPS units. The contribution suspended PM larger than the 560-nm EEPS mobility cutoff, but smaller than the 2.5-µm cyclone removal that could contribute to filter tunnel background was calculated at 0.006 mg/mi for the test cell using a TSI Aerodynamic Particle Sizer (APS, 0.54-2.5 µm). In total, the suspended PM background is approximately 0.018 mg/mi based on measured values, which is about 10 times lower than the gravimetric detection limit, and more than 50 times lower than 1 mg/mi. Although CFR 1066 permits subtraction of measured tunnel PM background, our data suggest the tunnel blank mass is of gaseous origin, and no subtraction of any kind was conducted. The correlation between IPSD and gravimetric measurements are subject to variability originating from either method, especially for tests with gravimetric emissions below 0.17 mg/mi.

4.4.3 Comparing IPSD and Gravimetric Mass

Figure 4.6 presents a series of Pearson Least Squares linear regressions for M_{IPSD} versus M_{GRAV} by vehicle technology for FTP and US06 tests. Vehicles with FTP emissions exceeding 3.5 mg/mi were excluded here because their emissions exceeded the LEV III standards. Prediction intervals at the 95% confidence level are shown as the dashed lines. The standard error of the estimate (S_e) is reported for each panel, which quantifies the average residual error, in units of the dependent variable (M_{IPSD}) in the vertical direction, from the best fit line.

4.4.3.1 Goodness of Fit

PFI and GDI vehicles showed good agreement was achieved between IPSD and gravimetric measurements for FTP (R^2 = 0.70 and 0.86, respectively) and US06 (R^2 = 0.55 and 0.89, respectively) tests. Measurements generally lay within the 95% prediction intervals; the average residual error indicated by S_e ranged from 0.12 to 0.19 mg/mi for PFI, and from 0.12 to 0.20 for GDI vehicles. Despite nearly identical ranges of S_e for both GDI and PFI vehicle technologies, the larger magnitude of PM emissions from GDI vehicles manifested as improved R^2 statistics for both tests FTP and US06 tests compared to PFI vehicles.

LDD vehicles exhibited weaker correlation between the methods (R^2=0.11) compared to gasoline vehicles for FTP tests. One US06 test included an active DPF regeneration (ID=251, M_{GRAV}=69.7 mg/mi), resulting in a strong apparent correlation (R^2=0.998); however, this point was not an outlier as the slope was 0.17, which lay between the range of US06 slopes for gasoline vehicles (0.16-0.19). This regression analysis violates the assumption of heteroscedasticity; and, it demonstrates how R^2 alone is not always a useful parameter to assess goodness of fit. In this case, the average residual error indicated by S_e was 0.057 and 0.133

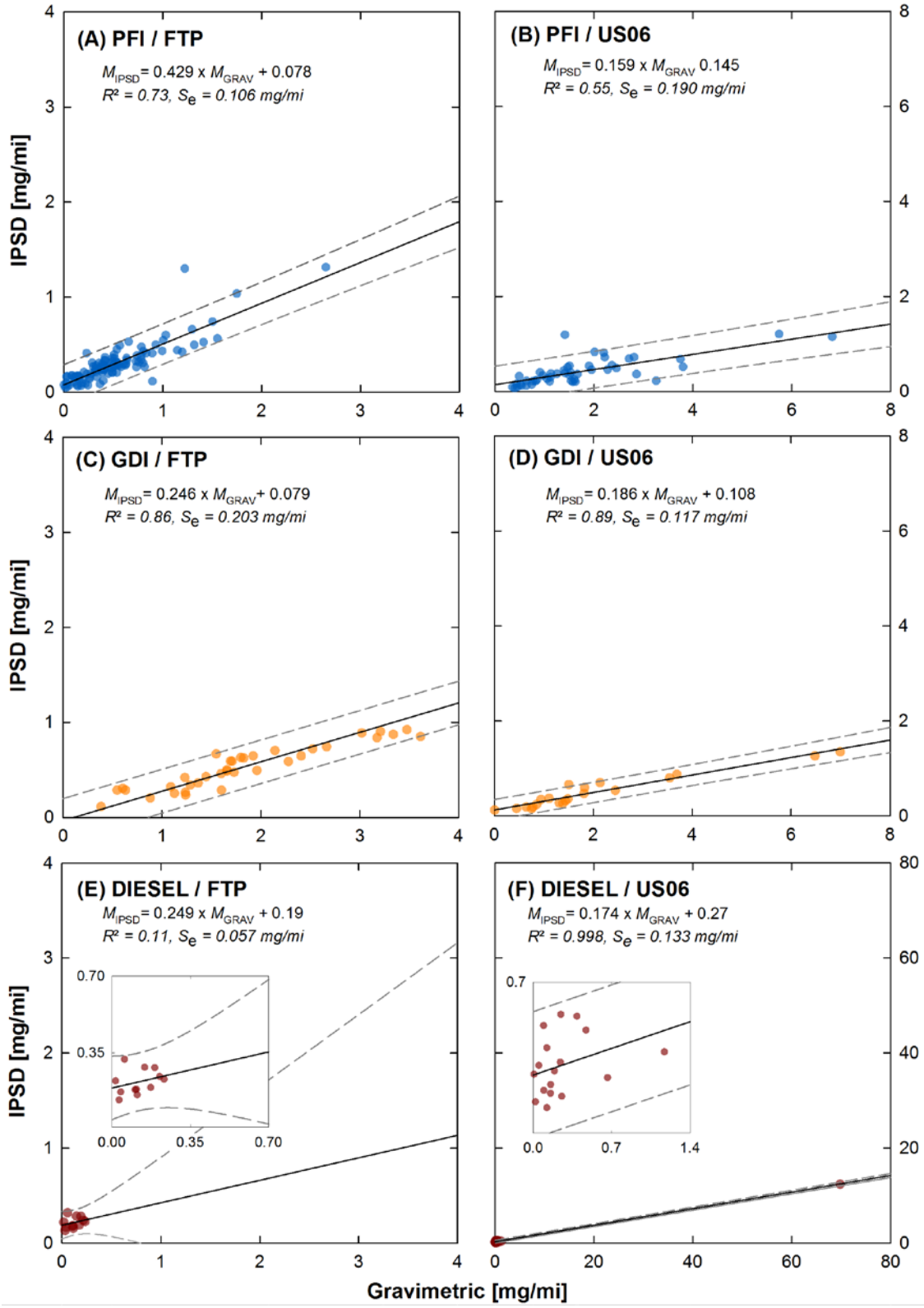

Figure 4.6. Correlations of M_{IPSD} versus M_{GRAV} for vehicle tests over the FTP (a, c, e), and US06 (b, d, f) test cycles.

mg/mi for the FTP and US06 tests respectively, indicating that the FTP tests actually exhibit less deviation from the best-fit line. Importantly, the relationship between IPSD and gravimetric mass for LDDs is poor as evidenced by the clustering of data between 0.1-0.2 mg/mi. This uncertainty could be a result of the unpredictable effective density function for LDD, and, gaseous artifact or background PM from the dilution air that result in variability associated with the gravimetric measurement below its detection limit of 0.17 mg/mi.

4.4.3.2 Understanding Methodological Bias

Theoretically, suspended (M_{IPSD}) and gravimetric mass collected on filters (M_{GRAV}) should be equivalent, and a one-to-one relationship between the two would result in a slope equal to unity. However, M_{IPSD} was virtually always lower than $M_{GRAV.}$ Predictive slopes ranged 0.25 - 0.43 over the FTP and 0.16-0.19 over the US06. These ranges are lower than our initial evaluation of a smaller dataset (slope = 0.63), which included multiple vehicle technologies with PM emissions between 0 and 6 mg/mi (Li et al. 2014). However, the slope of 0.63 was impacted by a single test with $M_{GRAV} \approx 6$ mg/mi; the remaining measurements follow a slope more consistent with the results in the presentation evaluation. In contrast to the initial heavy-duty evaluations of IPSD showing good one-to-one agreement with the gravimetric method (Liu et al. 2009; Liu et al. 2012), our work shows IPSD has a persistent negative bias when applied to a range of light-duty vehicle technologies. There are several possible contributing factors.

The effective density functions were derived during steady-state conditions and applied to transient FTP and US06 tests. Gasoline vehicle effective density was not a strong function of vehicle load, and application of a static effective density function for all FTP loading points was reasonable. Strategies used to accelerate catalyst light-off following cold start, such as retarded

spark timing and in some cases fuel enrichment (Bielaczyc and Merkisz 1999; Yi et al. 2014), result in higher hydrocarbon emissions that could condense onto combustion-generated fractal soot particles, or higher quantities of soot particles, possibly changing effective density for the brief period responsible for a large fraction of total FTP emissions. Figure 4.7 shows the slope of the relationship was steepest for Phase 1 for both PFI and GDI vehicles; however, substantial bias (>50%) was still observed relative to the gravimetric method. Because the slope of M_{IPSD} vs. M_{GRAV} for Phase 1 (Cold Start) was at least 60% lower than the identical Phase 3 (Hot Start, 0) as shown for both PFI and GDI, any error in effective density was likely not a major contributor to the negative bias.

The upper detection limit of the EEPS was briefly exceeded for some tests at the beginning of Phase 1 following cold start, but not during Phase 2 or Phase 3. This brief peak flattening would have resulted in reporting a lesser quantity of suspended PM mass, but the slope is higher for Phase 1 than Phase 3 as shown in Figure 4.7. Additionally, a linear relationship was observed over the entire measurement range with no positive or negative residual skewing (Figure 4.6). Therefore, the EEPS detection limit was also not a major contributor to the negative bias.

The adsorption or evaporation of semi-volatile constituents from filter media could also result in methodological bias, which would be indicated by a positive or negative intercept respectively, of the regression analysis. The magnitude of the intercepts annotated within each panel of Figure 4.6 for gasoline vehicles are within the scatter of the data expressed by S_e. For FTP tests, the intercept ranged from -0.0709 to 0.083 mg/mi, and the S_e ranged between 0.118 to 0.203 mg/mi; and for US06 tests the intercept ranged from 0.108 to 0.145 mg/mi, and S_e ranged 0.117 and 0.190 mg/mi. Figures 4.6(e) and Figures 4.6(f) suggest some evaporation may have

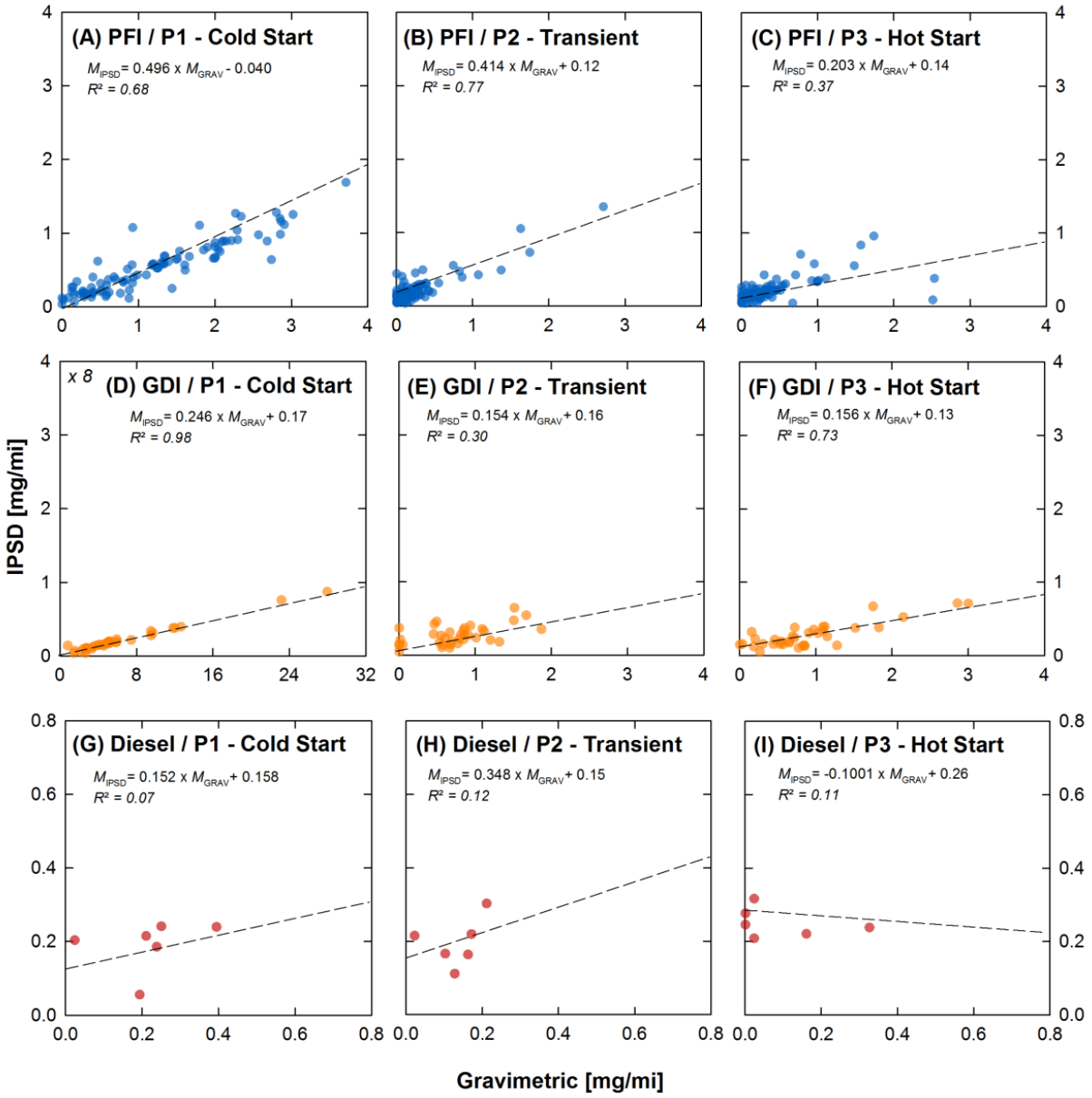

Figure 4.7. Correlations of M_{IPSD} versus M_{GRAV} for each vehicle over Phase 1, Phase, 2, and Phase 3 of the FTP.

occurred for the LDD vehicles, because the intercepts ranged from 0.19 to 0.27 mg/mi while S_e ranged from 0.057 to 0.133 mg/mi. However, negative IPSD bias would be caused by gaseous adsorption, not evaporation, from filters, and the magnitude of the gaseous artifact is insufficient to explain the large deviation from the one-to-one relationship.

Measurements in Chapter 3 included a TSI APS for measuring the contribution of particles up to 2.5-µm aerodynamic diameter during steady-state testing used for effective density determination. By aligning the IPSD and gravimetric measurement ranges to the d_{50} of the inlet cyclone, the slope of M_{IPSD} vs. M_{GRAV} increased from 0.50 to 1.03. Because Figure 4.4 suggests FTP mass distributions are bimodal with the larger peak centered above the EEPS measurement range, size range is likely the major contributor to the bias in the present evaluation as well. The origin of larger particles resulting in the bimodal mass distribution could be combustion or high-temperature entrainment from the exhaust manifold or sampling system lines. Fast-mobility instrumentation such as the Cambustion DMS 500 (Cambustion, Ltd, Cambridge, UK) that measure up to 1000 nm could capture more suspended PM mass, but it is still limited because it does not report size distributions between 1 and 2.5 µm. Combining multiple instruments, such as the EEPS and APS, for a larger dataset of FTP and US06 tests should be used to demonstrate agreement between IPSD and gravimetric mass.

4.4.4 Repeat FTP Testing and Methodological Variance

Table 4.2 presents five PFI and three GDI vehicles with at least eight repeat tests over the FTP. Figure 4.7 presents the average (x) and one standard deviation (s) of each repeat test, and the change in the coefficient of variance ($COV = s/x$) between methods ($\Delta COV = COV_{IPSD} - COV_{GRAV}$). Generally, reduced variance was observed for measurements of M_{IPSD} compared to M_{GRAV}, and the pooled test-to-test variance indicated ΔCOV was -8%, but a wide range of ΔCOV was observed for individual vehicles (-40% to +25%), indicating IPSD resulted in increased variability for some vehicles. The statistical significance of the 8% improvement in variability was evaluated for each vehicle using the Pitman-Morgan test, which is commonly applied to test

Table 4.2. Vehicles with eight or more repeat tests measured by IPSD and gravimetric methods.

ID	Vehicle	No. of Tests, n	M_{GRAV} mg/mi	M_{IPSD} mg/mi	Correlation, r	Pitman-Morgan, *t*-value	two-sided, p-value
PFI							
A	2013 Dodge Caravan	10	0.13±0.06	0.16±0.01	-0.65	10.4	< 0.001
B	2011 Nissan Altima	17	0.68±0.24	0.35±0.11	0.84	1.10	0.210
C	2012 Honda Civic	14	0.61±0.13	0.33±0.05	0.89	2.20	0.043
D	2012 GM Malibu	14	0.38±0.09	0.28±0.05	0.54	1.20	0.187
E	2009 Toyota Camry	14	0.54±0.14	0.35±0.14	0.36	-2.55	0.024
GDI							
F	2009 BMW 335i	9	1.20±0.51	0.40±0.13	0.78	0.78	0.174
G	2009 BMW 750i	8	2.60±0.86	0.70±0.25	0.99	-1.09	0.204
H	2010 Volkswagen Jetta	17	1.82±0.78	0.51±0.23	0.91	-0.30	0.374

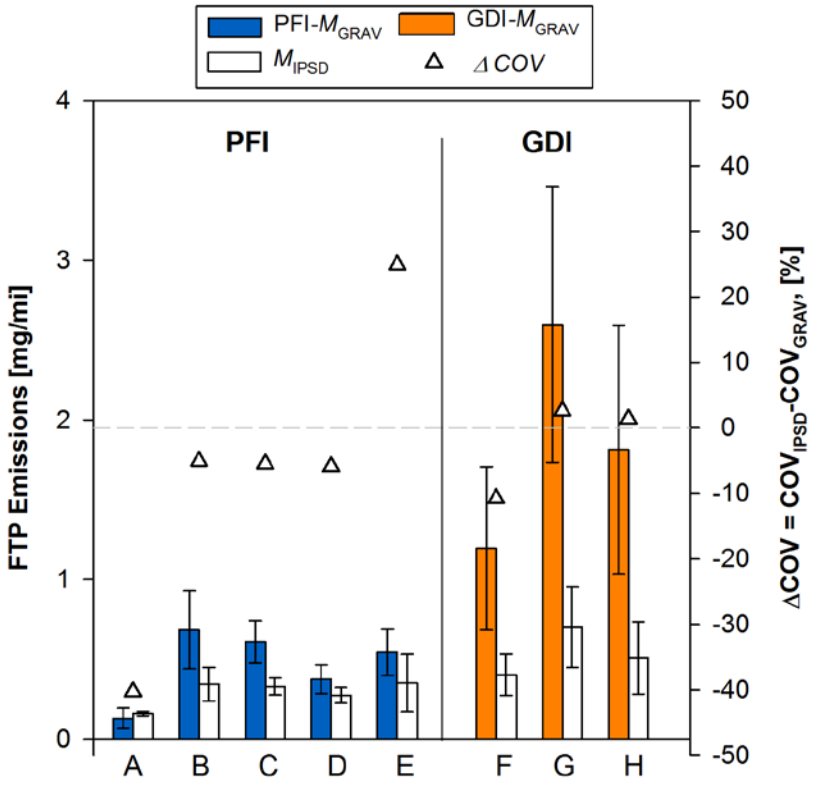

Figure 4.8. FTP emissions and coefficient of variation (COV) for IPSD and gravimetric methods for five PFI and three GDI vehicles with eight or more repeat tests.

the assumption of homogeneity of variance for paired-correlated data (Gardner 2001). The formula for the *t*-distribution test statistic is presented in Equation 4.3, where *n* equals the number of tests, *F* equals the ratio of the larger versus the smaller variances (e.g. gravimetric to IPSD variance, $s^2_{\mathrm{GRAV}}/s^2_{\mathrm{IPSD}}$), and *r* is the correlation between the methods of the paired data.

$$t = \frac{(\mathrm{F}-1)*\sqrt{(\mathrm{n}-2)}}{2*\sqrt{(\mathrm{F}*(1-\mathrm{r}^2))}} \qquad [4.3]$$

The null hypothesis was rejected for equal variance between the methods (H_o: F = 1) for all vehicles at the 0.05 alpha level. However, the Pitman-Morgan tests applied to the raw data indicated statistically significant differences between the variances but that was predominantly a manifestation of the negative bias of the IPSD method. When accounting for the bias by scaling the standard deviation of IPSD measurements by the unique measured ratio of gravimetric to IPSD mass for each vehicle, the null hypothesis was rejected only for Vehicle A (p-value < 0.001, M_{GRAV} = 0.13 mg/mi) and Vehicle C (p-value < 0.05, M_{GRAV} = 0.61 mg/mi). PM emissions from Vehicle A (M_{GRAV} = 0.06-0.19 mg/m) was below the gravimetric detection limit of 0.17 mg/mi. The IPSD method resulted in reduced COV for Vehicles B, D, and F, but these were not statistically significant, and COV was higher for ISPD than gravimetric measurements for Vehicles E, G, and H (Figure 4.8 and Table 4.2). One assumption made when performing these calculations is that the unresolved negative bias of the IPSD method does not affect the variability. Evaluations of IPSD achieving a one-to-one relationship with gravimetric measurements should re-assess the methodological variability.

Figure 4.9 presents the correlation of M_{IPSD} and M_{GRAV} for three selected vehicles (A, C, and H). A negative correlation was obtained between M_{IPSD} and M_{GRAV} for Vehicle A, which had PM emissions below the gravimetric detection limit of 0.17 mg/mi. Strong positive correlations were observed between IPSD and gravimetric measurements for Vehicles C and H –

demonstrating variability largely originates from an actual difference of PM emissions rather than the measurement method. Similar trends of moderate to strong positive correlation among repeat tests were observed for all other vehicles ($0.54 < r < 0.99$) as shown by Table 4.2. The spread of actual PM emissions contributing to test-to-test variability illustrates an important consideration when designing vehicles to meet low PM emissions standards.

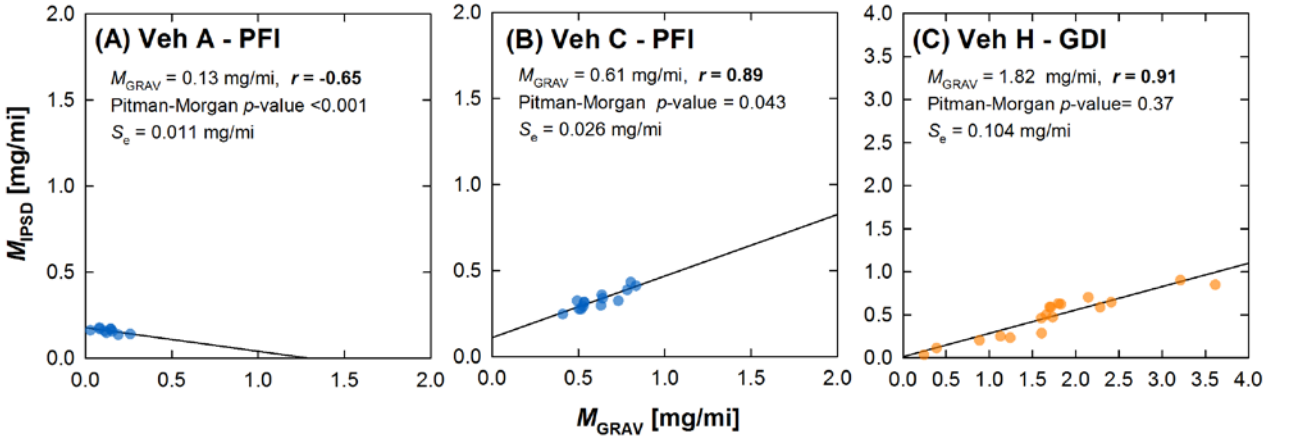

Figure 4.9. Correlation between IPSD and gravimetric mass for repeat tests of three vehicles.

4.4.5 Evaluating Future Number-Based Standards

Figure 4.10 presents total particle number (N_{IPSD}) and surface area (SA_{IPSD}) versus gravimetric mass (M_{GRAV}) for the FTP tests. Similar to the caveat of IPSD mass, the ISPD method is neither the reference method for measuring particle number (such as using a condensation particle counter with defined calibration criteria by ISO/DIS 27891 (Wang et al. 2010)), nor for measuring surface area (such as using a diffusion charger (Jung and Kittelson 2005)), and therefore the basis for new measurement and certification procedures would require

additional validation of this proof-of-concept. Additionally, the exponent of particle diameter used to estimate surface area varies by flow regime and morphology, therefore, a reference method is needed to further verify these calculations. The two dashed vertical lines indicate the 1 and 3-mg/mi standards that will be implemented starting with MY 2017 and MY 2025, respectively. Data are clustered by engine technology; most GDI vehicles have PM emissions below 3 mg/mi (average 2.65 mg/mi) and most PFI vehicles have PM emissions below 1 mg/mi (average 0.53 mg/mi).

The scatter plot shows a trend between both total number or surface area, and gravimetric PM mass for the FTP cycle. A slope of a linear regression was used to determine the ratio of N_{IPSD}/M_{GRAV} and SA_{IPSD}/M_{GRAV}. Conventional PFI gasoline vehicles emitted approximately 2.76 x 10^{12} #/mg, GDI vehicles 1.63 x 10^{12} #/mg, and LDD vehicles 8.74 x 10^{11} #/mg. Per unit mass, PFI vehicles emitted higher total particle number emissions than GDI vehicles, both of which emitted higher total particle number emissions than diesel vehicles. These ratios bound the widely recognized ratio of 2 x 10^{12} #/mg for total particle number to gravimetric PM for a variety of GDI vehicles (Maricq et al. 2011; Maricq et al. 2013). The corresponding surface area ratios were 8.64 x 10^{14} $d^{1.4}$/mg, 6.84 x 10^{14} $d^{1.4}$/mg, and 5.55 x 10^{14} $d^{1.4}$/mg for PFI, GDI, and LDD vehicles, respectively. Similar to the caveat of IPSD mass, the ISPD method is neither the reference method for measuring particle number (such as using a condensation particle counter with defined calibration criteria by ISO/DIS 27891 (Wang et al. 2010)), nor for measuring surface area (such as using a diffusion charger (Jung and Kittelson 2005)), and therefore the basis for new measurement and test procedures would require additional validation of this proof-of-concept.

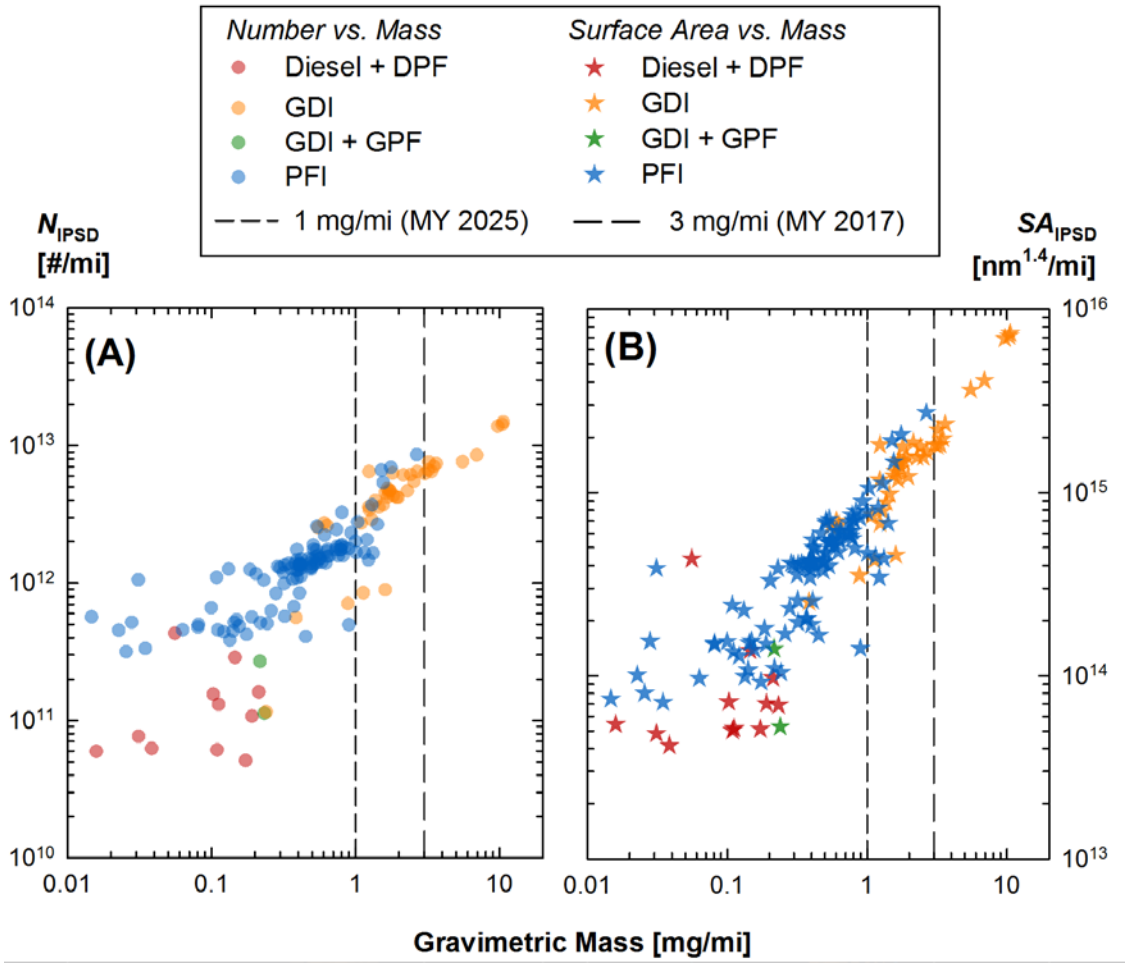

Figure 4.10. Scatter plots for (a) total particle number, and (b) surface area versus gravimetric PM mass for each vehicle technology.

The observed trend between total number and gravimetric PM mass emissions suggests control of particle number could be achieved through mass-based emissions standards (and conversely, that control of mass emissions could be achieved through particle number standards). In some situations, such as high-temperature events as a result of high-load or DPF regeneration events, the particle number to mass ratio may deviate from the observed trends (Herner et al. 2009; Dwyer et al. 2010). Nevertheless, the data suggest that further reduction of FTP particle

number emissions would be expected with a reduction in the mass standard until PM emissions decrease below the gravimetric detection limit.

One limitation of IPSD is defining the upper cutoff size, which is parallel to the debate of lower cutoff size when setting the Euro 5/6 *solid* particle number (SPN, >23 nm) standards. An approach that is more robust to upper and lower cutoff size is measurement of active surface area (Swanson et al. 2010), which may be also be a more appropriate dose metric than mass for predicting health outcomes (Sager and Castranova 2009). Figure 4.11 shows average particulate mass by gravimetric and IPSD method, surface area ($d^{1.4}$) and number emissions calculated using the EEPS size distributions between 5.6-560 nm. Data are split into two datasets: vehicles meeting the 3 mg/mi standard, and the subset of those that meet the 1 mg/mi standard. The relative difference among vehicle technologies is similar for mass, surface area, and number emissions. That is, the relative differences between average PM emissions are consistent regardless of which metric is used for density mass determination. Calculations from all the FTP tests in this evaluation indicate that the contribution of particles below 23 nm decreased from 28% for total number (d^0) to 5% for active surface area ($d^{1.4}$), and a small fraction of surface area originated from particles larger than 365 nm as shown in Figure 4.11. Thus, surface area is a metric that appears more robust to upper and lower cutoff size, could be operationally defined without inversion matrices converting charge into size distribution, and would not require measuring effective density to estimate suspended PM mass.

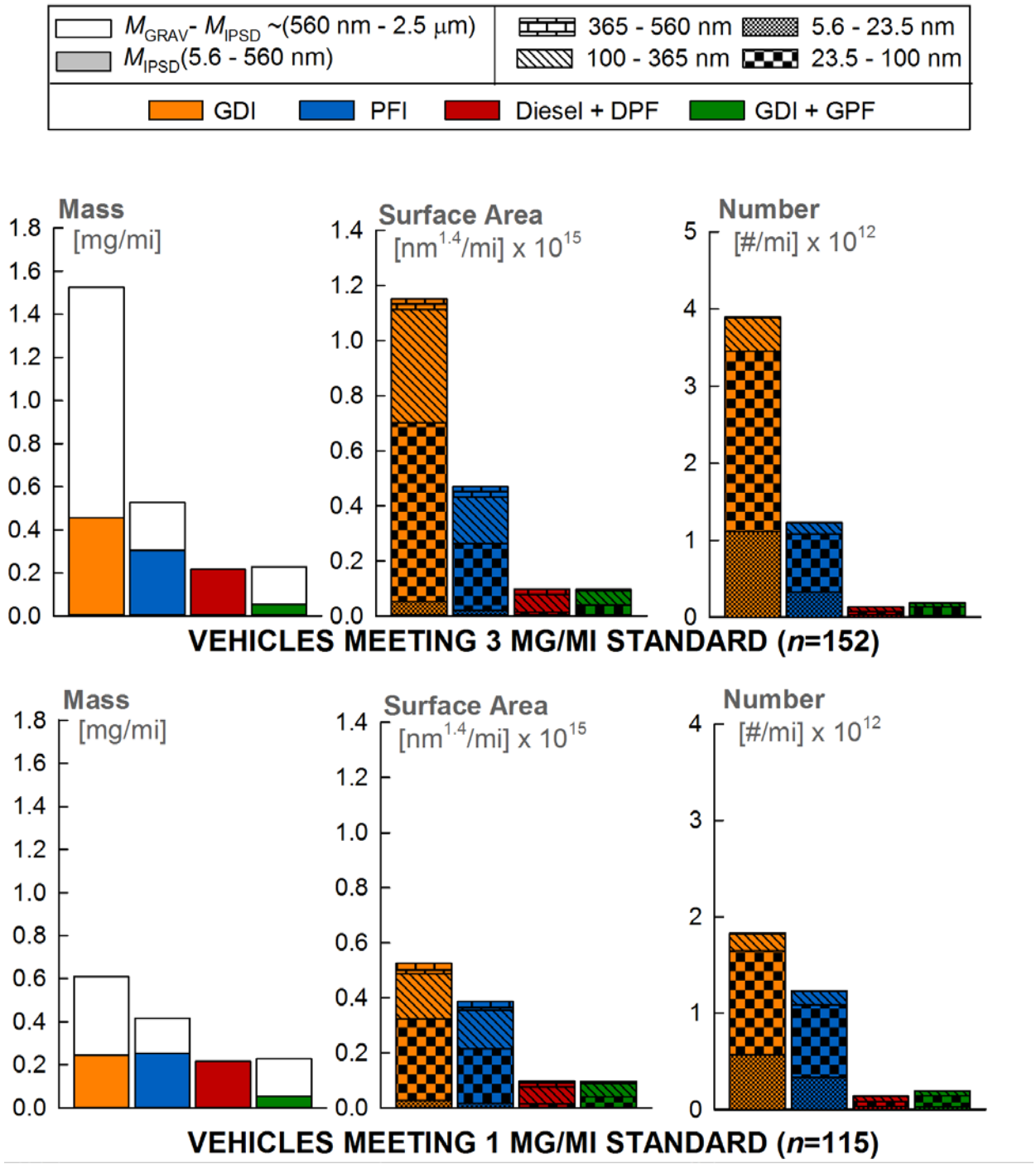

Figure 4.11. Size resolved particle emissions for vehicles meeting the 3 mg/mi and 1 mg/mi standards.

4.4.6 Evaluation of GPF and DPF Aftertreatment

Figure 4.12 presents the additional mass, surface area, and number emissions benefits of advanced aftertreatment control technologies, namely the GPF and the DPF. The figure shows the average emissions from DPF-equipped diesel vehicles have been 72 and 95% lower than gasoline PFI vehicles meeting 1 mg/mi, and 81 and 92% lower than GDI vehicles meeting 1 mg/mi. This cross-technology evaluation was made to compare PM emissions over the FTP and actual filtration efficiencies are likely greater; the DPF in heavy-duty applications has been shown highly (>90%) effective in reducing PM mass emissions (Khalek 2005; CRC 2009; Herner et al. 2011; CRC 2013). The prototype GPF installed on Vehicle H (Table 4.2) resulted in higher removal efficiencies (92-95%) for the two FTP tests conducted. This limited dataset suggests large emissions benefits are associated with the GPF as a control strategy.

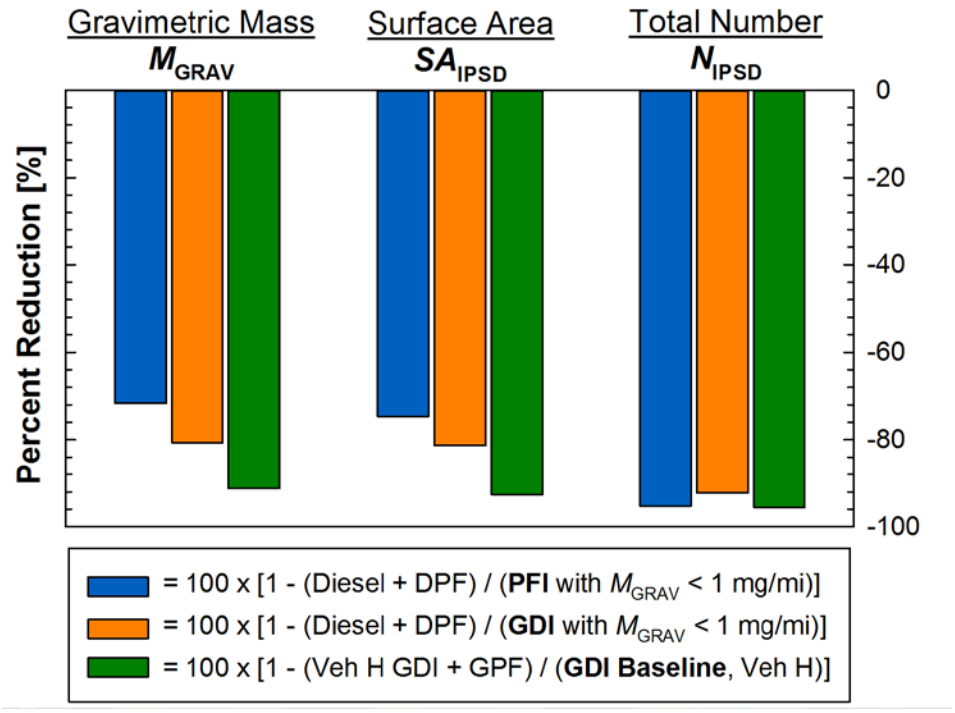

Figure 4.12. Emissions benefits associated with DPF and GPF after treatment technologies.

4.5 Conclusions

This evaluation of IPSD included a comprehensive dataset of 250 tests representing 34 light-duty vehicles. The IPSD method is free of gaseous artifact associated with filters, had approximately a 10 times lower detection limit based on tunnel blank concentrations, and resulted in a marginal 8% reduction in test-to-test variability as measured by the COV. However, the use of IPSD at this time as a standalone method for mass measurement is precluded by the persistent negative bias (slope = 0.25-0.43 over the FTP, and slope = 0.16-0.19 over the US06). Nevertheless, strong covariance between IPSD and gravimetric methods suggest that emissions variability is largely due to actual differences in vehicle PM emissions, and does not originate from IPSD or gravimetric measurements. The negative bias of the IPSD method likely results from the 560 nm upper size limit of the TSI EEPS. Future investigations of alternative methods should explore other metrics, such as number or active surface area, but could also further explore the size range of IPSD to achieve a better one-to-one relationship with the existing filter-based gravimetric method.

4.6 Appendix 1

Table 4.A. List of tests over the FTP cycle.

ID	MY	Make	Model	Engine	Mileage (mi)	Engine Family	Test Cell	# Phases	Gravimetric Mass (mg/mi)	IPSD Mass (mg/mi)	Total Number (#/mi)	Surface Area ($nm^{1.4}$/mi)
1	2009	BMW	335i	GDI	2,443	9BMXV03.0ULR	7	3	1.443	0.429	3.561E+12	9.808E+14
2	2009	BMW	335i	GDI	2,454	9BMXV03.0ULR	7	3	1.657	0.490	4.225E+12	1.180E+15
3	2009	BMW	335i	GDI	2,465	9BMXV03.0ULR	7	3	1.958	0.494	4.198E+12	1.221E+15
4	2009	BMW	335i	GDI	2,551	9BMXV03.0ULR	7	3	1.547	0.668	3.708E+12	1.238E+15
5	2009	BMW	750i	GDI	600	9BMXV04.4N63	7	3	3.171	0.839	6.625E+12	1.801E+15
6	2009	BMW	750i	GDI	742	9BMXV04.4N63	7	3	2.663	0.745	6.452E+12	1.669E+15
7	2009	BMW	750i	GDI	762	9BMXV04.4N63	7	3	3.337	0.874	6.469E+12	1.823E+15
8	2009	BMW	750i	GDI	773	9BMXV04.4N63	7	3	3.476	0.923	7.046E+12	1.973E+15
9	2009	BMW	750i	GDI	796	9BMXV04.4N63	7	3	3.017	0.890	6.244E+12	1.829E+15
10	2009	BMW	750i	GDI	926	9BMXV04.4N63	7	3	2.522	0.721	5.491E+12	1.559E+15
11	2009	BMW	335i	GDI	2,985	9BMXV03.0ULR	7	3	0.602	0.306	2.736E+12	6.989E+14
12	2009	BMW	335i	GDI	3,004	9BMXV03.0ULR	7	3	0.546	0.287	2.532E+12	6.534E+14
13	2009	BMW	335i	GDI	3,023	9BMXV03.0ULR	7	3	0.630	0.287	2.622E+12	6.644E+14
14	2010	Volkswagen	Jetta	GDI	76	AADXV02.03PA	7	3	1.824	0.626	4.337E+12	1.482E+15
15	2009	BMW	750i	GDI	1,008	9BMXV04.4N63	7	3	1.365	0.363	3.971E+12	8.837E+14
16	2010	Volkswagen	Jetta	GDI	162	AADXV02.03PA	7	3	1.692	0.592	4.579E+12	1.507E+15
17	2009	BMW	750i	GDI	1,019	9BMXV04.4N63	7	3	1.234	0.263	6.465E+12	1.822E+15
18	2010	Volkswagen	Jetta	GDI	458	AADXV02.03PA	7	3	1.237	0.236	3.415E+12	6.779E+14
19	2009	BMW	335i	GDI	3,909	9BMXV03.0ULR	7	3	1.286	0.341	2.899E+12	7.931E+14
20	2009	BMW	335i	GDI	3,932	9BMXV03.0ULR	7	3	1.087	0.324	2.724E+12	7.505E+14
21	2010	Volkswagen	Jetta	GDI	4,297	AADXV02.03PA	7	3	1.654	0.500	4.864E+12	1.440E+15
22	2010	Volkswagen	Jetta	GDI	4,536	AADXV02.03PA	7	3	1.728	0.475	4.708E+12	1.355E+15
23	2010	Volkswagen	Jetta	GDI	4,572	AADXV02.03PA	7	3	1.709	0.591	4.755E+12	1.418E+15
24	2010	Volkswagen	Jetta	GDI	4,643	AADXV02.03PA	7	3	1.596	0.463	4.535E+12	1.307E+15

25	2010	Volkswagen	Jetta	GDI	5,804	AADXV02.03PA	7	3	1.600	0.250	8.922E+11	4.566E+14
26	2010	Volkswagen	Jetta	GDI	5,856	AADXV02.03PA	7	3	0.880	0.224	7.090E+11	3.530E+14
27	2010	Volkswagen	Jetta	GDI	5,878	AADXV02.03PA	7	3	1.124	0.253	8.488E+11	4.298E+14
28	2010	Volkswagen	Jetta	GDI	6,611	AADXV02.03PA	7	3	3.207	0.842	7.611E+12	2.202E+15
29	2010	Volkswagen	Jetta	GDI	6,622	AADXV02.03PA	7	3	2.406	0.647	6.135E+12	1.773E+15
30	2010	Volkswagen	Jetta	GDI	6,777	AADXV02.03PA	7	3	1.796	0.632	6.311E+12	1.775E+15
31	2010	Volkswagen	Jetta	GDI	6,999	AADXV02.03PA	7	3	0.384	0.115	5.582E+11	2.531E+14
32	2010	Volkswagen	Jetta	GDI	7,209	AADXV02.03PA	7	3	3.612	0.850	7.398E+12	2.365E+15
33	2010	Volkswagen	Jetta	GDI	7,220	AADXV02.03PA	7	3	2.141	0.704	6.103E+12	1.866E+15
34	2012	GM	Acadia	GDI	5,746	CGMXT03.6151	7	3	6.900	1.816	8.532E+12	4.087E+15
35	2012	GM	Acadia	GDI	5,757	CGMXT03.6151	7	3	5.495	1.640	7.623E+12	3.639E+15
36	2013	Ford	Fusion	GDI	8,985	DFMXV01.6VZF	7	3	1.920	0.648	4.213E+12	1.568E+15
37	2013	Ford	Fusion	GDI	9,020	DFMXV01.6VZF	7	3	1.231	0.420	3.587E+12	1.168E+15
38	2011	Nissan	Juke	GDI	51,341	BNSXV01.6GDA	7	3	10.369	3.280	1.421E+13	7.122E+15
39	2011	Nissan	Juke	GDI	51,376	BNSXV01.6GDA	7	3	10.553	3.327	1.484E+13	7.393E+15
40	2011	Nissan	Juke	GDI	51,427	BNSXV01.6GDA	7	3	9.635	3.142	1.380E+13	6.931E+15
41	2010	Volkswagen	Jetta	GDI	11,302	AADXV02.03PA	7	3	2.277	0.589	4.689E+12	1.559E+15
42	2010	Volkswagen	Jetta	GDI+GPF	8,252	AADXV02.03PA	3	3	0.239	0.038	1.148E+11	5.267E+13
43	2010	Volkswagen	Jetta	GDI+GPF	8,580	AADXV02.03PA	3	3	0.216	0.073	2.695E+11	1.402E+14
44	2009	Hummer	H3	PFI	20,978	9GMXT03.7178	7	3	0.733	0.266	2.446E+12	6.124E+14
45	2009	Hummer	H3	PFI	21,351	9GMXT03.7178	7	3	0.536	0.451	2.581E+12	7.179E+14
46	2010	Toyota	Camry	PFI	5,449	ATYXV02.5HE2	7	3	0.407	0.282	8.448E+11	2.565E+14
47	2010	Toyota	Camry	PFI	5,484	ATYXV02.5HE2	7	3	0.372	0.259	6.744E+11	2.055E+14
48	2010	Toyota	Camry	PFI	5,495	ATYXV02.5HE2	7	3	0.321	0.279	5.708E+11	1.949E+14
49	2005	Toyota	Camry	PFI	115,688	5TYXV02.4MXA	7	3	1.221	1.302	1.475E+12	3.444E+14
50	2005	Toyota	Camry	PFI	115,723	5TYXV02.4MXA	7	3	0.390	0.284	1.475E+12	3.446E+14
51	2005	Toyota	Camry	PFI	115,735	5TYXV02.4MXA	7	3	0.783	0.478	1.750E+12	5.612E+14
52	2008	Ford	F-150	PFI	73,588	8FMXT04.63AB	7	3	1.003	0.545	1.666E+12	4.658E+14
53	2008	Ford	F-150	PFI	73,600	8FMXT04.63AB	7	3	1.317	0.499	1.645E+12	4.363E+14
54	2008	Ford	F-150	PFI	73,655	8FMXT04.63AB	7	3	1.147	0.442	1.656E+12	4.464E+14
55	2008	Ford	F-150	PFI	73,667	8FMXT04.63AB	7	3	1.411	0.527	2.676E+12	6.801E+14

56	2008	Nissan	Altima	PFI	99,787	8NSXV02.585A	7	3	0.230	0.413	1.053E+12	3.852E+14
57	2008	Nissan	Altima	PFI	99,806	8NSXV02.585A	7	3	0.416	0.369	1.122E+12	3.918E+14
58	2008	Nissan	Altima	PFI	99,817	8NSXV02.585A	7	3	0.654	0.532	1.568E+12	6.107E+14
59	2008	Nissan	Altima	PFI	99,852	8NSXV02.585A	7	3	0.565	0.493	1.513E+12	5.520E+14
60	2010	Kia	Forte	PFI	20,896	AKMXV02.0TPC	7	3	0.318	0.209	9.885E+11	2.579E+14
61	2010	Kia	Forte	PFI	20,989	AKMXV02.0TPC	7	3	0.279	0.199	8.403E+11	2.338E+14
62	1997	Ford	Taurus	PFI	129,825	VFM3.0V8G3EK	7	3	0.031	0.167	1.056E+12	3.863E+14
63	1997	Ford	Taurus	PFI	129,849	VFM3.0V8G3EK	7	2	0.131	0.171	1.264E+12	2.279E+14
64	1997	Ford	Taurus	PFI	129,868	VFM3.0V8G3EK	7	2	0.184	0.092	1.252E+12	1.809E+14
65	1997	Ford	Taurus	PFI	129,880	VFM3.0V8G3EK	7	2	0.397	0.122	1.235E+12	1.900E+14
66	2009	Dodge	Caravan	PFI	24,557	9CRXT03.8YP0	7	2	1.550	0.566	5.375E+12	1.475E+15
67	2009	Dodge	Caravan	PFI	24,616	9CRXT03.8YP0	7	2	1.502	0.743	6.620E+12	1.913E+15
68	2009	Dodge	Caravan	PFI	24,720	9CRXT03.8YP0	7	2	2.647	1.316	8.572E+12	2.733E+15
69	2009	Dodge	Caravan	PFI	24,772	9CRXT03.8YP0	7	2	1.746	1.040	6.935E+12	2.066E+15
70	2009	Dodge	Caravan	PFI	24,791	9CRXT03.8YP0	7	2	1.295	0.662	3.693E+12	1.122E+15
71	2008	Toyota	Prius	PFI	8,984	8TYXV01.5HC3	1	2	0.025	0.079	3.165E+11	8.027E+13
72	2008	Toyota	Prius	PFI	9,006	8TYXV01.5HC3	1	2	0.099	0.106	6.607E+11	1.539E+14
73	2008	Toyota	Prius	PFI	9,029	8TYXV01.5HC3	1	2	0.023	0.096	4.521E+11	1.011E+14
74	2011	Nissan	Altima	PFI	29,689	BNSXV02.585A	3	3	0.449	0.195	4.077E+11	1.664E+14
75	2011	Nissan	Altima	PFI	29,728	BNSXV02.585A	3	2	0.548	0.291	1.587E+12	5.369E+14
76	2011	Nissan	Altima	PFI	29,766	BNSXV02.585A	3	2	0.738	0.387	1.846E+12	6.856E+14
77	2011	Nissan	Altima	PFI	30,097	BNSXV02.585A	3	3	0.620	0.283	1.400E+12	4.737E+14
78	2011	Nissan	Altima	PFI	30,135	BNSXV02.585A	3	3	1.030	0.602	2.785E+12	1.060E+15
79	2011	Nissan	Altima	PFI	30,178	BNSXV02.585A	3	3	0.783	0.342	1.745E+12	6.168E+14
80	2011	Nissan	Altima	PFI	30,216	BNSXV02.585A	3	3	0.992	0.435	2.006E+12	7.874E+14
81	2011	Nissan	Altima	PFI	30,239	BNSXV02.585A	3	3	1.196	0.424	2.067E+12	8.244E+14
82	2011	Nissan	Altima	PFI	30,666	BNSXV02.585A	3	3	0.892	0.411	1.786E+12	7.259E+14
83	2011	Nissan	Altima	PFI	30,704	BNSXV02.585A	3	3	0.927	0.500	2.311E+12	8.958E+14
84	2011	Nissan	Altima	PFI	30,916	BNSXV02.585A	1	2	0.580	0.270	1.419E+12	5.124E+14
85	2011	Nissan	Altima	PFI	30,962	BNSXV02.585A	1	2	0.537	0.290	1.404E+12	5.290E+14
86	2011	Nissan	Altima	PFI	31,001	BNSXV02.585A	1	2	0.390	0.212	1.086E+12	3.804E+14

87	2011	Nissan	Altima	PFI	31,039	BNSXV02.585A	1	2	0.556	0.279	1.497E+12	5.457E+14
88	2009	Toyota	Camry	PFI	67,377	9TYXV02.4HE2	7	3	0.512	0.297	1.277E+12	4.471E+14
89	2009	Toyota	Camry	PFI	67,388	9TYXV02.4HE2	7	3	0.739	0.916	2.537E+12	1.406E+15
90	2009	Toyota	Camry	PFI	67,417	9TYXV02.4HE2	7	3	0.491	0.467	1.559E+12	7.331E+14
91	2009	Toyota	Camry	PFI	67,569	9TYXV02.4HE2	7	3	0.528	0.301	1.519E+12	5.028E+14
88	2008	Chevrolet	Impala	PFI	44,071	8GMXV03.9052	7	3	0.492	0.205	7.146E+13	2.040E+14
89	2008	Chevrolet	Impala	PFI	44,105	8GMXV03.9052	7	3	0.231	0.191	6.197E+13	1.733E+14
90	2008	Chevrolet	Impala	PFI	44,116	8GMXV03.9052	7	3	0.332	0.164	4.943E+13	1.372E+14
91	2008	Chevrolet	Impala	PFI	44,127	8GMXV03.9052	7	3	0.265	0.162	5.228E+13	1.476E+14
92	2011	Nissan	Altima	PFI	31,144	BNSXV02.585A	1	3	0.510	0.359	1.754E+12	6.802E+14
93	2011	Nissan	Altima	PFI	31,179	BNSXV02.585A	1	3	0.414	0.269	1.276E+12	5.026E+14
94	2011	Nissan	Altima	PFI	31,213	BNSXV02.585A	1	3	0.471	0.307	1.514E+12	5.988E+14
95	2012	Toyota	Corolla	PFI	22,956	CTYXV01.8BEA	7	3	0.108	0.159	1.098E+12	2.431E+14
96	2012	Toyota	Corolla	PFI	23,015	CTYXV01.8BEA	7	3	0.217	0.090	5.142E+11	1.100E+14
97	2012	Nissan	Maxima	PFI	19,285	CNSXV03.5G7B	1	3	0.015	0.048	5.669E+11	7.455E+13
98	2012	Toyota	Corolla	PFI	23,049	CTYXV01.8BEA	7	3	0.894	0.115	4.977E+11	1.409E+14
99	2012	Nissan	Maxima	PFI	19,320	CNSXV03.5G7B	1	3	0.000	0.078	5.159E+11	8.111E+13
100	2012	Nissan	Maxima	PFI	19,355	CNSXV03.5G7B	1	3	0.063	0.079	4.552E+11	9.714E+13
101	2009	Toyota	Camry	PFI	64,022	9TYXV02.4HE2	7	3	0.605	0.297	2.232E+12	6.165E+14
102	2009	Toyota	Camry	PFI	64,056	9TYXV02.4HE2	7	3	0.815	0.268	1.583E+12	4.969E+14
103	2013	Chevrolet	Spark	PFI	23,913	DGMXV01.8011	1	3	0.365	0.087	1.066E+12	2.048E+14
104	2013	Chevrolet	Spark	PFI	23,948	DGMXV01.8011	1	3	0.140	0.063	4.469E+11	1.075E+14
105	2013	Chevrolet	Spark	PFI	23,983	DGMXV01.8011	1	3	0.133	0.079	3.839E+11	9.895E+13
106	2009	Ford	Explorer	PFI	52,809	9FMXT04.03DC	1	3	0.242	0.074	5.068E+11	1.043E+14
107	2009	Ford	Explorer	PFI	52,844	9FMXT04.03DC	1	3	0.174	0.069	4.218E+11	9.271E+13
108	2009	Ford	Explorer	PFI	52,879	9FMXT04.03DC	1	3	0.035	0.057	3.340E+11	7.146E+13
109	2008	Smart	Fortwo	PFI	76,636	8MBXV01.0U2A	7	3	0.390	0.239	1.750E+12	4.220E+14
110	2008	Smart	Fortwo	PFI	76,671	8MBXV01.0U2A	7	3	0.534	0.208	1.732E+12	3.984E+14
111	2008	Smart	Fortwo	PFI	76,706	8MBXV01.0U2A	7	3	0.799	0.309	3.268E+12	7.114E+14
112	2012	GM	Malibu	PFI	26,760	CGMXV02.4026	7	3	0.507	0.396	1.886E+12	6.994E+14
113	2009	Toyota	Camry	PFI	67,406	9TYXV02.4HE2	7	3	0.755	0.318	1.581E+12	5.800E+14

114	2012	Honda	Civic	PFI	32,024	CHNXV01.8VC2	7	3	0.832	0.413	1.813E+12	7.905E+14
115	2009	Toyota	Camry	PFI	67,428	9TYXV02.4HE2	7	3	0.408	0.337	1.394E+12	5.522E+14
116	2012	Honda	Civic	PFI	32,043	CHNXV01.8VC2	7	3	0.782	0.388	1.864E+12	7.485E+14
117	2009	Toyota	Camry	PFI	67,439	9TYXV02.4HE2	7	3	0.485	0.209	1.297E+12	3.740E+14
118	2009	Toyota	Camry	PFI	67,458	9TYXV02.4HE2	7	3	0.490	0.360	1.265E+12	4.164E+14
119	2012	Honda	Civic	PFI	32,080	CHNXV01.8VC2	7	3	0.638	0.340	1.758E+12	6.127E+14
120	2009	Toyota	Camry	PFI	67,543	9TYXV02.4HE2	7	3	0.354	0.306	1.275E+12	3.982E+14
121	2009	Toyota	Camry	PFI	67,554	9TYXV02.4HE2	7	3	0.481	0.255	1.382E+12	4.145E+14
122	2012	Honda	Civic	PFI	32,118	CHNXV01.8VC2	7	3	0.408	0.248	1.381E+12	4.273E+14
123	2012	Honda	Civic	PFI	32,129	CHNXV01.8VC2	7	3	0.629	0.298	1.689E+12	5.573E+14
124	2009	Toyota	Camry	PFI	67,566	9TYXV02.4HE2	7	3	0.411	0.245	1.343E+12	4.053E+14
125	2012	Honda	Civic	PFI	32,148	CHNXV01.8VC2	7	3	0.802	0.433	1.893E+12	6.996E+14
126	2012	GM	Malibu	PFI	26,780	CGMXV02.4026	7	3	0.417	0.334	1.495E+12	4.930E+14
127	2012	Honda	Civic	PFI	32,159	CHNXV01.8VC2	7	3	0.532	0.318	1.562E+12	5.322E+14
128	2012	GM	Malibu	PFI	26,791	CGMXV02.4026	7	3	0.415	0.282	1.354E+12	4.173E+14
129	2012	GM	Malibu	PFI	26,802	CGMXV02.4026	7	3	0.498	0.285	1.500E+12	4.695E+14
130	2012	Honda	Civic	PFI	32,170	CHNXV01.8VC2	7	3	0.728	0.326	1.743E+12	5.873E+14
131	2012	GM	Malibu	PFI	26,483	CGMXV02.4026	7	3	0.287	0.310	1.319E+12	4.108E+14
132	2012	Honda	Civic	PFI	32,181	CHNXV01.8VC2	7	3	0.634	0.360	1.559E+12	5.413E+14
133	2012	GM	Malibu	PFI	26,844	CGMXV02.4026	7	3	0.315	0.231	1.192E+12	3.555E+14
134	2013	Dodge	Caravan	PFI	40,293	DCRXJ03.6VPA	7	3	0.028	0.164	5.176E+11	1.543E+14
135	2013	Dodge	Caravan	PFI	40,304	DCRXJ03.6VPA	7	3	0.080	0.178	4.776E+11	1.483E+14
136	2012	GM	Malibu	PFI	26,855	CGMXV02.4026	7	3	0.298	0.272	1.291E+12	4.022E+14
137	2012	GM	Malibu	PFI	26,874	CGMXV02.4026	7	3	0.381	0.237	1.386E+12	4.183E+14
138	2013	Dodge	Caravan	PFI	40,334	DCRXJ03.6VPA	7	3	0.258	0.142	6.277E+11	1.699E+14
139	2012	GM	Malibu	PFI	26,885	CGMXV02.4026	7	3	0.405	0.239	1.348E+12	4.291E+14
140	2013	Dodge	Caravan	PFI	40,346	DCRXJ03.6VPA	7	3	0.189	0.138	5.648E+11	1.489E+14
141	2012	GM	Malibu	PFI	26,896	CGMXV02.4026	7	3	0.492	0.259	1.310E+12	4.225E+14
142	2012	GM	Malibu	PFI	26,908	CGMXV02.4026	7	3	0.321	0.256	1.347E+12	4.064E+14
143	2013	Dodge	Caravan	PFI	40,357	DCRXJ03.6VPA	7	3	0.155	0.158	4.880E+11	1.392E+14
144	2013	Dodge	Caravan	PFI	40,376	DCRXJ03.6VPA	7	3	0.143	0.171	5.173E+11	1.510E+14

145	2012	GM	Malibu	PFI	26,927	CGMXV02.4026	7	3	0.340	0.237	1.387E+12	4.109E+14
146	2012	GM	Malibu	PFI	26,938	CGMXV02.4026	7	3	0.387	0.297	1.231E+12	4.125E+14
147	2012	GM	Malibu	PFI	26,949	CGMXV02.4026	7	3	0.203	0.212	1.167E+12	3.297E+14
148	2013	Dodge	Caravan	PFI	40,387	DCRXJ03.6VPA	7	3	0.149	0.171	5.397E+11	1.547E+14
149	2012	Honda	Civic	PFI	32,200	CHNXV01.8VC2	7	3	0.514	0.276	1.381E+12	4.635E+14
150	2013	Dodge	Caravan	PFI	40,417	DCRXJ03.6VPA	7	3	0.121	0.149	4.407E+11	1.281E+14
151	2013	Dodge	Caravan	PFI	40,428	DCRXJ03.6VPA	7	3	0.110	0.160	4.565E+11	1.352E+14
152	2013	Dodge	Caravan	PFI	40,439	DCRXJ03.6VPA	7	3	0.081	0.172	4.990E+11	1.511E+14
153	2012	Honda	Civic	PFI	32,219	CHNXV01.8VC2	7	3	0.490	0.326	4.971E+11	1.506E+14
154	2012	Honda	Civic	PFI	32,238	CHNXV01.8VC2	7	3	0.526	0.293	1.464E+12	4.897E+14
155	2012	Honda	Civic	PFI	32,249	CHNXV01.8VC2	7	3	0.502	0.277	1.489E+12	4.762E+14
156	2012	Honda	Civic	PFI	32,260	CHNXV01.8VC2	7	3	0.532	0.318	1.503E+12	5.190E+14
157	2010	Volkswagen	Jetta	Diesel	53,305	AVWXV02.0U5N	3	3	0.031	0.135	7.641E+10	4.831E+13
158	2011	BMW	335d	Diesel	26,315	BBMXV03.0M57	3	3	0.145	0.284	2.869E+11	1.376E+14
159	2011	BMW	335d	Diesel	26,399	BBMXV03.0M57	3	3	0.056	0.321	4.306E+11	4.346E+14
160	2011	BMW	335d	Diesel	26,467	BBMXV03.0M57	3	3	0.102	0.182	1.548E+11	7.191E+13
161	2011	BMW	335d	Diesel	26,489	BBMXV03.0M57	3	3	0.212	0.242	1.604E+11	9.723E+13
162	2011	Mercedes	E350	Diesel	7,078	BMBXV03.0U2B	3	3	0.038	0.171	6.238E+10	4.155E+13
163	2013	Volkswagen	Jetta Tdi	Diesel	4,868	DVWXV02.0U5N	3	3	0.172	0.191	5.110E+10	5.108E+13
164	2013	Volkswagen	Jetta Tdi	Diesel	4,924	DVWXV02.0U5N	3	3	0.109	0.183	6.089E+10	5.014E+13
165	2012	Volkswagen	Passat Tdi	Diesel	15,363	CVWXV02.0U4S	3	3	0.016	0.222	5.956E+10	5.431E+13
166	2012	Volkswagen	Passat Tdi	Diesel	15,450	CVWXV02.0U4S	3	3	0.190	0.282	1.073E+11	7.049E+13
167	2012	Volkswagen	Passat Tdi	Diesel	15,535	CVWXV02.0U4S	3	3	0.232	0.230	1.122E+11	6.908E+13
168	2011	Mercedes	E350	Diesel	24,412	BMBXV03.0U2B	3	3	0.111	0.158	1.306E+11	5.153E+13

4.7 Appendix 2.

Table 4.B. List of tests over the US06 cycle.

ID	Year	Make	Model	Engine	Mileage (mi)	Engine Family	Cell	Gravimetric Mass (mg/mi)	IPSD Mass (mg/mi)
169	2010	Volkswagen	Jetta	GDI	5,746	AADXV02.03PA	7	0.747	0.156
170	2010	Volkswagen	Jetta	GDI	5,763	AADXV02.03PA	7	1.380	0.264
171	2010	Volkswagen	Jetta	GDI	5,780	AADXV02.03PA	7	0.851	0.243
172	2010	Volkswagen	Jetta	GDI	5,815	AADXV02.03PA	7	1.305	0.279
173	2010	Volkswagen	Jetta	GDI	5,831	AADXV02.03PA	7	1.434	0.318
174	2010	Volkswagen	Jetta	GDI	5,911	AADXV02.03PA	7	0.774	0.191
175	2010	Volkswagen	Jetta	GDI	6,634	AADXV02.03PA	7	3.685	0.876
176	2010	Volkswagen	Jetta	GDI	6,683	AADXV02.03PA	7	2.132	0.703
177	2010	Volkswagen	Jetta	GDI	7,029	AADXV02.03PA	7	0.444	0.160
178	2010	Volkswagen	Jetta	GDI	7,045	AADXV02.03PA	7	1.467	0.126
179	2010	Volkswagen	Jetta	GDI	7,112	AADXV02.03PA	7	1.482	0.358
180	2010	Volkswagen	Jetta	GDI	7,128	AADXV02.03PA	7	1.806	0.474
181	2010	Volkswagen	Jetta	GDI	7,145	AADXV02.03PA	7	2.439	0.540
182	2010	Volkswagen	Jetta	GDI	7,161	AADXV02.03PA	7	1.820	0.599
183	2012	GM	Acadia	GDI	5,820	CGMXT03.6151	7	0.639	0.193
184	2013	Ford	Fusion	GDI	8,996	DFMXV01.6VZF	7	1.502	0.663
185	2013	Ford	Fusion	GDI	9,031	DFMXV01.6VZF	7	0.935	0.347
186	2013	Ford	Fusion	GDI	9,047	DFMXV01.6VZF	7	1.102	0.372
187	2011	Nissan	Juke	GDI	51,387	BNSXV01.6GDA	7	6.476	1.266
188	2011	Nissan	Juke	GDI	51,404	BNSXV01.6GDA	7	6.986	1.348
189	2011	Nissan	Juke	GDI	51,439	BNSXV01.6GDA	7	3.537	0.803
190	2008	Ford	F-150	PFI	73,612	8FMXT04.63AB	7	1.044	0.272
191	2008	Ford	F-150	PFI	73,629	8FMXT04.63AB	7	0.835	0.243
192	2008	Ford	F-150	PFI	73,729	8FMXT04.63AB	7	1.243	0.376
193	2008	Ford	F-150	PFI	73,768	8FMXT04.63AB	7	1.600	0.254

194	2008	Ford	F-150	PFI	73,785	8FMXT04.63AB	7	1.533	0.229
195	2008	Nissan	Altima	PFI	99,828	8NSXV02.585A	7	2.853	0.368
196	2008	Nissan	Altima	PFI	99,863	8NSXV02.585A	7	0.759	0.218
197	2008	Nissan	Altima	PFI	99,900	8NSXV02.585A	7	0.427	0.163
198	2008	Nissan	Altima	PFI	99,916	8NSXV02.585A	7	0.812	0.222
199	2010	Kia	Forte	PFI	20,907	AKMXV02.0TPC	7	0.447	0.098
200	2010	Kia	Forte	PFI	20,923	AKMXV02.0TPC	7	0.348	0.095
201	2010	Kia	Forte	PFI	20,966	AKMXV02.0TPC	7	0.623	0.129
202	2010	Kia	Forte	PFI	21,032	AKMXV02.0TPC	7	0.525	0.129
203	1997	Ford	Taurus	PFI	129,939	VFM3.0V8G3EK	7	3.250	0.227
204	2009	Dodge	Caravan	PFI	24,568	9CRXT03.8YP0	7	3.741	0.684
205	2009	Dodge	Caravan	PFI	24,585	9CRXT03.8YP0	7	2.702	0.692
206	2009	Dodge	Caravan	PFI	24,627	9CRXT03.8YP0	7	2.804	0.724
207	2009	Dodge	Caravan	PFI	24,643	9CRXT03.8YP0	7	2.210	0.724
208	2009	Dodge	Caravan	PFI	24,748	9CRXT03.8YP0	7	2.006	0.836
209	2011	Nissan	Altima	PFI	29,704	BNSXV02.585A	3	3.793	0.520
210	2011	Nissan	Altima	PFI	29,743	BNSXV02.585A	3	0.628	0.225
211	2011	Nissan	Altima	PFI	29,781	BNSXV02.585A	3	1.500	0.343
212	2011	Nissan	Altima	PFI	30,112	BNSXV02.585A	3	1.944	0.459
213	2011	Nissan	Altima	PFI	30,150	BNSXV02.585A	3	1.894	0.538
214	2011	Nissan	Altima	PFI	30,193	BNSXV02.585A	3	1.462	0.510
215	2011	Nissan	Altima	PFI	30,681	BNSXV02.585A	3	1.661	0.366
216	2011	Nissan	Altima	PFI	30,719	BNSXV02.585A	3	2.190	0.820
217	2011	Nissan	Altima	PFI	30,931	BNSXV02.585A	1	1.522	0.403
218	2011	Nissan	Altima	PFI	30,977	BNSXV02.585A	1	1.112	0.302
219	2011	Nissan	Altima	PFI	31,015	BNSXV02.585A	1	1.410	0.391
220	2011	Nissan	Altima	PFI	31,054	BNSXV02.585A	1	1.383	0.445
221	2011	Nissan	Altima	PFI	31,155	BNSXV02.585A	1	0.959	0.341
222	2007	Chevrolet	Suburban	PFI	0	7GMXT05.3381	7	1.407	1.195
223	2011	Nissan	Altima	PFI	31,190	BNSXV02.585A	1	1.123	0.378
224	2011	Nissan	Altima	PFI	31,224	BNSXV02.585A	1	0.482	0.324

225	2007	Chevrolet	Suburban	PFI	127,920	7GMXT05.3381	7	0.902	0.405
226	2007	Chevrolet	Suburban	PFI	127,920	7GMXT05.3381	7	1.499	0.543
227	2012	Toyota	Corolla	PFI	22,992	CTYXV01.8BEA	7	0.392	0.074
228	2012	Toyota	Corolla	PFI	23,060	CTYXV01.8BEA	7	0.511	0.154
229	2013	Chevy	Spark	PFI	23,925	DGMXV01.8011	1	1.563	0.206
230	2013	Chevy	Spark	PFI	23,959	DGMXV01.8011	1	0.734	0.148
231	2009	Toyota	Camry	PFI	64,083	9TYXV02.4HE2	7	2.358	0.552
232	2009	Ford	Explorer	PFI	52,820	9FMXT04.03DC	1	5.737	1.213
233	2009	Ford	Explorer	PFI	52,855	9FMXT04.03DC	1	2.447	0.494
234	2009	Ford	Explorer	PFI	52,890	9FMXT04.03DC	1	2.270	0.463
235	2009	Ford	Explorer	PFI	52,906	9FMXT04.03DC	1	1.617	0.208
236	2009	Ford	Explorer	PFI	52,923	9FMXT04.03DC	1	1.097	0.214
237	2013	Kia	Forte	PFI	12,674	9FMXT04.03DC	1	6.810	1.156
238	2010	Volkswagen	Jetta/Golf	Diesel	53,040	AVWXV02.0U5N	3	0.244	0.553
239	2010	Volkswagen	Jetta/Golf	Diesel	53,229	AVWXV02.0U5N	3	0.004	0.279
240	2011	BMW	335d	Diesel	26,414	BBMXV03.0M57	3	0.239	0.334
241	2011	BMW	335d	Diesel	26,451	BBMXV03.0M57	3	0.151	0.192
242	2011	Mercedes	E 350 Bluet	Diesel	6,747	BMBXV03.0U2B	3	0.252	0.178
243	2011	Mercedes	E 350 Bluet	Diesel	6,826	BMBXV03.0U2B	3	0.118	0.125
244	2011	Mercedes	E 350 Bluet	Diesel	6,862	BMBXV03.0U2B	3	0.016	0.153
245	2011	Mercedes	E 350 Bluet	Diesel	7,049	BMBXV03.0U2B	3	0.469	0.480
246	2011	Mercedes	E 350 Bluet	Diesel	7,145	BMBXV03.0U2B	3	0.092	0.205
247	2013	Volkswagen	Jetta Tdi	Diesel	4,844	9FMXT04.03DC	3	0.089	0.502
248	2013	Volkswagen	Jetta Tdi	Diesel	4,900	9FMXT04.03DC	3	1.168	0.381
249	2013	Volkswagen	Jetta Tdi	Diesel	4,935	9FMXT04.03DC	3	0.047	0.319
250	2012	Volkswagen	Passat Tdi	Diesel	15,427	9FMXT04.03DC	3	0.388	0.544
251	2012	Volkswagen	Passat Tdi	Diesel	15,482	9FMXT04.03DC	3	69.713	12.424
252	2012	Volkswagen	Passat Tdi	Diesel	15,546	9FMXT04.03DC	3	0.119	0.400
253	2011	Mercedes	E350	Diesel	24,444	9FMXT04.03DC	3	0.153	0.231
254	2011	Mercedes	E350	Diesel	24,499	9FMXT04.03DC	3	0.660	0.264
255	2011	Mercedes	E350	Diesel	24,515	9FMXT04.03DC	3	0.186	0.294

5 CONCLUSIONS AND FUTURE WORK

The conclusions of the work presented in Chapters 2, 3, and 4 are broken into the following four topic areas that cross between measurement and control of the light-duty or heavy-duty sectors.

Section 5.1 summarizes the work demonstrating how the DPF is an effective control strategy, but that the regeneration process is an important area for controlling total PM emissions, and how this may change as technologies evolve and the fleet turns over as a result of natural and accelerated vehicle retirement.

Sections 5.2 and 5.3 discuss the measurement methods for PM using the gravimetric and real-time methods. Although the IPSD method is not yet suitable as a standalone measurement method, it helps better understand gravimetric variability, and highlights new areas for new paradigms in PM measurement.

Section 5.4 presents discusses the results from Chapter 2 which links dilution of exhaust emissions and measurement of PM using ambient rather than filtered dilution air.

5.1 Controlling PM Emissions from Light- and Heavy-Duty Vehicles by the DPF

The characteristics of PM emissions from vehicles equipped with the DPF as a control technology are evaluated from several angles as part of this dissertation. Chapter 2 presents the emissions during parked active DPF regeneration from two trucks certified to the MY 2007 (PM) and 2010 (PM and NOx) heavy-duty emissions standards. PM emissions during parked active DPF regeneration were about ten times lower for the MY 2010 engine than MY 2007 engine following about equivalent durations of low-speed on-road driving to load the DPFs. Although both engines are certified to the same PM emissions standard over the FTP (0.01 g/bhp-hr),

regeneration emissions were substantially reduced for MY 2010 engines, and emissions during non-regeneration periods are also typically lower for MY 2010 engines (CRC 2013).

Chapter 4 showed the emissions from several light-duty diesel vehicles equipped with DPFs were substantially lower relative to PFI conventional gasoline vehicles over the FTP and US06 test cycles. The DPF-equipped diesel vehicles had emissions at least 80% below FTP and US06 emissions standards, except for one US06 test (70 mg/mi) that coincided with an active regeneration that was automatically triggered by the ECM. Based on the steady-state testing described in Chapter 3, an active regeneration is triggered about every 200 mi of driving around 50 mi/hr, and elevated PM emissions are observed between 10 and 20 minutes. However, the frequency and emissions during DPF regeneration may vary depending on the quantity of PM loaded on the DPF and in the case of active DPF regeneration, the operating state of the engine. Therefore, further study of the interaction between PM emissions during regular operation, passive regeneration, and active regenerations would provide a better understanding of the PM emissions over the lifetime of a vehicle in the real world.

In California, trucks with MY 2007 engine technology will mostly be replaced with MY 2010 engine technology by 2023 as required by the Truck and Bus Regulation. Some exceptions to this rule were given for economic considerations, such as trucks with low annual mileages, some classifications of trucks used for general construction purposes, and those operating exclusively in NOx exempt areas that are not expected to be non-attainment areas for ozone. At least over the next ten years, the in-use California heavy-duty truck fleet will include MY 2007 trucks which emit a significantly larger quantity of PM during parked active regeneration compared to the MY 2010 trucks. Current emissions inventories should account for these emissions as the MY 2007-2009 engines will remain operational in California over the next

decade, and for longer periods in other regions of the country without similar in-use programs requiring accelerated adoption.

A specific element of DPF regeneration that could be further explored to control PM emissions from cars and trucks is the effect of stored sulfur on the catalyzed aftertreatment systems. The reduction in regeneration emissions between MY 2007 and 2010 was because the Soot Combustion Regime was less dominant and only accounted for 5% of total PM emissions for the MY 2010 truck. However, both engines reached high aftertreatment temperatures (>500 °C) during active regeneration, which resulted in the repression of stored sulfur and high particle number emissions as a Fuel Combustion Regime. The impact of stored sulfur on catalyst efficiency, and its emission as hydrated sulfate particles during other types of regeneration (e.g. passive or active on-road regeneration), should be further explored. The light-duty diesel vehicle used for effective density determination in Chapter 3 had a mileage consistent with less than 1% of its regulatory useful life, and the effect of sulfur on loaded active DPF regeneration, effective density, and PM emissions during an FTP or US06 test are interesting from a research perspective. From a regulatory perspective, the effect of stored sulfur is more important for heavy-duty vehicles because only about 0.2% of the California light-duty fleet is diesel-powered, according to the latest emissions factor model (CARB 2011a).

5.2 Evaluation of the Gravimetric Method for Measuring PM

The gravimetric filter-based method has been the regulatory basis for measuring PM mass emissions during vehicle and engine certification. Regulations for PM emissions are defined on a mass basis because of the direct linkage to the preponderance of epidemiological

studies showing PM mass is associated with adverse health effects (Pope and Dockery 2006), which lead to establishing a NAAQS for PM as a criteria pollutant.

The existing method using gravimetric PM analysis also provides a rapid indicator of theoretical PM emissions, regardless of size range, composition, or morphology of PM. A key analysis of the PM mass emissions during parked active DPF regeneration in Chapter 2 was the normalization of alternative metrics to the gravimetric values. However, the impending need to further reduce PM emissions has raised questions regarding the repeatability and accuracy at low levels, such as below 1 mg/mi over the FTP light-duty vehicles. Accordingly, this was the basis and motivation for exploring the IPSD method in Chapter 3 for steady-state emissions and Chapter 4 for transient emissions for several vehicles with emissions near or below the LEV III PM standards.

The detection limit at ARB LDV laboratories has been described as 0.17 mg/mi over the FTP (Hu et al. 2014), which is defined as the average tunnel background level when sealing the exhaust transfer tube and measuring PM from the filtered dilution air. The correlation between IPSD and gravimetric mass over both the steady-state and transient cycles diverges below about 0.2 mg/mi as presented in Chapters 3 and 4. Particle number and gravimetric mass emissions followed a similar trend during steady-state and transient conditions, indicating the mass-based standard also offers an indirect control of particle number emissions, at least as measured over the FTP cycle.

5.3 Evaluation of the Real-Time Methods for Measuring PM

Several instruments to measure real-time PM characteristics, such as mass, surface area, and number were evaluated as part of this dissertation. In Chapter 2, the DustTrak DRX, DMM,

SMPS, and EEPS were used to PM emissions during parked active DPF regeneration. In Chapters 3 and 4, the EEPS and APS were used in the light-duty laboratory to measure size distribution and estimate PM mass.

The DustTrak DRX is a useful instrument for providing a direct PM mass reading and size fractionation using a newly developed optical method (Wang et al. 2009a). The DustTrak DRX data collected in Chapter 2 indicated that a large fraction of emissions may be larger than 1 µm during the Soot Combustion Regime. The measurement range of the instrument was limited to PM larger than 0.1 µm, and indeed, the instrument exhibited poor response to ultrafine particles below this size cutoff. The DustTrak is factory calibrated to Arizona Test Dust, and it measured about 3.9 times higher PM mass than filter-based gravimetric measurements during parked active regeneration. The DustTrak DRX reports a handful of real-time PM mass size fractions and may be useful in the light-duty laboratory where the emission of particles larger than 1 µm was reported. However, the APS, which uses an optical time-of-flight measurement, provided a sensitive and high-resolution size distribution of particles between 0.54 to over 2.5 µm for the evaluation presented in Chapter 3 over steady-state cycles, and therefore was an ideal instrument for covering the same size range as gravimetric filters. The aerodynamic distribution reported by the APS can be more rapidly and accurately converted into a mass distribution. Although the DustTrak DRX directly reports PM mass, it requires calibration to a source aerosol using a gravimetric filter.

The Dekati Mass Monitor (DMM) exhibited good sensitivity to both smaller ultrafine and larger fine particles in Chapter 2 when evaluating DPF regeneration emissions. Some of the discrepancies with other mass measurements may have been due to its assumption of unimodal mass distribution, which appears incorrect for vehicle emissions based on the results presented in

Chapters 3 and 4. In addition, the DMM assumes a static mass-mobility scaling exponent for the effective density function, and only changes the coefficient constant based on the distribution fitting between the mobility and aerodynamic channels. The instrument may therefore not be useful for accurately measuring mass emissions from aftertreatment equipped vehicles, during non-regeneration conditions where the exhaust emissions may be more spherical and less fractal than exhaust emissions during standard operation. Because the emissions of particles larger than the upper size cutoff of 1.2 μm appear to influence total PM mass emissions, the use of other Dekati instruments, such as the Electrical Low Pressure Impactor (ELPI) that is capable of measuring up to 10 μm may be more applicable for engine exhaust studies than the DMM, despite its marketed application for exhaust emissions.

Particle size distribution was measured using an SMPS in Chapters 2 and 3, and an EEPS in Chapters 2, 3, and 4. The adopted lognormal fitting approach was a novel application of an existing theory that provided a rapid and simple method for comparing size distributions with from the same source that differ by concentration, GSD, and CMD. The SMPS is regarded as the reference measurement for size distribution; however, it is limited to measuring steady-state emissions that do not change over the span of the approximate two-minute scan time. Parked active DPF regeneration emissions reported in Chapter 2 were sufficiently steady-state for proper characterization by the SMPS. When measuring more transient emissions, such as during FTP or US06 testing of light-duty vehicles on the chassis dynamometer, fast sizing response is required and the measurement biases of the EEPS need to be handled appropriately. The SMPS correction applied to EEPS measurements in Chapter 3 indicated about a 10% reduction in bias; however, the variability was equal or greater compared to without the correction. Therefore, a more robust and accurate inversion approach for EEPS measurements of engine exhaust particles

is needed. Other instruments operating using the same principle, such as the Cambustion DMS 500, employ other inversion techniques that may offer improved real-time measurement. Nevertheless, at least four different EEPS units were used to collect size distribution data from three test cells at the ARB HSL over the FTP and US06 tests. Mass distributions calculated from number-based size distributions indicated that measurements were at least as precise as gravimetric mass measurements. Furthermore, the detection limit of the EEPS if free from gaseous artifact and other variability affecting filter-based measurements, and the IPSD method has an estimated detection limit of 0.018 mg/mi over the FTP.

The application of an accurate effective density function is critical to calculate mass emissions from mobility-diameter size distribution measurements made from an EEPS or SMPS. The DMA-CPMA method adopted for measuring light-duty effective density functions was highly sensitive and accurate relative to laboratory-generated DOS materials over a wide size range. However, it cannot be used to measure transient effective density, which to some degree may change during transient events such as the cold start during the first phase of the FTP. Nevertheless, the correlation between IPSD and gravimetric mass indicates that these fluctuations are negligible compared to the other variables affecting measurement precision. The effective density from gasoline engines has remained similar over the past decade, and therefore additional measurements would only improve upon the fundamental understanding of the nature and morphology of particles emitted from the engine. Improved accuracy and repeatability of suspended PM mass estimates would be secondary objectives. In contrast, the effective density functions of the DPF-equipped light-duty diesel vehicle reported in Chapter 3 were drastically different among engine operating conditions and the relationship between density and vehicle specific power or engine load was not clear. Although light-duty diesel vehicles are predicted to

remain a very small fraction (<1%) of the on-road fleet in California, they are used widely in Europe, and the diesel engine with DPF aftertreatment is the predominant technology for heavy-duty sectors around the world. Therefore, additional measurement of particle effective density from engines equipped with DPF aftertreatment could vastly improve the ability to estimate PM mass using particle size distribution measurements.

The common objective between Chapters 2, 3, and 4 was to use particle size distribution to reconstruct or estimate PM mass over a size distribution of interest. However, new measurement paradigms may provide additional benefit for emissions control if alternative parameters can be considered. For example, a surface area metric could be adopted for light-duty or heavy-duty applications, which could utilize currently available electrometer-based detection methods without requiring the application of a complex inversion matrix to estimate size distribution and applying an appropriate effective density function. Chapter 4 presented some metrics based on estimates of surface area, and demonstrated how the surface area distribution is well contained within a range of approximately 23-560 nm particles, and therefore robust to stochastic measurements related to small nucleation-mode particles that contribute to number-based variability, or larger sub-micron fine particles that would contribute to mass-based variability. Further work should explore the performance of commercially developed diffusion chargers, such as the TSI Electrical Aerosol Detector (EAD).

5.4 Utility of Ambient Dilution for Measuring PM

A novel ambient dilution wind tunnel was used to dilute emissions during parked active DPF regeneration before measurement. One objective of Chapter 2 was to evaluate the relationship of dilution air from the ambient rather than filtering out the larger particles that can

serve as adsorption sites for condensation of gases during the rapid cooling of the dilution process. The range of ambient PM mass concentrations spanned about an order of magnitude, and thus allowed for a comparison of the emissions between two different conditions. Although the field studies and ambient observations have indicated there is a relationship between particle number and mass in the ambient air (Wichmann et al. 2000), data obtained during this study showed no evidence of larger particle adsorbing or affecting the formation of nucleation mode particles. It is possible that exhaust emissions were not mixed with a sufficient quantity of dilution air, and that increasing the dilution ratio beyond ~35 to more roadway-relevant ratios of 1000 or more could enable some finding due to the larger effective size. As part of this evaluation, the comparison to filtered dilution air should be included, because for some of the Subsequent Regenerations in Chapter 2, where only a Fuel Combustion Regime was observed, the contribution of ambient dilution sometimes exceeded the contribution from exhaust emissions. One of the motivations for measuring emissions using ambient dilution air is to establish number-based emissions limits according to how quickly they are taken up during typical ambient dilution air. For instance, if repression of stored sulfur on a DPF must occur periodically to maintain DOC performance, then a future regulation could specify the maximum rate of nucleation-mode particles at any given point during a certification test cycle. Although these particles would still contribute to PM mass emissions from on-road vehicles, any additional health concerns associated with enhanced pulmonary deposition could be mitigated.

5.5 Final Remarks

The implications of the research conducted and summarized in this dissertation span from new vehicle certification standards to controlling emissions from the in-use real-world fleet. The

evaluation of PM measurement in the real-world and in laboratory settings provided insight into the capabilities that could be used to adopt or implement standards for either the light-duty or heavy-duty sectors. The control of emissions from the in-use fleet, especially for heavy-duty vehicles that have longer typical useful life periods, is also important for reducing total emissions and meeting federal obligations set forth by the CAA. As projections of fleet size, in-use emissions inventory, and ambient pollutant standards change over time, California will need to adopt its in-use programs and control in-use emissions adequately and effectively to protect public health and welfare associated with PM emissions from mobile sources.

6 BIBLIOGRAPHY

Ahlvik, P., L. Ntziachristos, J. Keskinen and A. Virtanen (1998). "Real-time measurements of diesel particle size distribution with an electrical low-pressure impactor, SAE 98-0410." SAE Transactions **107**(4): 95-113.

Asbach, C., H. Kaminski, H. Fissan, C. Monz, D. Dahmann, S. Mülhopt, H. Paur, H. Kiesling, F. Herrmann, M. Voetz and T. J. Kuhlbusch (2009). "Comparison of four mobility particle sizers with different time resolution for stationary exposure measurements." Journal of Nanoparticle Research **11**(7): 1593-1609.

Ayala, A., S. Zhang, J. Collins, T. Zhan, H. Dwyer, T. Huai, J. Herner and W. Chau (2008). California's Informal Participation in the Particle Measurement Programme (PMP) Light-Duty Inter-Laboratory Correlation Exercise. CARB. Sacramento, CA.

Barone, T. L., A. A. Lall, J. M. E. Storey, G. W. Mulholland, V. Y. Prikhodko, J. H. Frankland, J. E. Parks and M. R. Zachariah (2011). "Size-Resolved Density Measurements of Particle Emissions from an Advanced Combustion Diesel Engine: Effect of Aggregate Morphology." Energy & Fuels **25**(5): 1978-1988.

Barone, T. L., J. M. E. Storey and N. Domingo (2010). "An Analysis of Field-Aged Diesel Particulate Filter Performance: Particle Emissions before, during, and after Regeneration." Journal of the Air & Waste Management Association **60**(8): 968-976.

Beelen, R., G. Hoek, P. A. van den Brandt, R. A. Goldbohm, P. Fischer, L. J. Schouten, M. Jerrett, E. Hughes, B. Armstrong and B. Brunekreef (2007). "Long-Term Effects of Traffic-Related Air Pollution on Mortality in a Dutch Cohort (NLCS-AIR Study)." Environ Health Perspect **116**(2).

Bielaczyc, P. and J. Merkisz (1999). Euro III/Euro IV Emissions-A Study of Cold Start and Warm up Phases with a SI (Spark Ignition) Engine, SAE Technical Paper.

Biswas, S., S. Hu, V. Verma, J. D. Herner, W. H. Robertson, A. Ayala and C. Sioutas (2008). "Physical properties of particulate matter (PM) from late model heavy-duty diesel vehicles operating with advanced PM and NO x emission control technologies." Atmospheric Environment **42**(22): 5622-5634.

Biswas, S., V. Verma, J. J. Schauer, F. R. Cassee, A. K. Cho and C. Sioutas (2009). "Oxidative Potential of Semi-Volatile and Non Volatile Particulate Matter (PM) from Heavy-Duty Vehicles Retrofitted with Emission Control Technologies." Environmental Science & Technology **43**(10): 3905-3912.

Brook, R. D., S. Rajagopalan, C. A. Pope, J. R. Brook, A. Bhatnagar, A. V. Diez-Roux, F. Holguin, Y. Hong, R. V. Luepker and M. A. Mittleman (2010). "Particulate matter air pollution and cardiovascular disease an update to the scientific statement from the American heart association." Circulation **121**(21): 2331-2378.

Burtscher, H. (2005). "Physical characterization of particulate emissions from diesel engines: a review." Journal of Aerosol Science **36**(7): 896-932.

Bushkuhl, J., W. Silvis, M. M. Maricq and J. Szente (2013). "A New Approach for Very Low Particulate Mass Emissions Measurement." SAE 2013-01-1557.

CARB (1998). Proposed Identification of Diesel Exhaust as a Toxic Air Contaminant (Initial Statement of Reasons). Sacramento, CA.

CARB (2007). Amendments To Adopt More Stringent Emission Standards for 2007 and Subsequetn Model Year New Heavy-Duty Diesel Engines. Sacramento, CA.

CARB (2011a). Emissions Factor (EMFAC2011) Database. Sacramento, CA.

CARB (2011b). LEV III PM, Technical Support Document, Development of Particulate Matter Mass Standards for Future Light-Duty Vehicles. CARB. Sacramento, CA, CARB. **Appendix P**.

CARB (2012a). Development of Particulate Matter Mass Standards for Future Light-Duty Vehicles. Technical Support Document. Sacramento, CA. **Appendix P:** 165.

CARB (2012b). Procedure for Preparation and Handling of Aerosol Sampling Media, California Air Resources Board. Monitoring and Laboratory Division. El Monte, CA.

Cauda, E., D. Fino, G. Saracco and V. Specchia (2007). "Secondary nanoparticle emissions during diesel particulate trap regeneration." Topics in Catalysis **42-43**(1-4): 253-257.

CFR (2011). Engine Testing Procedures. 40 CFR 1065. United States of America.

Chan, T. W., E. Meloche, J. Kubsh and R. Brezny (2014). "Black Carbon Emissions in Gasoline Exhaust and a Reduction Alternative with a Gasoline Particulate Filter." Environmental Science & Technology.

Chase, R. E., G. J. Duszkiewicz, T. E. Jensen, D. Lewis, E. J. Schlaps, A. T. Weibel, S. Cadle and P. Mulawa (2000). "Particle Mass Emission Rates from Current-Technology, Light-Duty Gasoline Vehicles." Journal of the Air & Waste Management Association **50**(6): 930-935.

Choi, W., S. Hu, M. He, K. Kozawa, S. Mara, A. M. Winer and S. E. Paulson (2013). "Neighborhood-scale air quality impacts of emissions from motor vehicles and aircraft." Atmospheric Environment **80**(0): 310-321.

CRC (2009). Final Report, Phase 1 of the Advanced Collaborative Emissions Study, Coordinating Research Council, Health Effects Institute (HEI).

CRC (2013). Final Report, Phase 2 of the Advanced Collaborative Emissions Study, Coordinating Research Council, Health Effects Institute (HEI). Alpharetta, GA.

Dallmann, T. R. and R. A. Harley (2010). "Evaluation of mobile source emission trends in the United States." Journal of Geophysical Research: Atmospheres **115**(D14): n/a-n/a.

Donaldson, K., V. Stone, A. Clouter, L. Renwick and W. MacNee (2001). "Ultrafine particles." Occupational and Environmental Medicine **58**(3): 211-216.

Dwyer, H. (2013). Final Report, Agreement Number 11-329. Measurement of Emissions from both Active and Parked Regenerations of a Diesel Particulate Fitler from Heavy Duty Trucks. Sacramento, CA, California Air Resources Board.

Dwyer, H., A. Ayala, S. Zhang, J. Collins, T. Huai, J. Herner and W. Chau (2010). "Emissions from a diesel car during regeneration of an active diesel particulate filter." Journal of Aerosol Science **41**(6): 541-552.

Ehara, K., C. Hagwood and K. J. Coakley (1996). "Novel method to classify aerosol particles according to their mass-to-charge ratio—aerosol particle mass analyser." Journal of Aerosol Science **27**(2): 217-234.

EPA, U. S. (2002). Health Assessment Document for Diesel Engine Exhaust. Washington, DC, United States Environmental Protection Agency, EPA/600/8-90/057F.

Fenger, J. (1999). "Urban air quality." Atmospheric Environment **33**(29): 4877-4900.

Gardner, R. C. (2001). Psychological statistics using SPSS for Windows, Prentice Hall.

Gauderman, W. J., H. Vora, R. McConnell, K. Berhane, F. Gilliland, D. Thomas, F. Lurmann, E. Avol, N. Kunzli and M. Jerrett (2007). "Effect of exposure to traffic on lung development from 10 to 18 years of age: a cohort study." The Lancet **369**(9561): 571-577.

Grose, M., H. Sakurai, J. Savstrom, M. R. Stolzenburg, W. F. Watts, C. G. Morgan, I. P. Murray, M. V. Twigg, D. B. Kittelson and P. H. McMurry (2006). "Chemical and Physical Properties of Ultrafine Diesel Exhaust Particles Sampled Downstream of a Catalytic Trap." Environmental Science & Technology **40**(17): 5502-5507.

Harrison, R. M., J. P. Shi, S. Xi, A. Khan, D. Mark, R. Kinnersley and J. Yin (2000). "Measurement of number, mass and size distribution of particles in the atmosphere." Philosophical Transactions of the Royal Society of London. Series A: Mathematical, Physical and Engineering Sciences **358**(1775): 2567-2580.

HEI (2012). Advanced Collaborative Emissions Study (ACES) Subchronic Exposure Results: Biologic Responses in Rats and Mice and Assessment of Genotoxicity, Health Effects Institute. Research Report 166. Boston, MA, HEI.

HEI (2013). Understanding the Health Effects of Ultrafine Particles, Health Effects Institute. HEI Perspectives 3. Boston, MA.

Herner, J. D., S. Hu, W. H. Robertson, T. Huai, M. C. O. Chang, P. Rieger and A. Ayala (2011). "Effect of Advanced Aftertreatment for PM and NOx Reduction on Heavy-Duty Diesel

Engine Ultrafine Particle Emissions." Environmental Science & Technology **45**(6): 2413-2419.

Herner, J. D., S. Hu, W. H. Robertson, T. Huai, J. F. Collins, H. Dwyer and A. Ayala (2009). "Effect of Advanced Aftertreatment for PM and NOx Control on Heavy-Duty Diesel Truck Emissions." Environmental Science & Technology **43**(15): 5928-5933.

Hesterberg, T. W., C. M. Long, S. N. Sax, C. A. Lapin, R. O. McClellan, W. B. Bunn and P. A. Valberg (2011). "Particulate Matter in New Technology Diesel Exhaust (NTDE) is Quantitatively and Qualitatively Very Different from that Found in Traditional Diesel Exhaust (TDE)." Journal of the Air & Waste Management Association **61**(9): 894-913.

Hill, J., S. Polasky, E. Nelson, D. Tilman, H. Huo, L. Ludwig, J. Neumann, H. Zheng and D. Bonta (2009). "Climate change and health costs of air emissions from biofuels and gasoline." Proceedings of the National Academy of Sciences **106**(6): 2077-2082.

Hinds, W. C. (1999). Aerosol Technology, Properties Behavior and Measurement of Airborne Particles.

Hu, S., S. E. Paulson, S. Fruin, K. Kozawa, S. Mara and A. M. Winer (2012). "Observation of elevated air pollutant concentrations in a residential neighborhood of Los Angeles California using a mobile platform." Atmospheric Environment **51**(0): 311-319.

Hu, S., S. Zhang, S. Sardar, S. Chen, I. Dzhema, S.-M. Huang, D. Quiros, H. Sun, C. Laroo, L. J. Sanchez, J. Watson, O. M.-C. Chang, T. Huai and A. Ayala (2014). Evaluation of Gravimetric Method to Measure Light-Duty Vehicle Particulate Matter Emissions at Levels below One Milligram per Mile (1 mg/mile), Paper 2014-01-1571, SAE Technical Paper.

Jeong, C.-H. and G. J. Evans (2009). "Inter-Comparison of a Fast Mobility Particle Sizer and a Scanning Mobility Particle Sizer Incorporating an Ultrafine Water-Based Condensation Particle Counter." Aerosol Science and Technology **43**(4): 364-373.

Johnson, T., R. Caldow, A. Pocher, A. Mirme and D. Kittelson (2004). "A New Electrical Mobility Particle Sizer Spectrometer for Engine Exhaust Particle Measurements." SAE 2004-01-1341.

Johnson, T., R. Caldow, A. Pucher, A. Mirme and D. Kittelson (2003). An engine exhaust particle sizer spectrometer for transient emission particle measurements. 9th Diesel Engine Emissions Reduction (DEER) Workshop 2003. Newport, RI.

Johnson, T. J., J. P. R. Symonds and J. S. Olfert (2013). "Mass–Mobility Measurements Using a Centrifugal Particle Mass Analyzer and Differential Mobility Spectrometer." Aerosol Science and Technology **47**(11): 1215-1225.

Jung, H. and D. B. Kittelson (2005). "Characterization of Aerosol Surface Instruments in Transition Regime." Aerosol Science and Technology **39**(9): 902-911.

Kado, N. Y., R. A. Okamoto, P. A. Kuzmicky, R. Kobayashi, A. Ayala, M. E. Gebel, P. L. Rieger, C. Maddox and L. Zafonte (2005). "Emissions of toxic pollutants from compressed natural gas and low sulfur diesel-fueled heavy-duty transit buses tested over multiple driving cycles." Environmental Science & Technology **39**(19): 7638-7649.

Kamboures, M. (2015). "ARB's Evaluation of the AVL Method using two BC measurement principles."

Kaminski, H., T. A. J. Kuhlbusch, S. Rath, U. Götz, M. Sprenger, D. Wels, J. Polloczek, V. Bachmann, N. Dziurowitz, H.-J. Kiesling, A. Schwiegelshohn, C. Monz, D. Dahmann and C. Asbach (2013). "Comparability of mobility particle sizers and diffusion chargers." Journal of Aerosol Science **57**(0): 156-178.

Kelly, W. P. and P. H. McMurry (1992). "Measurement of Particle Density by Inertial Classification of Differential Mobility Analyzer–Generated Monodisperse Aerosols." Aerosol Science and Technology **17**(3): 199-212.

Keskinen, J., K. Pietarinen and M. Lehtimäki (1992). "Electrical low pressure impactor." Journal of Aerosol Science **23**(4): 353-360.

Khalek, I. A. (2005). Final Report, Project E-66 Phase I. Diesel Particulate Measurement Research. Alpharetta, GA, Coordinating Research Council.

Khalek, I. A., T. L. Bougher, P. M. Merritt and B. Zielinska (2011). "Regulated and Unregulated Emissions from Highway Heavy-Duty Diesel Engines Complying with U.S. Environmental Protection Agency 2007 Emissions Standards." Journal of the Air & Waste Management Association **61**(4): 427-442.

Khan, M. Y., K. C. Johnson, T. D. Durbin, H. Jung, D. R. Cocker III, D. Bishnu and R. Giannelli (2012). "Characterization of PM-PEMS for In-Use Measurements Conducted During Validation Testing for the PM-PEMS Measurement Allowance Program." Atmospheric Environment **55**: 311-318.

Khlystov, A., C. Stanier and S. N. Pandis (2004). "An Algorithm for Combining Electrical Mobility and Aerodynamic Size Distributions Data when Measuring Ambient Aerosol Special Issue of Aerosol Science and Technology on Findings from the Fine Particulate Matter Supersites Program." Aerosol Science and Technology **38**(sup1): 229-238.

Kinsey, J. S., W. A. Mitchell, W. C. Squier, K. Linna, F. G. King, R. Logan, Y. Dong, G. J. Thompson and N. N. Clark (2006). "Evaluation of methods for the determination of diesel-generated fine particulate matter: Physical characterization results." Journal of Aerosol Science **37**(1): 63-87.

Kittelson, D. B., W. F. Watts, J. P. Johnson, C. Rowntree, M. Payne, S. Goodier, C. Warrens, H. Preston, U. Zink, M. Ortiz, C. Goersmann, M. V. Twigg, A. P. Walker and R. Caldow (2006). "On-road evaluation of two Diesel exhaust aftertreatment devices." Journal of Aerosol Science **37**(9): 1140-1151.

Kozawa, K. H., S. S. Park, S. L. Mara and J. D. Herner (2014). "Verifying Emission Reductions from Heavy-Duty Diesel Trucks Operating on Southern California Freeways." Environmental Science & Technology **48**(3): 1475-1483.

Kulmala, M., G. Mordas, T. Petäjä, T. Grönholm, P. P. Aalto, H. Vehkamäki, A. I. Hienola, E. Herrmann, M. Sipilä, I. Riipinen, H. E. Manninen, K. Hämeri, F. Stratmann, M. Bilde, P. M. Winkler, W. Birmili and P. E. Wagner (2007). "The condensation particle counter battery (CPCB): A new tool to investigate the activation properties of nanoparticles." Journal of Aerosol Science **38**(3): 289-304.

Laden, F., J. Schwartz, F. E. Speizer and D. W. Dockery (2006). "Reduction in Fine Particulate Air Pollution and Mortality." American Journal of Respiratory and Critical Care Medicine **173**(6): 667-672.

Lall, A. A. and S. K. Friedlander (2006). "On-line measurement of ultrafine aggregate surface area and volume distributions by electrical mobility analysis: I. Theoretical analysis." Journal of Aerosol Science **37**(3): 260-271.

Lehmann, U., V. Niemelä and M. Mohr (2004). "New Method for Time-Resolved Diesel Engine Exhaust Particle Mass Measurement." Environmental Science & Technology **38**(21): 5704-5711.

Li, Y., J. Xue, K. Johnson, T. Durbin, M. Villela, L. Pham, S. Hosseini, Z. Zheng, D. Short and G. Karavalakis (2014). "Determination of Suspended Exhaust PM Mass for Light-Duty Vehicles, 2014-01-1594." SAE Technical Paper.

Liang, B., Y. Ge, J. Tan, X. Han, L. Gao, L. Hao, W. Ye and P. Dai (2013). "Comparison of PM emissions from a gasoline direct injected (GDI) vehicle and a port fuel injected (PFI) vehicle measured by electrical low pressure impactor (ELPI) with two fuels: Gasoline and M15 methanol gasoline." Journal of Aerosol Science **57**(0): 22-31.

Liu, B. Y. H., D. Y. H. Pui, K. L. Rubow and W. W. Szymanski (1985). "Electrostatic Effects in Aerosol Sampling and Filtration." Annals of Occupational Hygiene **29**(2): 251-269.

Liu, Z., J. Swanson, D. B. Kittelson and D. Y. H. Pui (2012). "Comparison of Methods for Online Measurement of Diesel Particulate Matter." Environmental Science & Technology **46**(11): 6127-6133.

Liu, Z. G., V. N. Vasys, M. E. Dettmann, J. J. Schauer, D. B. Kittelson and J. Swanson (2009). "Comparison of Strategies for the Measurement of Mass Emissions from Diesel Engines Emitting Ultra-Low Levels of Particulate Matter." Aerosol Science and Technology **43**(11): 1142-1152.

Lloyd, A. C. and T. A. Cackette (2001). "Diesel Engines: Environmental Impact and Control." Journal of the Air & Waste Management Association **51**(6): 809-847.

Lucking, A. J., M. Lundbäck, S. L. Barath, N. L. Mills, M. K. Sidhu, J. P. Langrish, N. A. Boon, J. Pourazar, J. J. Badimon and M. E. Gerlofs-Nijland (2011). "Particle traps prevent

adverse vascular and prothrombotic effects of diesel engine exhaust inhalation in men." Circulation **123**(16): 1721-1728.

Mamakos, A., L. Ntziachristos and Z. Samaras (2006). "Evaluation of the Dekati Mass Monitor for the Measurement of Exhaust Particle Mass Emissions." Environmental Science & Technology **40**(15): 4739-4745.

Maricq, M. M. (2008). "Bipolar Diffusion Charging of Soot Aggregates." Aerosol Science and Technology **42**(4): 247-254.

Maricq, M. M. (2013). "Monitoring Motor Vehicle PM Emissions: An Evaluation of Three Portable Low-Cost Aerosol Instruments." Aerosol Science and Technology **47**(5): 564-573.

Maricq, M. M., D. H. Podsiadlik and R. E. Chase (1999). "Examination of the Size-Resolved and Transient Nature of Motor Vehicle Particle Emissions." Environmental Science & Technology **33**(10): 1618-1626.

Maricq, M. M., D. H. Podsiadlik and R. E. Chase (2000). "Size Distributions of Motor Vehicle Exhaust PM: A Comparison Between ELPI and SMPS Measurements." Aerosol Science and Technology **33**(3): 239-260.

Maricq, M. M., J. Szente, M. Loos and R. Vogt (2011). "Motor Vehicle PM Emissions Measurement at LEV III Levels." SAE International Journal of Engines **4**(1): 597-609.

Maricq, M. M., J. J. Szente, J. Adams, P. Tennison and T. Rumpsa (2013). "Influence of Mileage Accumulation on the Particle Mass and Number Emissions of Two Gasoline Direct Injection Vehicles." Environmental Science & Technology **47**(20): 11890-11896.

Maricq, M. M. and N. Xu (2004). "The effective density and fractal dimension of soot particles from premixed flames and motor vehicle exhaust." Journal of Aerosol Science **35**(10): 1251-1274.

Matti Maricq, M. (2007). "Chemical characterization of particulate emissions from diesel engines: A review." Journal of Aerosol Science **38**(11): 1079-1118.

May, A. A., N. T. Nguyen, A. A. Presto, T. D. Gordon, E. M. Lipsky, M. Karve, A. Gutierrez, W. H. Robertson, M. Zhang, C. Brandow, O. Chang, S. Chen, P. Cicero-Fernandez, L. Dinkins, M. Fuentes, S.-M. Huang, R. Ling, J. Long, C. Maddox, J. Massetti, E. McCauley, A. Miguel, K. Na, R. Ong, Y. Pang, P. Rieger, T. Sax, T. Truong, T. Vo, S. Chattopadhyay, H. Maldonado, M. M. Maricq and A. L. Robinson (2014). "Gas- and particle-phase primary emissions from in-use, on-road gasoline and diesel vehicles." Atmospheric Environment **88**(0): 247-260.

May, A. A., A. A. Presto, C. J. Hennigan, N. T. Nguyen, T. D. Gordon and A. L. Robinson (2013). "Gas-particle partitioning of primary organic aerosol emissions: (2) diesel vehicles." Environmental Science & Technology **47**(15): 8288-8296.

McDonald, J. D., K. S. Harrod, J. Seagrave, S. K. Seilkop and J. L. Mauderly (2004). "Effects of low sulfur fuel and a catalyzed particle trap on the composition and toxicity of diesel emissions." Environmental Health Perspectives **112**(13): 1307-1312.

McMurry, P. H., X. Wang, K. Park and K. Ehara (2002). "The Relationship between Mass and Mobility for Atmospheric Particles: A New Technique for Measuring Particle Density." Aerosol Science and Technology **36**(2): 227-238.

Mulawa, P. A., S. H. Cadle, K. Knapp, R. Zweidinger, R. Snow, R. Lucas and J. Goldbach (1997). "Effect of Ambient Temperature and E-10 Fuel on Primary Exhaust Particulate Matter Emissions from Light-Duty Vehicles." Environmental Science & Technology **31**(5): 1302-1307.

Oh, H., H. Park and S. Kim (2004). "Effects of Particle Shape on the Unipolar Diffusion Charging of Nonspherical Particles." Aerosol Science and Technology **38**(11): 1045-1053.

Olfert, J. S. and N. Collings (2005). "New method for particle mass classification—the Couette centrifugal particle mass analyzer." Journal of Aerosol Science **36**(11): 1338-1352.

Olfert, J. S., K. S. Reavell, M. G. Rushton and N. Collings (2006). "The experimental transfer function of the Couette centrifugal particle mass analyzer." Journal of Aerosol Science **37**(12): 1840-1852.

Olfert, J. S., J. P. R. Symonds and N. Collings (2007). "The effective density and fractal dimension of particles emitted from a light-duty diesel vehicle with a diesel oxidation catalyst." Journal of Aerosol Science **38**(1): 69-82.

Park, K., F. Cao, D. B. Kittelson and P. H. McMurry (2003). "Relationship between Particle Mass and Mobility for Diesel Exhaust Particles." Environmental Science & Technology **37**(3): 577-583.

Pope, C. A. and D. W. Dockery (2006). "Health Effects of Fine Particulate Air Pollution: Lines that Connect." Journal of the Air & Waste Management Association **56**(6): 709-742.

Quiros, D. C., E. S. Lee, R. Wang and Y. Zhu (2013). "Ultrafine particle exposures while walking, cycling, and driving along an urban residential roadway." Atmospheric Environment **73**(0): 185-194.

Ristimäki, J., A. Virtanen, M. Marjamäki, A. Rostedt and J. Keskinen (2002). "On-line measurement of size distribution and effective density of submicron aerosol particles." Journal of Aerosol Science **33**(11): 1541-1557.

Ristovski, Z. D., E. R. Jayaratne, M. Lim, G. A. Ayoko and L. Morawska (2006). "Influence of Diesel Fuel Sulfur on Nanoparticle Emissions from City Buses." Environmental Science & Technology **40**(4): 1314-1320.

Rostedt, A., M. Marjamäki and J. Keskinen (2009). "Modification of the ELPI to measure mean particle effective density in real-time." Journal of Aerosol Science **40**(9): 823-831.

Russell, L. M., R. C. Flagan and J. H. Seinfeld (1995). "Asymmetric Instrument Response Resulting from Mixing Effects in Accelerated DMA-CPC Measurements." Aerosol Science and Technology **23**(4): 491-509.

Sager, T. M. and V. Castranova (2009). "Surface area of particle administered versus mass in determining the pulmonary toxicity of ultrafine and fine carbon black: comparison to ultrafine titanium dioxide." Part Fibre Toxicol **6**(15): 1-11.

Samuel, S., A. Hassaneen and D. Morrey (2010). Particulate matter emissions and the role of catalytic converter during cold start of GDI engine, SAE Technical Paper.

Schmidt-Ott, A., U. Baltensperger, H. W. Gäggeler and D. T. Jost (1990). "Scaling behaviour of physical parameters describing agglomerates." Journal of Aerosol Science **21**(6): 711-717.

Skillas, G., S. Künzel, H. Burtscher, U. Baltensperger and K. Siegmann (1998). "High fractal-like dimension of diesel soot agglomerates." Journal of Aerosol Science **29**(4): 411-419.

Sorensen, C. M. (2011). "The Mobility of Fractal Aggregates: A Review." Aerosol Science and Technology **45**(7): 765-779.

Swanson, J., D. Kittelson, D. Pui and W. Watts (2010). "Alternatives to the Gravimetric Method for Quantification of Diesel Particulate Matter near the Lower Level of Detection." Journal of the Air & Waste Management Association **60**(10): 1177-1191.

Swanson, J. J., D. B. Kittelson, W. F. Watts, D. D. Gladis and M. V. Twigg (2009). "Influence of storage and release on particle emissions from new and used CRTs." Atmospheric Environment **43**(26): 3998-4004.

Symonds, J. P. R., K. S. J. Reavell and J. S. Olfert (2013). "The CPMA-Electrometer System—A Suspended Particle Mass Concentration Standard." Aerosol Science and Technology **47**(8): i-iv.

Timko, M. T., Z. Yu, J. Kroll, J. T. Jayne, D. R. Worsnop, R. C. Miake-Lye, T. B. Onasch, D. Liscinsky, T. W. Kirchstetter, H. Destaillats, A. L. Holder, J. D. Smith and K. R. Wilson (2009). "Sampling Artifacts from Conductive Silicone Tubing." Aerosol Science and Technology **43**(9): 855-865.

TSI (2011). Fast Mobility Sizers, FMPS 3091, EEPS 3090, Standard Operating Procedure. Fast Sizing Workshop 2011. TSI. Shoreview, MN.

Tzamkiozis, T., T. Stoeger, K. Cheung, L. Ntziachristos, C. Sioutas and Z. Samaras (2010). "Monitoring the inflammatory potential of exhaust particles from passenger cars in mice." Inhalation Toxicology **22**(S2): 59-69.

U.S. EPA (2001). Control of Air Pollution from New Motor Vehicles: Heavy-Duty Engine and Vehicle Standards and Highway Diesel Fuel Sulfur Control Requirements. 40 CFR Part 69, 80, 86, Federal Register.

U.S. EPA (2012). Vehicle-Testing Procedures. 40 CFR 1066, Fedreal Register.

Vaaraslahti, K., A. Virtanen, J. Ristimäki and J. Keskinen (2004). "Nucleation mode formation in heavy-duty diesel exhaust with and without a particulate filter." Environmental Science and Technology **38**(18): 4884-4890.

Van Gulijk, C., J. C. M. Marijnissen, M. Makkee, J. A. Moulijn and A. Schmidt-Ott (2004). "Measuring diesel soot with a scanning mobility particle sizer and an electrical low-pressure impactor: performance assessment with a model for fractal-like agglomerates." Journal of Aerosol Science **35**(5): 633-655.

Verma, V., M. M. Shafer, J. J. Schauer and C. Sioutas (2010). "Contribution of transition metals in the reactive oxygen species activity of PM emissions from retrofitted heavy-duty vehicles." Atmospheric Environment **44**(39): 5165-5173.

Virtanen, A., J. Ristimäki and J. Keskinen (2004a). "Method for Measuring Effective Density and Fractal Dimension of Aerosol Agglomerates." Aerosol Science and Technology **38**(5): 437-446.

Virtanen, A., J. Ristimäki, M. Marjamäki, K. Vaaraslahti, J. Keskinen and M. Lappi (2002). "Effective Density of Diesel Exhaust Particles as a Function of Size, 2002-01-0056." SAE Technical Paper.

Virtanen, A. K. K., J. M. Ristimäki, K. M. Vaaraslahti and J. Keskinen (2004b). "Effect of Engine Load on Diesel Soot Particles." Environmental Science & Technology **38**(9): 2551-2556.

Wang, J., J. Storey, N. Domingo, S. Huff, J. Thomas and B. West (2006). "Studies of Diesel Engine Particle Emissions During Transient Operations Using an Engine Exhaust Particle Sizer." Aerosol Science and Technology **40**(11): 1002-1015.

Wang, S. C. and R. C. Flagan (1990). "Scanning Electrical Mobility Spectrometer." Aerosol Science and Technology **13**(2): 230-240.

Wang, X., R. Caldow, G. J. Sem, N. Hama and H. Sakurai (2010). "Evaluation of a condensation particle counter for vehicle emission measurement: Experimental procedure and effects of calibration aerosol material." Journal of Aerosol Science **41**(3): 306-318.

Wang, X., G. Chancellor, J. Evenstad, J. E. Farnsworth, A. Hase, G. M. Olson, A. Sreenath and J. K. Agarwal (2009a). "A Novel Optical Instrument for Estimating Size Segregated Aerosol Mass Concentration in Real Time." Aerosol Science and Technology **43**(9): 939-950.

Wang, X., M. Grose, R. Caldow, J. Swanson, W. Watts and D. Kittelson (2009b). Improvement of engine exhaust particle sizer spectrometer for engine emissions measurement. American Association for Aerosol Research, Minneapolis, MN.

Wentzel, M., H. Gorzawski, K.-H. Naumann, H. Saathoff and S. Weinbruch (2003). "Transmission electron microscopical and aerosol dynamical characterization of soot aerosols." Journal of Aerosol Science **34**(10): 1347-1370.

Westerdahl, D., S. Fruin, T. Sax, P. M. Fine and C. Sioutas (2005). "Mobile platform measurements of ultrafine particles and associated pollutant concentrations on freeways and residential streets in Los Angeles." Atmospheric Environment **39**(20): 3597-3610.

WHO (2005). World Health Organization (WHO) air quality guidlines global update, Report on a working group meeting, Bonn, Germany, 18-20 October 2005., World Health Organization.

Wichmann, H. E., C. Spix, T. Tuch, G. Wölke, A. Peters, J. Heinrich, W. Kreyling and J. Heyder (2000). Daily Mortality and Fine and Ultrafine Particles in Erfurt, Germany. Part I: Role of Particle Number and Particle Mass. J. Heinrich.

Xue, J., Y. Li, X. Wang, T. D. Durbin, K. C. Johnson, G. Karavalakis, A. Asa-Awuku, M. Villela, D. C. Quiros, S. Hu, T. Huai, A. Ayala and H. S. Jung (2014). "Comparison of vehicle exhaust particle size distributions measured by SMPS and EEPS during steady-state conditions." Submitted to Aerosol Science and Technology.

Yanosky, J. D., P. L. Williams and D. L. MacIntosh (2002). "A comparison of two direct-reading aerosol monitors with the federal reference method for PM2.5 in indoor air." Atmospheric Environment **36**(1): 107-113.

Yi, S.-J., H. K. Kim, S. Quelhas, C. Giler, D. Dang and S. B. Kim (2014). Investigation of a Catalyst and Engine Management Solution to Meet LEV III-SULEV with Reduced PGM, SAE Technical Paper.

Zelenyuk, A., Y. Cai, L. Chieffo and D. Imre (2005). "High Precision Density Measurements of Single Particles: The Density of Metastable Phases." Aerosol Science and Technology **39**(10): 972-986.

Zelenyuk, A., J. Yang, E. Choi and D. Imre (2009). "SPLAT II: An Aircraft Compatible, Ultra-Sensitive, High Precision Instrument for In-Situ Characterization of the Size and Composition of Fine and Ultrafine Particles." Aerosol Science and Technology **43**(5): 411-424.

Zhang, S., W. McMahon, B. Frodin, H. Toutoundijan and M. Cruz (2010). Particulate Emissions from California LEV II Certified Gasoline Direct Injection Vehicles. 20th CRC On-Road Vehicle Emissions Workshop, San Diego, CA.

Zheng, Z., K. C. Johnson, Z. Liu, T. D. Durbin, S. Hu, T. Huai, D. B. Kittelson and H. S. Jung (2011). "Investigation of solid particle number measurement: Existence and nature of

sub-23 nm particles under PMP methodology." Journal of Aerosol Science **42**(12): 883-897.

Zhu, Y. F., W. C. Hinds, S. Kim, S. Shen and C. Sioutas (2002a). "Study of Ultrafine Particles Near a Major Highway with Heavy-Duty Diesel Traffic." Atmospheric Environment **36**(27): 4323-4335.

Zhu, Y. F., W. C. Hinds, S. Kim and C. Sioutas (2002b). "Concentration and size distribution of ultrafine particles near a major highway." Journal of the Air & Waste Management Association **52**(9): 1032-1042.

Zimmerman, N., K. J. Godri Pollitt, C.-H. Jeong, J. M. Wang, T. Jung, J. M. Cooper, J. S. Wallace and G. J. Evans (2014). "Comparison of three nanoparticle sizing instruments: The influence of particle morphology." Atmospheric Environment **86**(0): 140-147.